UNIVERSITY OF BERGEN

Department of Physics and Technology

MASTER'S THESIS IN OCEAN TECHNOLOGY

Multidisciplinary Moorings in the Arctic and Coastal Areas

Author: Bjørnar Hallaråker Røsvik

June 15, 2022

Abstract

When measuring long-term changes in the ocean, it is essential to have moorings or other observation systems that can reliably provide high-quality measurements. Accordingly, it would be valuable to simulate how it acts in the water column with different designs and environmental conditions. As a result, good simulations could help optimize the mooring design before deployment. Part one of this thesis focuses on reviewing moorings from the UNDER-ICE experiment in the Arctic Ocean by using currents from the GECCO ocean model and ADCPs as input to a mooring design software. The aim is to compare the simulated and observed mooring motions to evaluate how good the design approach is. If the results are promising, this approach can help optimize mooring design.

Part two of the thesis focuses on designing, deploying, and recovering a multidisciplinary mooring near a fish farm. After recovery, the measurements and modeling results have been analyzed to investigate how well the observation mooring has performed. In particular, to show the strengths and weaknesses of the mooring design and explain how the aquaculture industry can take advantage of the data obtained.

The main result from the simulation using currents from the GECCO ocean model, the simulations disagreed with the observed mooring motion because of insufficient movement. However, when using currents from the ADCPs installed in the moorings, the results were in better agreement. In part two, the design, deployment, and recovery operations went well, despite ending up as a surface mooring instead of the planned subsurface mooring. Still, it proved to be capable of conducting measurements in coastal areas.

Acknowledgment

I want to express my gratitude to my supervisors, who have helped me with valuable input and helpful advice in my research work. First, thank my main supervisors, Hanne Sagen and Espen Storheim, at the Nansen Environmental and Remote Sensing Center (NERSC), co-supervisor Camilla Sætre at the University of Bergen, and co-supervisor Thore Clifford Thuestad at the Western Norway University of Applied Sciences.

In addition, a special thanks to the staff at NERSC for including me in their work environment. NERSC has also helped me with a lot of resources to be able to deploy an observation mooring. They were lending me both instruments and hardware components. Also, I want to express my gratitude to Inger Graves and Aanderaa Data Instruments AS for lending me two SeaGuard instruments that have been important in my research.

Bremnes Seashore AS has also been a key in conducting the field experiment safely and well. Especially the people in Team Holevik have been supportive in providing ship time and helping complete the deployment and recovery operations. In addition, Geir Magne Knutsen has also been supportive in the process and permitted me to use data from Bremnes Seashore in my thesis.

I am particularly grateful for the assistance given by Espen Storheim at NERSC. I have learned a lot from his guidance, helpful critiques, technical support, and valuable tips and tricks that I will take with me further. He was also an essential part of conducting the field experiment.

I am also grateful to my friends, especially Parkveiens Venner, for their entertainment and moral support throughout my studies. Finally, I want to thank my girlfriend Frida and my family for keeping my spirits high and supporting and encouraging me.

This work has been supported by SFI Smart Ocean, funded by the Research Council of Norway. Data and mooring design for the Arctic were obtained from the UNDER-ICE project number: 226373.

Contents

List of Figures

List of Tables

Chapter 1

Introduction

1.1 Motivation

In order to monitor the long-term changes of the ocean, it is necessary to have equipment that can measure essential water parameters in various ocean environments worldwide. Buoys and moorings are utilized for this purpose with all sorts of applications. For example, it is related to observing temperature changes, algae blooms, currents, salinity, etc. Furthermore, buoys are relevant when monitoring the motion of water and studying the variability between different ocean locations. However, moored observatories are necessary when specific areas are critical to observe.

Moorings come in different shapes and types, and various applications and methods have been tested throughout the years. However, in most situations, the configuration consists of one mooring line connected to an anchor at the seafloor and a flotation element at the top. This means that the deployment and recovery operations are more efficient and safe. Therefore, this report focuses on either single-point surface or single-point subsurface moorings.

In remote areas like the Arctic Ocean, moorings are an essential tool since there is little infrastructure to establish, e.g., observatories with real-time data. To conduct scientific cruises in environments like this requires a lot of resources and time. Due to sea-ice, it is also critical to have a vessel that is an ice-breaker and certified to handle sea-ice. This amplifies the importance of what is called multipurpose moorings. When cruises like this are arranged, it is about using the time effectively to obtain as much valuable data as possible. Hence, when deploying moorings here, it is a goal to have as many instruments as possible in the mooring design. However, avoiding large knockdowns is recommended in specific applications, for instance, when acoustic instruments are on the moorings.

Regarding moorings in the Arctic, some other aspects must be considered. First, the sea-ice

makes the deployment and recovery operations much more complicated. When deploying in sea-ice, the anchor must be deployed first, which means that the mooring line will be under high tension during the operation. Since the depth also often is great, the procedure takes time. That increases the risk of injuries on both personal and equipment. This situation also increases the risk of drifting sea-ice damaging the mooring line. That is also why nylon ropes like kevlar are more typically used in open waters than in conditions with sea-ice.

Based on all these factors, it is essential to have a mooring design that fulfills the requirements of the mooring system. Unfortunately, after deployment under the sea-ice and generally on subsurface moorings, there is no possibility of getting confirmation that all the instrument operates as planned before recovery. It means that there is a possibility that the mooring has failed because of too large pulldowns on the top float, which have made it implode. Alternatively, the mooring line could not withstand the tension, detached from the anchor, and was lost under the sea-ice.

This makes it exciting to investigate if there is software that can predict how moorings will act in the water column during various environmental conditions. If it is possible to verify the movement from the simulations, mooring design software could be used to optimize mooring design. In addition, it is interesting to compare currents from ocean models with *in situ* data to evaluate how good the model is. With reliable models that satisfactorily represent the current in the area, it would be possible to use this when deploying in new places. Furthermore, if specific locations or depths with strong currents could be identified, it would be possible to avoid placing mooring elements with much drag in these positions. Consequently, if it is situations where precise depth or location is essential, necessary measures could be implemented to avoid unwanted mooring motion.

Different multidisciplinary projects in the Arctic Ocean have been investigated to obtain more information about essential projects in the area. For example, the Alfred Wegener Institute, Helmholtz-Centre for Polar and Marine Research (AWI) established the LTER (Long-Term Ecological Research) observatory HAUSGARTEN in the Fram Strait in 1999 [5]. This project focus on measuring long-term changes regarding important ocean parameters like heat fluxes, freshwater fluxes, sea-ice concentration, water circulation, etc., in the Fram Strait. Another interesting experiment is called the Beaufort Gyre Exploration Project. This project focuses on monitoring the circulation in the Canadian Basin [6]. It is conducted by the Woods Hole Oceanographic Institution (WHOI). An additional example of a more small-scale experiment is the UNDER-ICE experiment, which had five different moorings with acoustic and oceanographic instruments and is discussed further in Chapter 4.

Furthermore, it is critical to avoid the acoustic instruments' pulldowns since they can ruin the quality of the measurements. An essential element in these projects is observation moor-

ings monitoring the long-term changes. Henceforth, it is important to understand how they will act in the water column in different flows. In open waters, it is possible to have surface buoys that transmit the data in near real-time via satellites. In addition, closer to shore, real-time data can be transmitted via fiber-optic cables or an internet connection. However, systems like this are not applicable under the sea-ice. Consequently, reliable subsurface moorings are needed under the sea-ice to measure the long-term changes.

Several software solutions are applicable for modeling moorings and simulating mooring motion. The mooring engineers at WHOI use a software called NOYFB [7] coded in FORTRAN II. Even though it was created in 1976, it is still in use. Another more modern software that is getting popular within the marine dynamic analysis field is ProteusDS [8]. However, it requires a license to operate. There is also another software coded in MATLAB called Mooring Design & Dynamics MD&D.

Based on the experiences from working with moorings already deployed and evaluating their design, there is an ambition to try and implement some of the knowledge obtained in designing an observation mooring to deploy in coastal areas. Of course, it is an entirely different environment, but many of the same considerations must be taken when deploying. There are also some new aspects that would be interesting to evaluate and compare. There is, for instance, typically more ship traffic and also shallow water with variable bathymetry. In addition, more obstacles like fishing gear and aquaculture facilities in the area must be considered to find a suitable location to deploy the mooring.

Furthermore, it is interesting to investigate how multipurpose mooring works in an environment like this. To look into the data obtained and evaluate how the aquaculture industry may take advantage of having an observation mooring nearby. Compare measurements from the fjord with real-time measurements done inside the fish net. How would the net, e.g., affect the oxygen levels inside the fish cage if there is much marine growth on the net? It could also help understand how currents affect salinity, temperature, and oxygen. Maybe evaluate how noise affects the fish when operations occur in the facility.

1.2 Objetive

This thesis has been divided into two main objectives, as described below. The first objective is to learn more about mooring design and obtain experiences with mooring motion. Lessons learned from objective one can be used to conduct objective number two more competently. Objective two is more practical and requires more resources to carry out.

Objective 1: Analysis of mooring motion in a deep-water environment. Model moorings

and simulate mooring motion using current data from an ocean model that covers the measurement period or *in situ* data from the mooring location. Furthermore, comparing the observed and simulated mooring motion.

Objective 2: Design, deploy, and recover a multidisciplinary mooring in a coastal area. Process and analyze the data obtained from the measurements to evaluate the performance of the mooring. Use the collected data to compare ocean parameters with other experiments or ocean model data vertically and horizontally.

The first objective aims to investigate two different moorings from the UNDER-ICE experiment conducted in the complex deep-water area in the Fram Strait. The modeling and simulations will be performed in the MD&D software using environmental input from the GECCO ocean model and ADCPs attached to the moorings.

The second objective aims to carry out a field experiment from planning and preparations to recovery. This will be conducted in cooperation with an aquaculture company. In a narrow fjord system, it is crucial to have a good design and avoid conflict with shipping and aquaculture moorings. After recovery, data from the observation mooring will be compared with measurements conducted inside a fish cage.

1.3 Literature Review

This section describes some important papers and studies conducted on simulations of mooring motion. The studies address simulations on surface and subsurface moorings and investigate their accuracy relative to observed motion.

In the paper Analysis of surface mooring dynamics from 1974 [9], a comparison of simulated dynamics and actual measurements was conducted. According to this study, the comparison agreed well, and simulations showed that the type and placement of mooring materials significantly influenced the system's behavior.

In [3] mooring motion was simulated in MD&D using ocean currents input from a local Acoustic Doppler Current Profiler (ADCP). The pulldowns from pressure data from the instruments were compared with simulated pulldowns. Based on this paper's findings, the pulldowns agreed with a few percent and showed promising results.

In [10] simulations have been conducted on a wave energy converter (WEC). To develop an economically competitive WEC, having accurate simulations is essential. However, the review shows that much computational power is required to achieve precise results. Consequently, a sensible choice of the model's environmental input data has to be made to get the best balance between computational requirements and the accuracy of the results.

1.4 Thesis Outline

This thesis consists of seven chapters. Below is a brief overview of what the various chapters contain.

Chapter 1, Introduction: Presents the motivation, objectives, and literature review.

Chapter 2, Theory: Describes the theory needed to understand how ocean currents influence different moorings.

Chapter 3, Software and Data: Description of the simulation software and the two ocean models utilized in the project.

Chapter 4, UNDER-ICE Experiment - Mooring Design and Results: Presents information about the UNDER-ICE experiment in the Fram Strait regarding mooring design and configuration. Before illustrating the results regarding current data and from the comparison between observed and simulated mooring motion.

Chapter 5, Field Experiment in Stokksundet: Description of the field experiment process from planning and preparations to design, configuration, deployment, and lastly, recovery of the observation mooring.

Chapter 6, Results - Field Experiment: Contains an evaluation of the data obtained from the field experiment, a comparison of temperature, salinity, and oxygen data, and an assessment of the observation mooring performance.

Chapter 7, Discussion, Conclusions, and Further Work: Describes essential discussions based on the results, conclusions drawn from the findings in the thesis, and suggestions for further work.

Chapter 2

Theory

This chapter presents the theory of importance to explain the motion of moorings induced by ocean currents.

2.1 Hydrodynamics on Subsurface Moorings

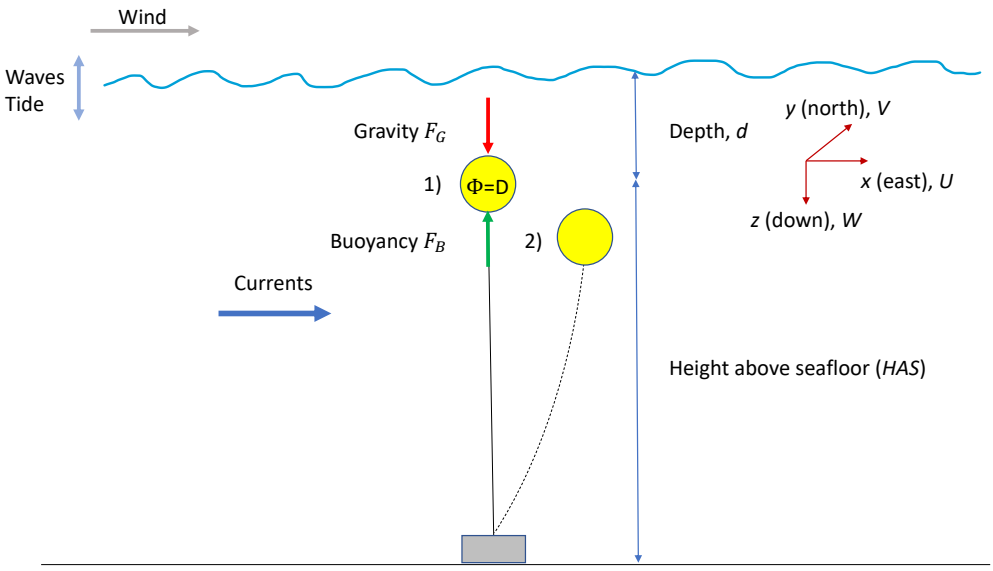

Figure 2.1: The various forces that are influencing a subsurface mooring at two different states. In state 1) the system is presented in a zero flow condition. In state 2), the mooring motion is shown when there is a flow, $\vec{u}$, Eq. (2.12) working on the sphere.

Consider a sphere at depth d attached to an anchor on the seafloor with a mooring line. Firstly, the system is considered at a state with zero flow in the water. That can be used to

describe the forces that keep the floatation sphere in place. F_B represents the buoyancy force that will try to move the sphere towards the surface. F_G is the gravity force that tries to pull it down. Finally, the wire's tension and anchor weight keep the sphere in position. The height above the seafloor (HAS) on a subsurface mooring will stay constant at a zero flow condition in state 1), but the depth will vary with tidal waters and waves. State 2) shows how the top float can be pulled down during strong currents. The distance between the initial depth of the sphere and the new depth when being pulled down is called dZ.

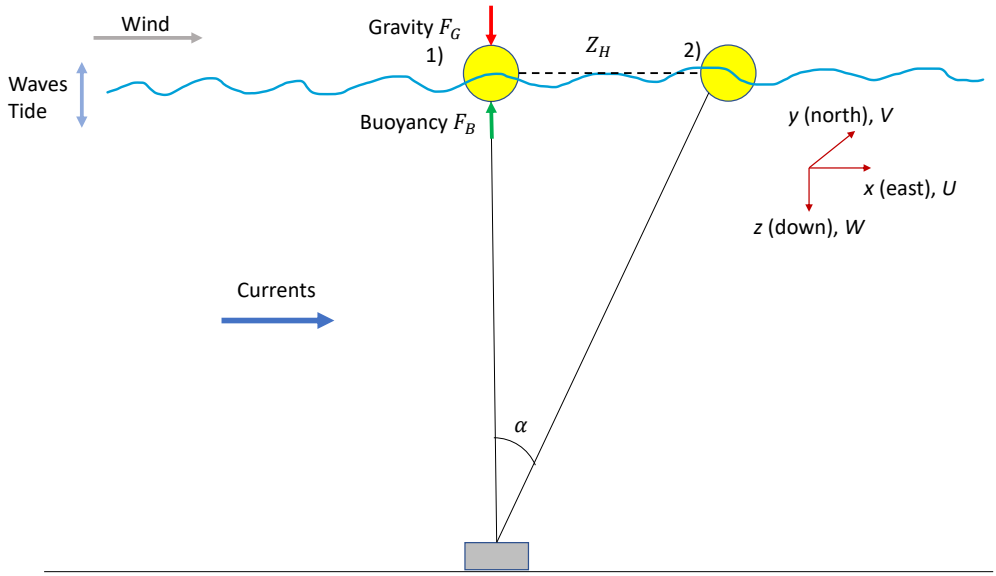

Figure 2.2: Mooring motion on a surface mooring at two different states. Firstly, in still water in case 1), and then in a condition with currents and wind influencing the system in case 2).

Figure 2.2 illustrates how a surface mooring might look in the water. At state 1) the mooring line will have some slack, and the top float position will be straight over the anchor. State 2) shows how the mooring will look if strong currents and winds occur. The distance Z_H is the distance from the starting position. The angle α between the straight mooring line and the stretched one can be used to calculate how far from the starting position the mooring can move. One thing that changes slightly with the tension on the mooring is instrument depths if attached. If the mooring line is fully stretched, the depths of instruments will decrease. This illustration shows how far the top float can move freely. The sphere could also be forced beneath the surface in certain environmental conditions depending on the sphere's characteristics. It is possible to calculate the horizontal distance Z_H by using this equation

$$Z_H = \sqrt{Z_m^2 - Z_d^2}, \tag{2.1}$$

where Z_m is the mooring line length, and Z_d is the depth at the mooring location.

2.2 Buoyancy

The net vertical force acting on an object due to hydrostatic pressure is called the buoyancy force [11]. Archimedes' principle states that a buoyancy force, F_B, operates in the opposite direction of the gravitational force, F_G, and has a magnitude equal to the weight of the displaced fluid. Since F_G working on the object is equal to the object weight, the net force F_{net} on a fully submerged object is the difference between its weight W_{obj} and the weight of the displaced water W_{fluid}. The net force can then be described as

$$F_{\text{net}} = F_G - F_B = W_{obj} - W_{fluid}. \tag{2.2}$$

In this case, the positive value of F_{net} represents a force in the direction of gravity. Conversely, a negative value describes an object being pushed towards the surface. Another way to describe the buoyancy force working on an element is by setting up Archimedes' principle mathematically as

$$F_{\text{B}} = \rho g V_f, \tag{2.3}$$

where g is the gravitational constant, V_f is the volume of the displaced fluid, and ρ is the density of the fluid. Archimedes' principle is the statement that the buoyant force on an object is equal to the weight of the fluid displaced by the object.

2.3 Drag Force

A structure immersed in and surrounded by a liquid will experience forces caused by static pressure from the surrounding fluid. If the flow starts to move, the submerged structures will also experience dynamic pressure caused by water particles pressed around the structure [12]. This effect is illustrated in Figure 2.3.

The drag force F_D [11] on a cylinder is defined with the geometric parameters diameter D, and length L. In addition, the density, velocity, and viscosity have to be taken into account. The relationship between these parameters is described mathematically with dimensional analysis [11] and is given as

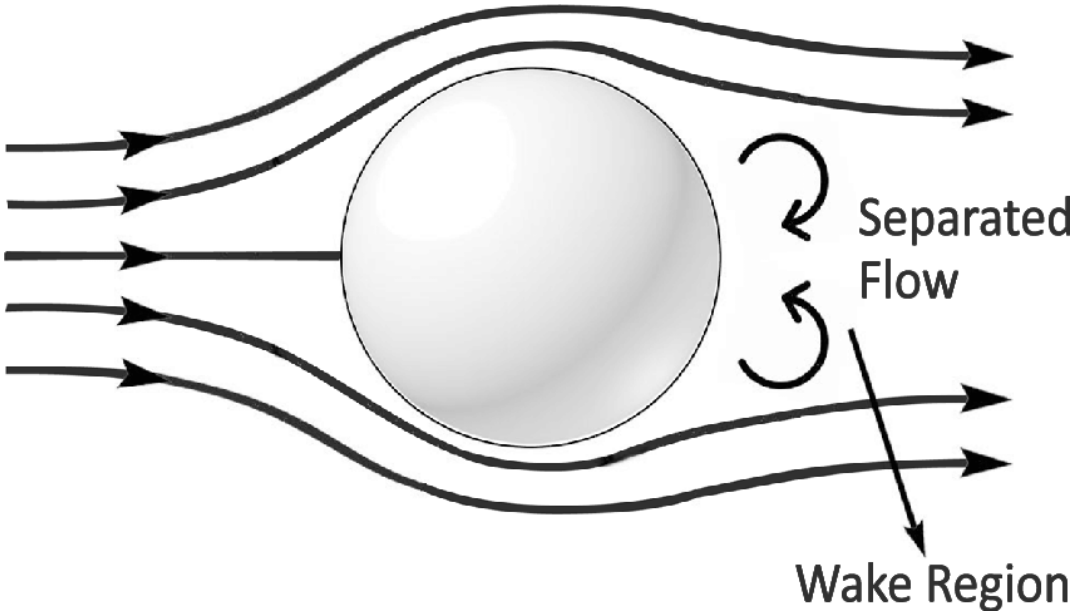

Figure 2.3: Illustrates how the flow around an object separates and formates a wake region behind object [1].

$$\frac{F_D}{\frac{1}{2}\rho v^2 DL} = g\left(\mathrm{Re}, \frac{L}{D}\right), \tag{2.4}$$

where the Reynolds number Re is based on the aspect ratio of the cylinder, v represents the flow speed, and ρ is the density. The drag force F_D is normally presented as

$$F_D = C_D \frac{1}{2}\rho v^2 DL, \tag{2.5}$$

where the drag coefficient C_D is described as

$$C_D = \frac{F_D}{\frac{1}{2}\rho v^2 DL}. \tag{2.6}$$

From Eq. (2.4) the drag coefficient is defined as

$$C_D = C_D\left(\mathrm{Re}, \frac{L}{D}\right). \tag{2.7}$$

Eq. (2.7) concludes that the drag force on a cylinder depends on the Reynolds number and the relationship between the geometric parameters.

Furthermore, the drag force F_D that works on a smooth sphere will be described. This will depend on the sphere's diameter D, fluid speed, density, and viscosity. Based on the dimensional analysis [11], the drag force F_D is given by

$$F_D = C_D \frac{1}{2} \rho v^2 \frac{\pi D^2}{4}, \tag{2.8}$$

Where the last part represents the projected area of the sphere. The drag coefficient C_D can then be described as

$$C_D = \frac{F_D}{\frac{1}{2}\rho v^2 \left(\pi D^2/4\right)}. \tag{2.9}$$

Since the sphere only has one dimension in the flow, the drag coefficient is simply only depending on the Reynolds number,

$$C_D = C_D(Re), \tag{2.10}$$

and the Reynolds number is based on the diameter of the sphere.

2.3.1 Reynolds Number

A fluid flow can be described by using flow lines. The movement pattern a given fluid particle will follow in a flow is the movement pattern. A flow can be divided into three types, laminar, transitional, and turbulent. In laminar flow, the particles move in nice straight paths. The fluid particles move in random and disordered paths in turbulent flow, while the transitional flow is something in between. Figure 2.4 illustrates the difference between the laminar and turbulent flow.

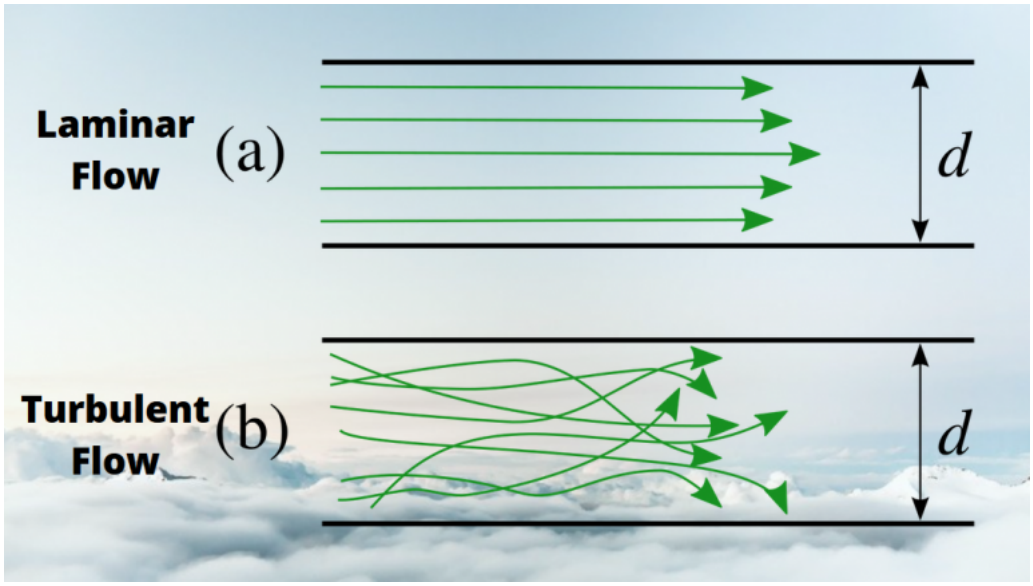

Figure 2.4: Laminar (a) and turbulent (b) flow [2]. The d presented in the figure is equivalent to the L in Eq. (2.11), and represent the pipe diameter in this situation.

An important factor in describing this is the Reynolds number, Re. Reynolds Number is a calculation that defines a fluid's flow as the ratio of the inertial forces to the viscous forces [2].

$$Re = \frac{\rho v L}{\mu}, \tag{2.11}$$

where ρ is the fluid density, v represents the fluid velocity, L is the characteristic length scale, and μ is the fluid viscosity. For flow in a pipe, L is typically represented as the inner diameter of the pipe. In open water, the characteristic length will typically be the diameter of the object that the flow passes.

At low Re numbers, the inertia is so small that the flow easily transports past a cylinder while remaining laminar. For flow in a pipe, for example, one has a laminar flow at $Re < 2300$, at $2300 < Re < 4000$, the flow will be transitional, and at $Re > 4000$, the flow is turbulent [2]. In the case of external influence or flow over other geometries, the transition from laminar to turbulent current occurs at other Re.

2.4 Ocean Currents

Ocean currents describe the movement of the water masses in the ocean. Three factors mainly drive these currents: tidal water, wind, and thermohaline circulation [13]. The tidally driven currents can be strong in the fjords and along the coast. These currents are regularly changing and can be predicted for future days. Another essential aspect is the wind-driven ocean current. They can significantly influence the currents in the upper water column. The last main factor to consider is thermohaline circulation. Density differences drive this process due to temperature and salinity variations in various ocean areas. The water flow in the ocean is described as,

$$\vec{u} = [u_x, u_y, u_z] = [U, V, W], \tag{2.12}$$

where the flow vector $\vec{u}$ is divided into three different components in the x, y, and z direction. These components are often referred to as U, V, and W, and from these, the magnitude of the current speed in all directions could be calculated by using,

$$\|\vec{u}\| = \sqrt{U^2 + V^2 + W^2}. \tag{2.13}$$

The various components represent different directions in the ocean. For example, the U

component refers to the current in the East-West direction, where East is the positive one. The V component represents the currents in the North-South direction, where North is the positive one, and lastly, the W component refers to the vertical motion.

2.5 Mooring Motion Induced by Currents

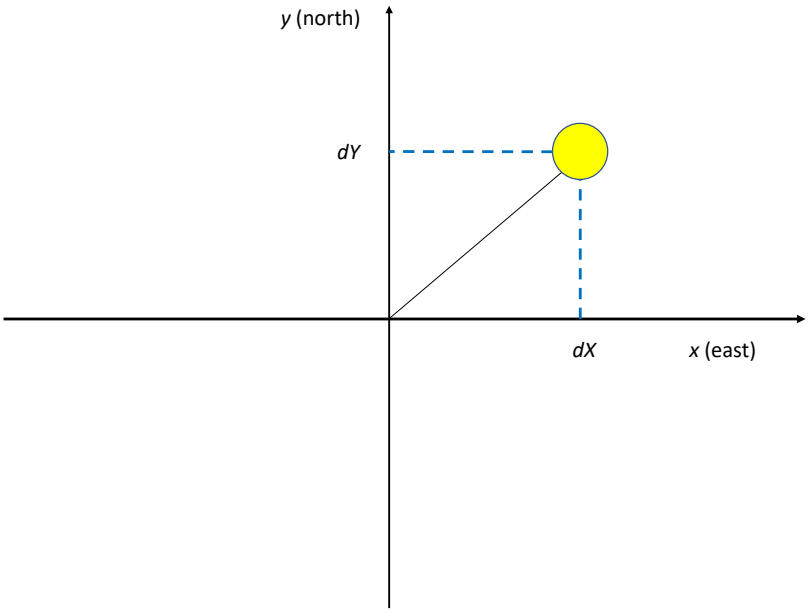

Figure 2.5: Displacement in the x and y direction when horizontal currents act on the mooring. It is, in this case, seen from a bird's-eye view.

Figure 2.5 illustrates the offset from the top float to the anchor position on a mooring. Again, especially considering surface moorings, it is essential to consider the movement in the horizontal direction. It can explain how the instrument depths vary because of the stretch on the mooring line during wind and currents. In subsurface moorings, the dX and dY parameters are also important, but the dZ considering pulldowns on the float is also very important.

Chapter 3

Software and Data

This section describes the different software utilized during the project. It also describes the two ocean models used as support to simulate various scenarios and compare data. The last part is about the *in situ* observations from the UNDER-ICE Experiment in the Fram Strait.

3.1 Mooring Design & Dynamics

Mooring Design & Dynamics (MD&D)[3] is a MATLAB [14] package used to design and analyze single-point oceanographic moorings. The package uses a set of MATLAB routines to recreate a good representation of the moorings and environmental conditions at various mooring sites.

The program runs a static model that will predict the tension and tilt at each mooring component at a given time, given input about the oceanographic conditions and properties of the mooring components. This means that MD&D provides a solution where each element has a static vector force balance in all directions. Through several iterations, the program solves the mooring position given the conditions. When a time-dependent solution is present, it is possible to use a simulation to predict the dynamic response of the mooring motion. The prediction accuracy depends on the environmental data's quality, especially the time-series of current data. The safe anchor mass is also estimated for each given situation. The vertical and horizontal tension, alongside the anchor material, is considered to ensure the mooring system has enough weight.

3.1.1 The Main Menu

This section looks at what capabilities the software has when designing a mooring. The software's main menu shows what kind of different possibilities the user has to design and analyze new or existing moorings. Figure 3.1 illustrates the main menu graphical user interface (GUI). The menu shows some of the most important functions available in the software. The upper left part is for moorings, which is investigated in the present work, while the upper right side shows options when analyzing towed bodies.

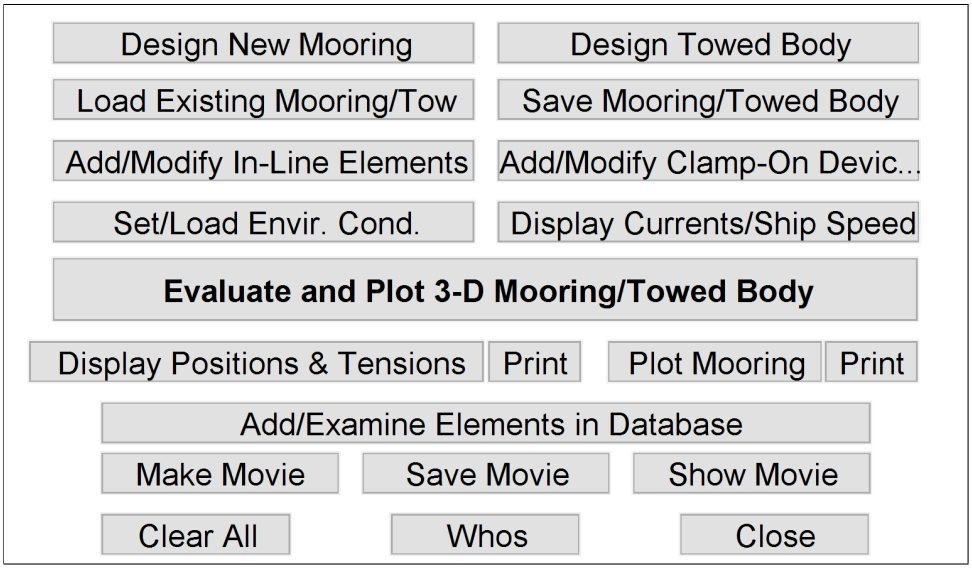

Figure 3.1: Main menu showing most of the functions available in the MD&D package.

The "Design New Mooring" function is used to build a new mooring from scratch. It starts with selecting the top float on the mooring, and then every in-line component is selected from top to bottom. This includes instruments, floatation, chains, and shackles to recreate the configuration as precisely as possible. Afterward, the clamp-on elements can be added to the mooring at given depths, and the software will automatically put it on the correct segment of the mooring line.

Another important function is the ability to set the environmental conditions. This allows the users to define currents, wind, density, and depth at the mooring location. That allows setting extreme values for the current and seeing if the mooring is capable of withstanding the forces that result from it. It is also possible to load current velocities datasets from text files. This allows for making time-dependent solutions in the software. Then it is possible to simulate how the mooring motion is predicted based on changing currents.

It is also an opportunity to illustrate the mooring displacement in 3-D. Therefore, when the mooring design is conducted and the environmental conditions are set, there is an option that shows a three-dimensional plot of how the mooring will act in the water column given

the environmental conditions.

The “Plot Mooring” button gives a simplified drawing of the components in the mooring. It shows the schematic of the most important instruments and where they are placed according to each other. It gives a good understanding of how the mooring is built up.

The “Add/Examine Elements in Database” function make it possible to create new components and look at existing ones. Many standard hardware components and instruments are already in the database and can be used when designing a mooring. The program has four important parameters when adding new parts: dimension, buoyancy, material, and drag coefficient. For example, it is only possible to define cylinders and spheres when inserting dimensions since most instruments are close to having that geometry. However, when instruments have other geometries, an appropriate selection of drag coefficient, C_D, Eq. (2.7) could help compensate for the differences in geometry.

The specifications of the top float used in the field experiment, described in Chapter 5, are illustrated in Figure 3.2. It shows the different parameters that have to be defined. The first value represents the component’s vertical height, and the second value is only for cylinders and represents the diameter of the cylinder. If the device is a sphere, the second value is set to be zero, and the third value is only used when defining spheres, representing the sphere’s diameter. Since the top float is a sphere, the diameter and vertical height are equal at 76.2 cm.

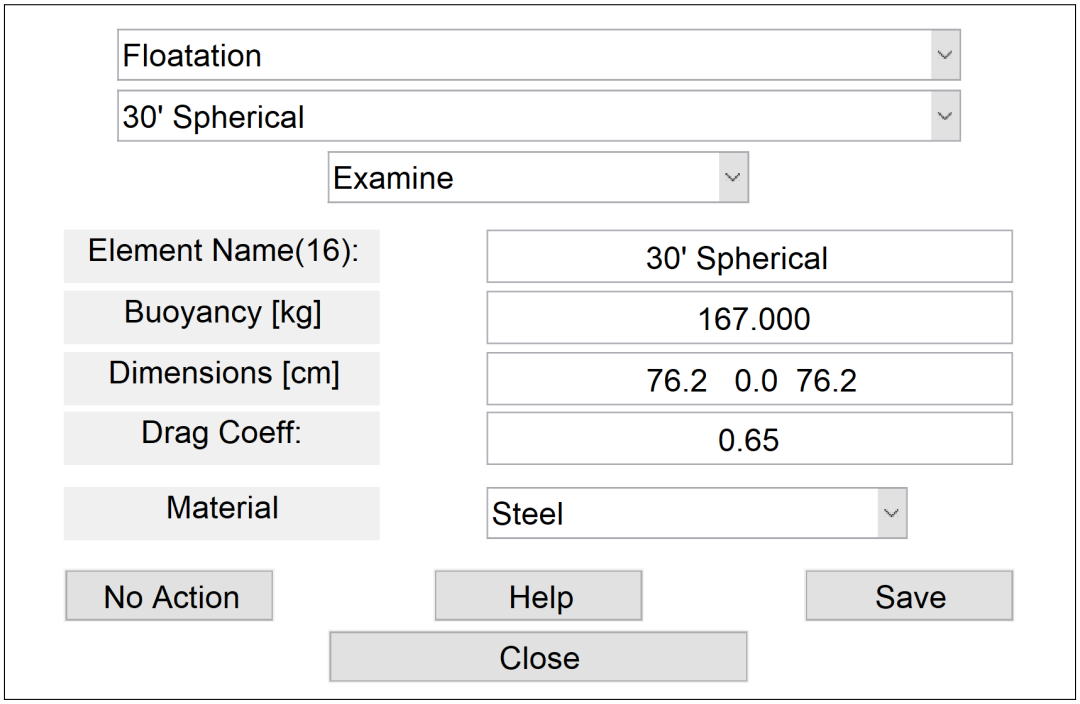

Figure 3.2: The add element graphical user interface.

3.1.2 Numerical Solution

This section covers the numerical solution of the software. To estimate the mooring motion, MD&D uses an iterative process to calculate the positions of every element under the given environmental conditions. That means that the mooring is standing vertically in the water column at the first calculation. Through several re-calculations, the new mooring position is estimated. At each new position, the drag force, tilt, and positions are calculated repeatedly until the mooring stabilizes. The equations used in this section are taken from the MD&D manual [3]. The current and density profiles and wire/chain sections are interpolated to approximately one-meter vertical resolution using linear interpolation. The drag force Q in each direction acting on each mooring element is calculated according to

$$Q_j = \frac{1}{2}\rho_w C_{Di} \cdot A_j \|\vec{u}\| U_j. \tag{3.1}$$

Q_j is the drag in newton that works on each element in water with density ρ_w in the direction "j" (x, y, or z). U_j is the velocity component at a given depth, with C_{Di} being the drag coefficient of a given element "i" at a given depth. A_j is the element's surface area that is perpendicular to the direction j. $\|\vec{u}\|$ represents the total vector magnitude of the velocity in all directions, and is calculated using Eq. (2.13). This calculation is conducted at every depth to understand the flow conditions on all mooring components. From this, the drag in all directions is calculated. Once the drag force for each mooring element has been calculated, including every segment of the mooring line, the tension and vertical angles required to keep the element in position when influenced by ocean currents can be estimated. There are three (x, y, z) component equations that have to be solved at each element to calculate this,

$$Q_{xi} + T_i \cos\theta_i \sin\psi_i = T_{i+1} \cos\theta_{i+1} \sin\psi_{i+1}, \tag{3.2}$$

$$Q_{yi} + T_i \sin\theta_i \sin\psi_i = T_{i+1}, \sin\theta_{i+1} \sin\psi_{i+1}, \tag{3.3}$$

$$B_i g + Q_{zi} + T_i \cos\psi_i = T_{i+1} \cos\psi_{i+1}. \tag{3.4}$$

T_i is defined as the wire tension from above, creating spherical angles in the x and y planes from the vertical. The angles are defined as θ_i and ψ_i. B_i represents the buoyancy force of the element, while g is the gravitational acceleration. Q_{xi}, Q_{yi}, and Q_{zi} are the drag forces in the different directions. The wire tension from below is described as T_{i+1} and the spherical angle from below as θ_{i+1} and ψ_{i+1}. All elements are considered to act dynamically as a hinge, even though they might be rigid in reality.

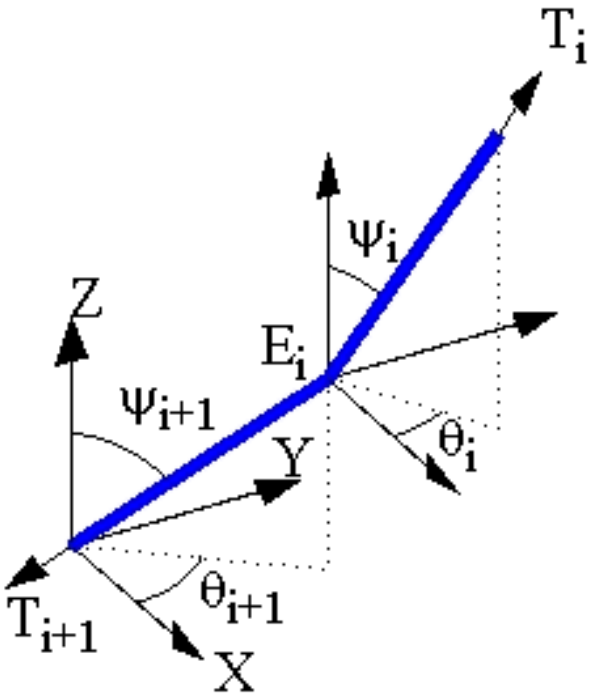

Figure 3.3: The orientation of the tension vectors, spherical angles, and hinge characteristics for an element E_i in a mooring [3].

Figure 3.3 shows the orientation of the tension vectors, spherical angles, and hinge characteristics of an element in the middle of a mooring. Wire and chain segments are divided into smaller segments of 1 m in length. That makes the mooring flexible, which means it can be adjusted to many different shapes based on what kind of current profile and associated drag is present on each element. Once the tension and angles of each element are calculated, the position of the elements relative to the anchor can be calculated. Consequently, it is possible to determine the position of each component by adding the length of each element L_i and adding them together from bottom to top,

$$\begin{aligned} X_i &= X_{i+1} + L_i \cos\theta_i \sin\psi_i, \\ Y_i &= Y_{i+1} + L_i \sin\theta_i \sin\psi_i, \\ Z_i &= Z_{i+1} + L_i \cos\psi_i. \end{aligned} \tag{3.5}$$

When using MD&D the position and tilt of every significant component are stored in the memory. The tilt of the elements is essential when calculating drag. Consequently, when looking at spheres, the main difference is the change of current at the new depth, but when looking at cylinders, there are more things to consider. For cylinders, once the mooring is tilting, several changes occur. The exposed surface area in both the horizontal and vertical directions changes. The drag gets divided into tangential and normal components for the

different currents acting on the element. Tilted elements like these have reduced area and drag coefficient to horizontal currents but increased drag force in the vertical direction.

3.1.3 Environmental Input Data

It is possible to add environmental parameters like ocean currents, wind, and density to the software. In this case, essential variables are the different components from the flow vector, $\vec{u}$ from Eq. (2.12). The U, V, and W represent the current in different directions. U represents the current going in the East-West direction, whereas the East is the positive direction. The V component represents the North-South direction, whereas the North is the positive one. The ocean current data used as input must be stated in m/s. When computed, the software automatically calculates the magnitude and direction of the current components together. The W component represents the vertical current and is, in most cases, neglected since it is much less than the horizontal currents [3].

These velocity profiles are computed as a function of depth. The first value should be the current at the surface, and the last value should be at z = 0, which is the origin of the coordinate system. There is no limitation to the number of data points present in a profile. Since it is often interesting to look at current data over time, it is also possible to have as many columns in the dataset representing the current at different times. However, the number of data points and time columns must be considered due to calculation times. How frequently it is appropriate to have the current measurements depends on the situation and time frame. The easiest way to import the data is by saving it as mat files in MATLAB. Instruments and ocean models often contain CSV files with data about depth and currents, which can be saved into mat files.

MD&D has a coordinate system with the origin at the seafloor beneath the anchor. In most other applications, the $z = 0$ is set at the sea surface and follows the pressure towards the bottom. This can lead to confusion when importing data from ocean models and in cases when comparing results from experiments with simulations. The difference between depth and height above seafloor is illustrated in Figure 2.1.

There are also possibilities to add wind data that will affect the current in the uppermost part of the water column. However, again, it depends on the wind speed how deep below the surface the wind speed will affect the current. It will decrease linearly with a decreasing rate of 1 m/s each meter. Density profiles are the last environmental input data that is important to consider. There has to be at least one density profile that matches the depths defined in the ocean current profile present. Preferably, the density profile changes with ocean current, salinity, and temperature in a time-dependent solution. If density data is unavailable, an

approximation of the density profile is utilized.

3.1.4 Output From Simulations

The software provides several possibilities once a complete mooring has been designed and the environmental conditions are set. First, there is a possibility to plot the positions of the various segments in a 3-D plot, which shows the mooring in the water column under given environmental conditions. This is illustrated in Figure 3.4.

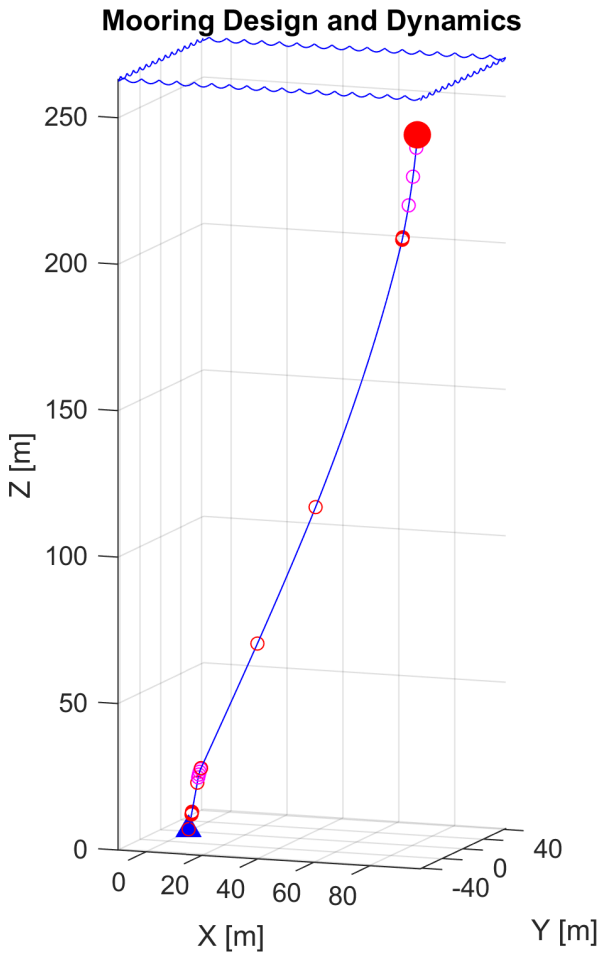

Figure 3.4: A 3-D plot of mooring motion during ocean currents. The filled red circle at the top represents the floatation element, the smaller red circles represent instruments or connections between segments of mooring lines. The triangle represents the anchor on the seafloor.

MD&D calculates the position of the different components and the tension they are exposed to at both the neutral and the moved locations. From this, the movement in the horizontal East/West direction, dX, horizontal North/South direction, dY, and vertical movement, dZ are shown to indicate how much motion the mooring will have. It also calculates the safe

wet anchor mass needed to prevent the mooring from moving from the set location.

If there is a time-dependent solution, it is also possible to plot the positions of an essential component to watch how it is expected to be pulled down in the water column during strong currents. Alternatively, determine when it would move furthest away from the neutral position. When adding the time-dependent solution, the software can create a movie. That option is suitable for visualizing how the mooring might move due to changing currents.

Furthermore, to compare simulations with *in situ* observations, there is a possibility to import ADCP data to have currents from the area as the input. This is conducted in the same way as importing data from ocean models. Firstly the data has to be converted to a mat file. Then, from this position, it is possible to compare, e.g., the movement in the vertical direction, dZ of an instrument by comparing the pressure data from the instrument with the simulation. Alternatively, if the mooring system has a transponder network deployed around it called Long Baseline Acoustic Navigation Network [15], instruments with communicating transducers can be compared in all directions.

3.2 Ocean Model Data

3.2.1 GECCO Reanalysis

The GECCO ocean model is an Arctic Ocean–sea ice reanalysis covering the period from 2007 to 2016 [16], [17], [18]. The model has a vertical resolution of 50 fixed depths, which means they are not following the seafloor but are the same at every location. The maximum fixed depth in the model is 5096 m. However, this causes some data points to be empty in locations with less depth. The model comes with one set of data points each day for ten years, which means that the day-to-day changes in velocities and other parameters can be monitored. However, the model does not consider the small-scale changes during the day.

It also has a rough grid with horizontal data points every 16 km, with higher resolution in some areas in the Arctic Ocean. That means the model is good at predicting the large-scale variabilities but struggles when observing details. The model has stored many different ocean parameters. It contains potential temperature, salinity, East-West current, North-South current, Eeas-West ice velocity, North-South ice velocity, sea surface height, ice thickness, ice concentration, heat flux, freshwater flux, and wind stress. These parameters are also described at different coordinates, varying with time and depth.

3.2.2 NorFjords Ocean Model

The NorFjord hydrodynamic fjord model was developed to get high-resolution data in narrow fjords. The model is defined in the western part of Norway in the Hardangerfjord and has data points every 160 m [19]. The data is obtained from the coastal model system of the Institute of Marine Research. The model has data points from every hour and indicates how the ocean parameters change throughout the day. Moreover, it contains temperature, salinity, East-West current velocity, North-South velocity, time, and depth. The depth data is divided into 35 data points following the terrain. That means that the distance between data points is less on shallower water.

Chapter 4

UNDER-ICE Experiment - Mooring Design and Results

The UNDER-ICE experiment was carried out from 2014 to 2016 in the Fram Strait, between Greenland and Svalbard. Figure 4.1 illustrates the mooring locations of the five moorings deployed as a part of the project. All the moorings are in the length range between 1066 m and 2798 m and include ten hydrophone modules, floatation, a DSTAR controller, and more. The DSTAR controller is connected to the hydrophones via an inductive link and is responsible for controlling them and keeping track of time. The experiment intended to measure the heat flux in and out of the Arctic Ocean. The Fram Strait is a crucial area to monitor to understand the warming of the Arctic Ocean. The West Spitsbergen Current transports warm Atlantic water into the Arctic Ocean, and the East Greenland Current transports cold fresh water out of the Arctic Ocean. The acoustic tomography technique monitors the temperature differences in such large areas.

Two moorings labeled UI2 and UI5 have acoustic sources attached, which is necessary to apply this technique. Figure 4.1 also shows the acoustic paths between the moorings. In addition, the northernmost moorings UI4 and UI5 were equipped with oceanographic instruments. This helps to improve the acoustic measurements and provides new data from an area that is not that well documented.

4.1 Mooring Design

In the beginning, all five moorings from the UNDER-ICE experiment were modeled and investigated in the MD&D software. This was useful for getting more experience with the software and better knowing the different functions. However, since the mooring design and

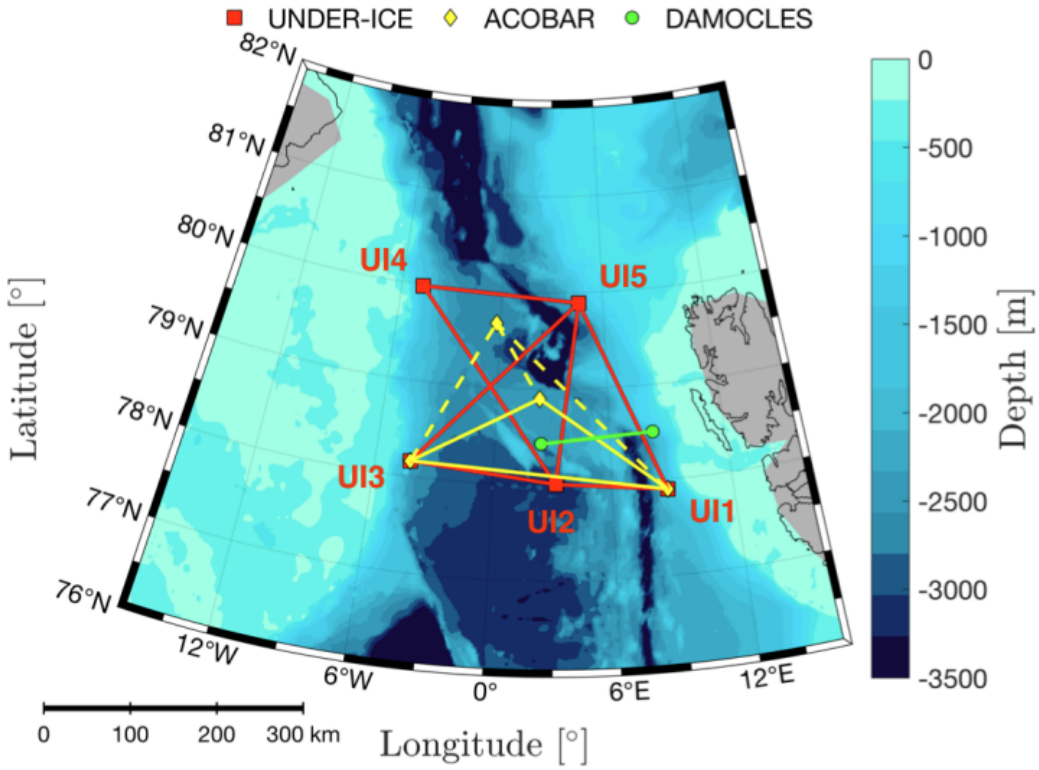

Figure 4.1: Locations of the moorings deployed in the Fram Strait between Greenland and Spitsbergen connected with the UNDER-ICE tomographic experiment. The red marks indicate the mooring locations [4]. The green and yellow marks are from previous experiments.

layout are similar, it was decided to examine two of the moorings more in-depth. The northernmost moorings, UI4 and UI5, were selected since they are in different areas of the Fram Strait and have different configurations. They are also the two moorings equipped with ADCPs, making it interesting to compare the observed current data with the ocean model data. UI5 mooring also has an acoustic source attached which seems to influence the mooring motion quite a bit.

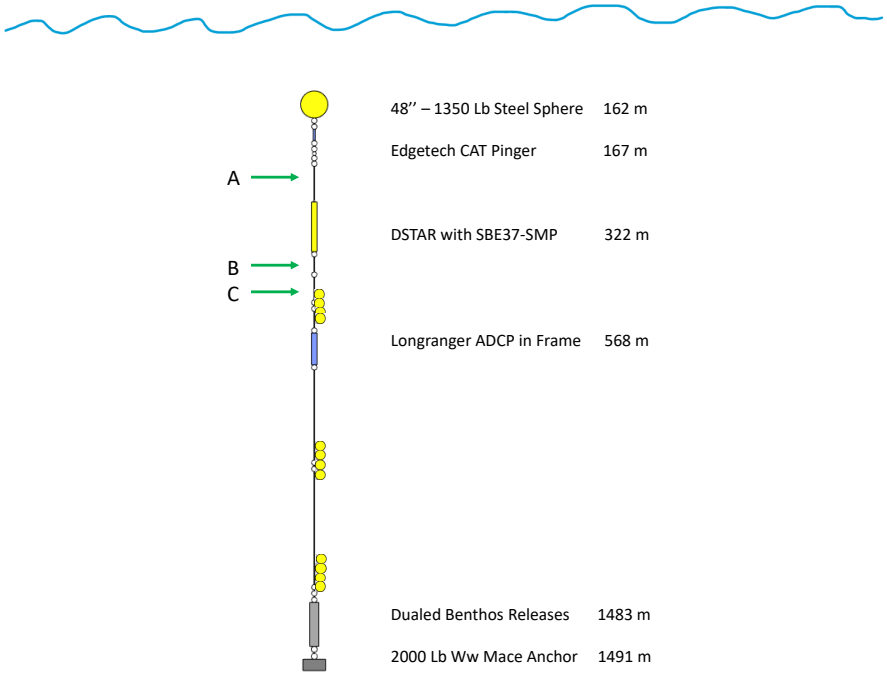

Figure 4.2: Schematic drawing of the UI4 mooring as planned before deployment in the Fram Strait.

Figure 4.2 shows the configuration and main components of the UI4 mooring. The figure illustrates an approximation of the distances between the instruments, even though the mooring line segments are proportionally much shorter than in reality. The different instrument placements are displayed in Table 4.1. At the top of the mooring, there is a floatation element with a positive buoyancy which tries to keep the mooring line straight. Below, A CAT-pinger is located, an instrument that is used to identify the position of the top float before activating the acoustic release during the recovery operation. It is essential to know the top floats' position when conducting these operations in areas with sea-ice, to prevent the mooring from rising beneath the ice.

After the CAT-pinger, the key instruments are located on a 150 m long cable which is connected to the DSTAR controller unit via an inductive termination. The hydrophone modules, two temperature sensors SBE39, and a moored CTD of the type SBE37 are attached by using clamp-on brackets to the mooring line above the DSTAR. In addition, some other SBE39s and SBE37s are attached. Table 4.1 describes the instrument depths and placement. The DSTAR

controller also observes the mooring motion by communicating with the transponder network [15] deployed around the mooring. The four transponders around the mooring will reply to the ping transmitted by the DSTAR with four unique frequency signals. The replies are recorded by the DSTAR and the hydrophone modules and can be used to track both vertical and horizontal movement. Typically, only pressure data is available on oceanographic moorings and can say something about the vertical motion.

In the acoustic tomography experiment, the hydrophones are vital for measuring the sound travel time. However, to control that the estimates from the travel time are correct, local instruments are critical to have as a control organ. That is one of the reasons there are temperature and salinity sensors attached to the mooring line.

Furthermore, a long-ranger ADCP in a frame is connected as an in-line element between two mooring line shots. This ADCP is configured to measure the flow in the upper water column. It is located at 568 m and measures the current at 70 different depths starting from 559 m and measuring every 8 m up to 7 m. Below this are mostly mooring lines and two sets of flotation glass balls before reaching the seafloor. At the end of the mooring, two benthos releases are attached to the anchor with 5 m of chain. This is a safety measure if one release does not respond or function properly. Suppose both releases fail, there would be difficult even to retrieve the instruments without an advanced and costly operation.

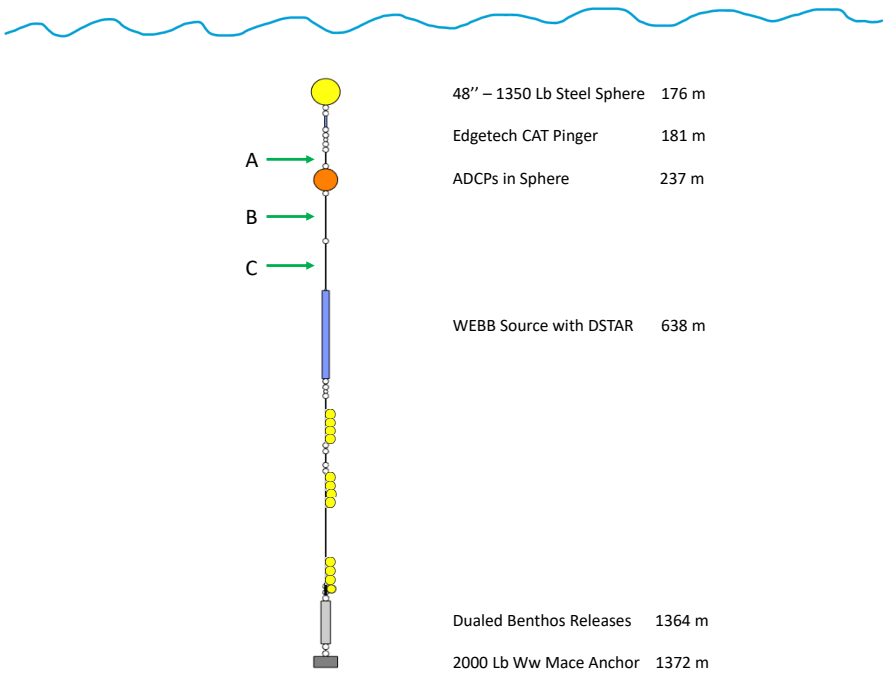

Figure 4.3: Schematic drawing of the UI5 mooring as planned before deployment in the Fram Strait.

Figure 4.3 shows the configuration of mooring five from the UNDER-ICE experiment. UI4 and UI5 have a similar design with many of the same instruments and components. Hence,

Table 4.1: Instruments mounted with clamp-on brackets on the mooring line, the green arrows with the letter labels in Figure 4.2 shows the positions of the instruments on the UI4 mooring.

Instrument	Depth (m)	Serial number	Location (A-D)
SBE39	177 m	3566	A
SBE39	202 m	3746	A
SBE37	227 m	9104	A
H9	232 m	540	A
H8	241 m	539	A
H7	250 m	538	A
H6	259 m	537	A
H5	268 m	536	A
H4	277 m	535	A
H3	286 m	534	A
H2	295 m	533	A
H1	304 m	532	A
H0	313 m	531	A
SBE39	368 m	3570	B
SBE39	419 m	3569	C
SBE37	469 m	9105	C
SBE39	568 m	3574	D

it is not necessary to describe all the details again. Despite this, some essential differences influence the mooring performance much. The main difference is that the UI5 mooring has a sizeable acoustic source as an in-line element at a depth of about 600 m. This source has a big area and wet weight and is used to transmit sound signals to create the acoustic thermometer. Another difference is that this mooring has two ADCPs mounted in a sphere with floatation. One is measuring the currents in the upper water column, and the other is looking down to measure currents down in the water column. The clamp-on devices' respective placement is presented in Table 4.2.

Table 4.2: Instruments mounted with clamp-on brackets on the mooring line, the green arrows with the letter labels in Figure 4.3 shows the positions of the instruments on the UI5 mooring.

Instrument	Depth (m)	Serial number	Location (A-C)
SBE39	187 m	6145	A
SBE37	212 m	8974	A
SBE39	283 m	3573	B
SBE39	333 m	3571	B
SBE39	383 m	3566	B
SBE37	438 m	5447	C
H9	493 m	550	C
H8	502 m	549	C
H7	511 m	548	C
H6	520 m	547	C
H5	529 m	546	C
H4	538 m	545	C
H3	547 m	544	C
H2	556 m	543	C
H1	565 m	542	C
H0	574 m	541	C

4.2 Results

This section covers the results of investigating mooring motion from the UNDER-ICE experiment. This has been conducted by modeling the moorings in MD&D and importing time-series of ocean current data from the GECCO reanalysis. Further, it was possible to simulate mooring motion during the measurement period from deployment in September 2014 to recovery in July 2016. Firstly the mooring design will be presented, and current information from the mooring sites of UI4 and UI5. It was decided to focus on the northernmost moor-

ings since they were subsurface moorings with ADCPs. They are also in two different areas in the Fram Strait, and the UI5 mooring has an acoustic source attached.

The simulated mooring motion is evaluated before comparing it with the observed mooring motion based on the acoustic transponder network.

4.2.1 Comparison of Ocean Current Data From ADCP With the GECCO Reanalysis

It was essential to compare trends from the whole measurement period to establish an overview of the differences between the GECCO current data and the *in situ* current data from the ADCP.

Furthermore, when trying to predict mooring motion, it is essential to have an idea of how the ocean currents in the area behave. Unfortunately, in remote places like the Arctic Ocean, there are not many *in situ* observations, which is why it is interesting to compare model data with measured ADCP data. In this situation, current data has been downloaded from the GECCO ocean model. Unfortunately, since the model has a low resolution, the closest data points available were about 3000 m away from the mooring locations. However, this is still relatively close considering the precision of the model, but it is still a source of error.

Figure 4.4 (b) illustrates the current direction and (a) the speed of the GECCO model in the UI4 location. Based on the thermohaline circulation in the Fram Strait, it is expected to see the strongest currents in the area heading towards the southwest transporting cold water out of the Arctic Ocean [20]. It is also somewhat in the middle of the Strait and probably slightly east of the most substantial part of the East Greenland Current. As shown in (b), at least from 300 m to 900 m, the direction is dominated by currents towards the southeast and somewhat towards the southwest in the upper part. There are also some currents in the upper section of the water column towards the North/Northwest from March to August 2015. .

Figure 4.5 shows the ocean current based on the measurements conducted by the current profiler attached to the mooring. From the first look at the directions in (b), it is clear that the purple shade that indicates currents towards the Southeast dominates. It is also current towards the East and West and barely any towards the North as anticipated. The yellow areas that show stronger currents also have a direction towards the South/Southeast. Something else that separates the ADCP data from the model data is that, especially towards the surface, the current reach levels much higher than predicted in the model. There are also some blank spots from about 50 m to 200 m from March 2015 to October 2015. It is hard to explain why this has happened since later in Figure 4.8 there is no sign of more mooring motion in this period.

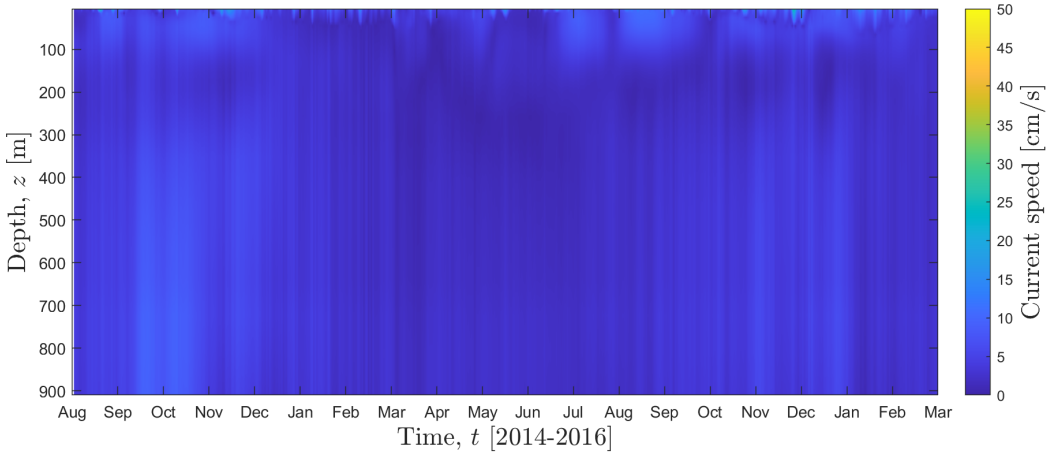

(a)

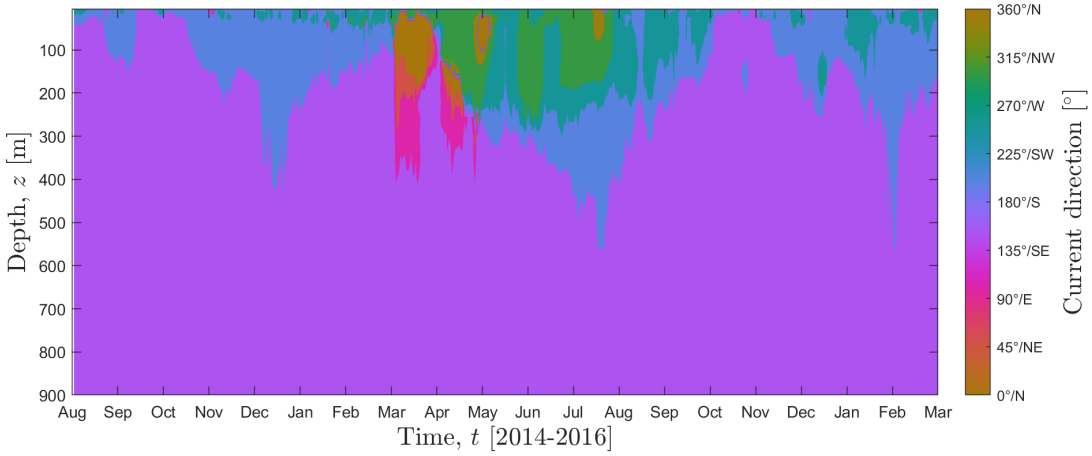

(b)

Figure 4.4: Time-series of the current speed (a) and direction (b) as described by the GECCO ocean model at the UI4 location.

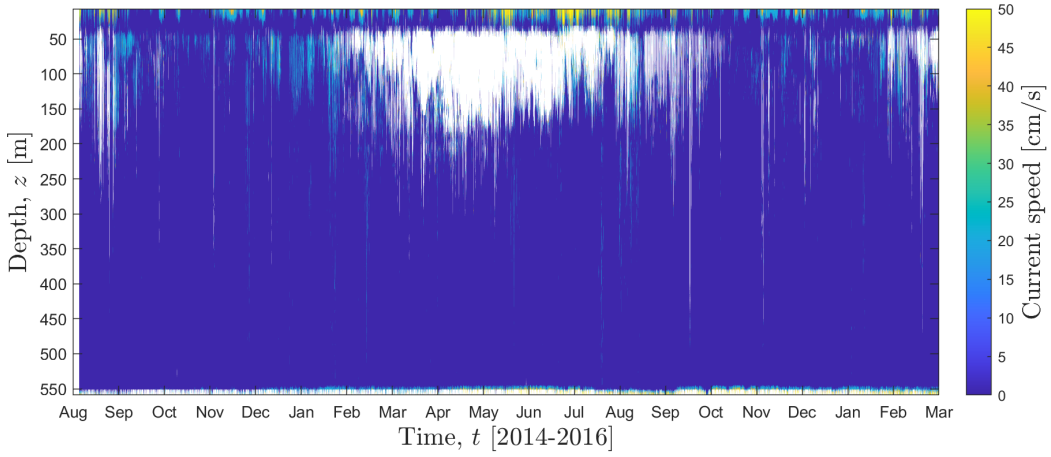

(a)

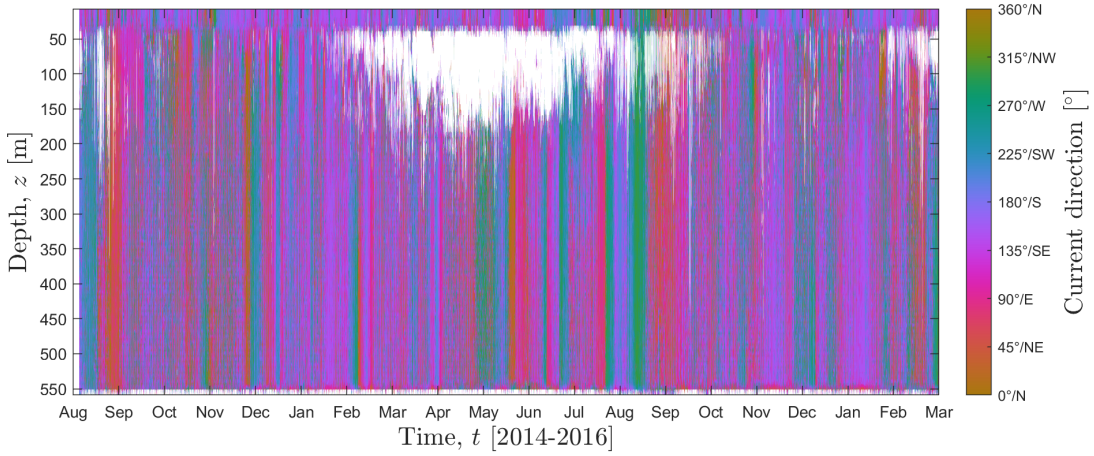

(b)

Figure 4.5: Time-series of the current speed (a) and direction (b) as measured by the upward-looking ADCP on UI4.

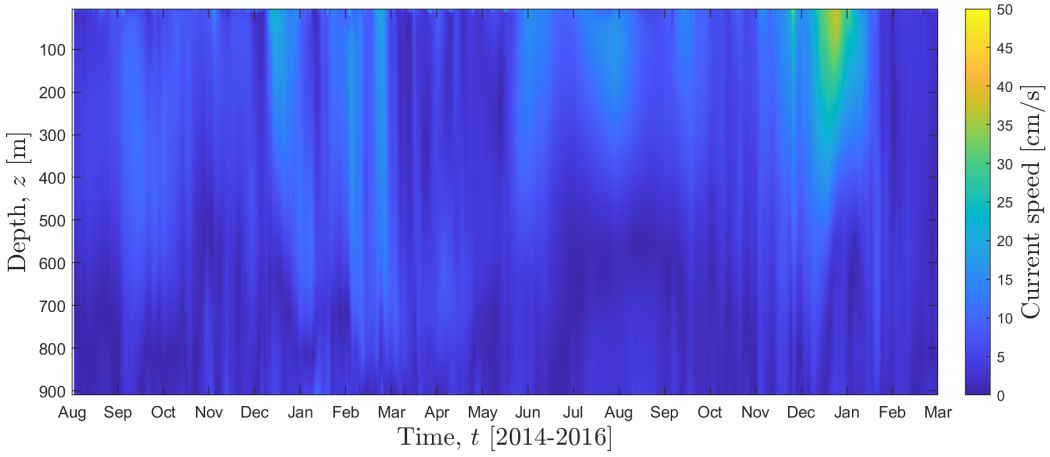

(a)

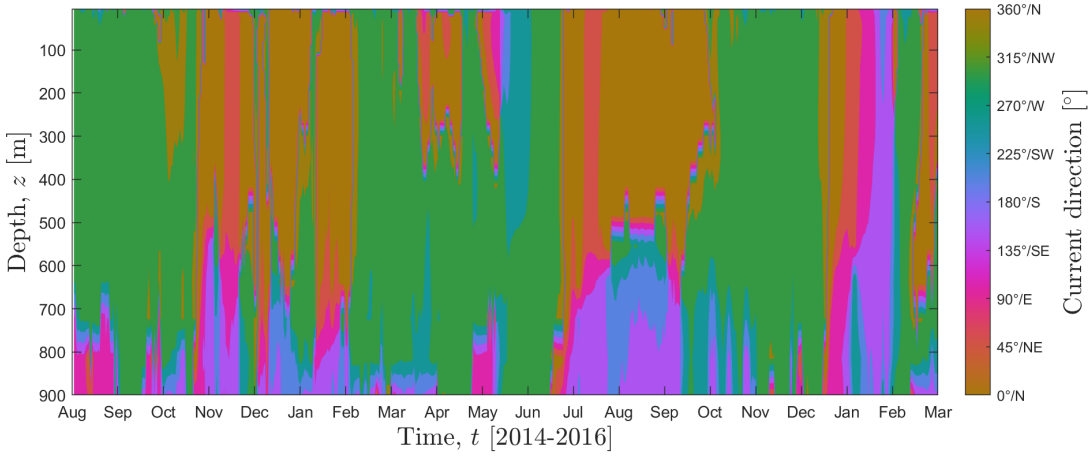

(b)

Figure 4.6: Time-series of the current speed (a) and direction (b) as described by the GECCO ocean model at the UI5 location.

Figure 4.6 shows the current speed (a) and current direction (b) from the GECCO ocean model at the mooring position of UI5. It is interesting to note that it is stronger currents in this case than what was shown in Figure 4.4. Especially in the period of late December 2015, it is current speeds up to 50 cm/s. It is also interesting to note that the current is pretty deep in the water column and not only towards the surface. Figure 4.6 (b) shows that the directions of the strongest currents are towards the North, Northwest, or Northeast. Consequently, this makes more sense based on what is expected in this part of the Fram Strait, sine the mooring is located in the West Spitsbergen Current.

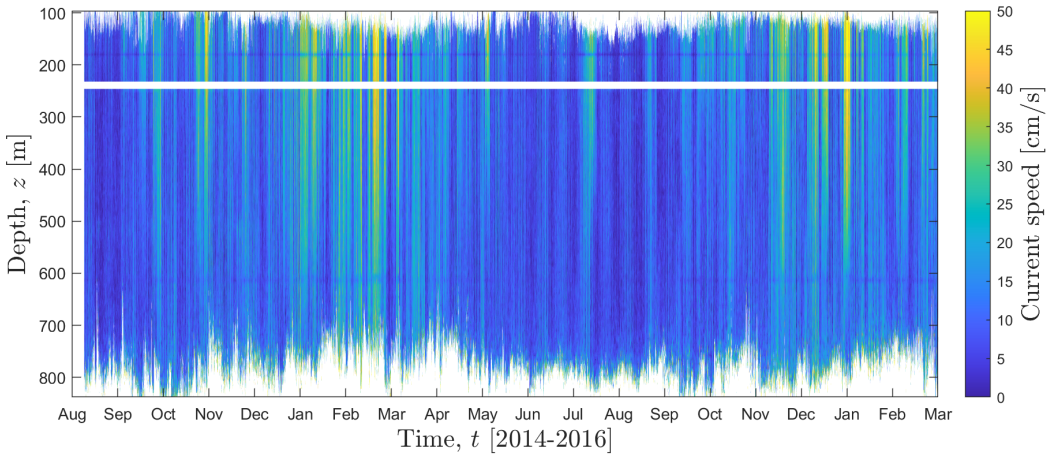

(a)

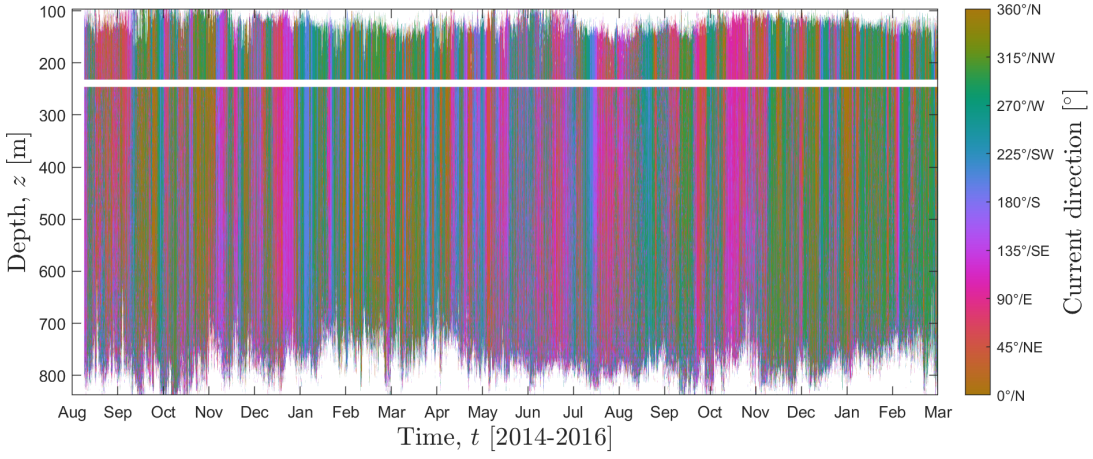

(b)

Figure 4.7: Time-series of the current speed (a) and direction (b) as measured by the downward- and upward-looking ADCPs on UI5.

Figure 4.7 shows the current speed (a) and direction (b) as measured by the two ADCPs attached to the mooring. Both ADCPs were attached to a floatation sphere with one short-range sentinel ADCP and one long-range ADCP. It was deployed at a depth of 237 m with the short-range looking upwards and measuring currents from 232 m to 96 m every 4 m, with a

sample rate of 3600 s. The long-ranger ADCP looked downwards and measured from 246 m to 838 m every 8 m, with a sample rate of 7200 s. Hence, the short-range ADCP conducted measurements more frequently but at fewer depths. The white line in the middle indicates the area of the ADCPs in the sphere. It is interesting to note that the observed current speed is higher than the GECCO current speed. It also follows the pattern from the GECCO model, with strong currents throughout the water column. It is even more visible with the ADCP. It also has many periods with powerful water flow not detected in the GECCO ocean model. During these events, the direction is usually towards the North/Northwest.

4.2.2 Observed Mooring Motion

This section covers the observed mooring motion on the two moorings, UI4 and UI5. At first, there are figures which show the dX, dY, and dZ displacement in a time series. The motion is based on data from the transponder network deployed around the moorings. The data used is from the communication between the transponders and the DSTAR. All the transponders have a unique frequency that the DSTAR records. This can be used to triangulate the position of the DSTAR in both x-, y-, and z-direction based on the travel time of the signals. This was done as part of data processing after the experiment, not in the present work.

Interestingly, the positive value in the x-displacement plot is the movement towards the North. Furthermore, in the y-displacement plot, the positive direction shows the motion towards the east. In February and March 2015, a good example is shown when strong currents towards the northwest occurred. Consequently, the mooring motion in the horizontal xy-plane is about 400 m towards the West and 400 m towards the North. The DSTAR also drops to its maximum depth of 784 m which is 184 m below the nominal depth.

UI4

This section investigates the observed mooring motion on the UI4 mooring. Any significant pulldowns were not expected from the current speeds measured by the ADCP on UI4, presented in Figure 4.4. The limits used on the y-axis are chosen like this, intending to be able to compare the mooring motion directly between UI4 and UI5.

Figure 4.8 shows the observed mooring motion both vertically and horizontally. The displacement in the x-direction shown in Figure 4.8 (a) indications that there are no significant currents in this direction during the measurement period. In the y-direction, as shown in Figure 4.8 (b), there is a little more movement, but on a mooring that is about 1300 m long, a horizontal movement of 100 m is not that much. Figure 4.8 (c) shows almost no pulldowns

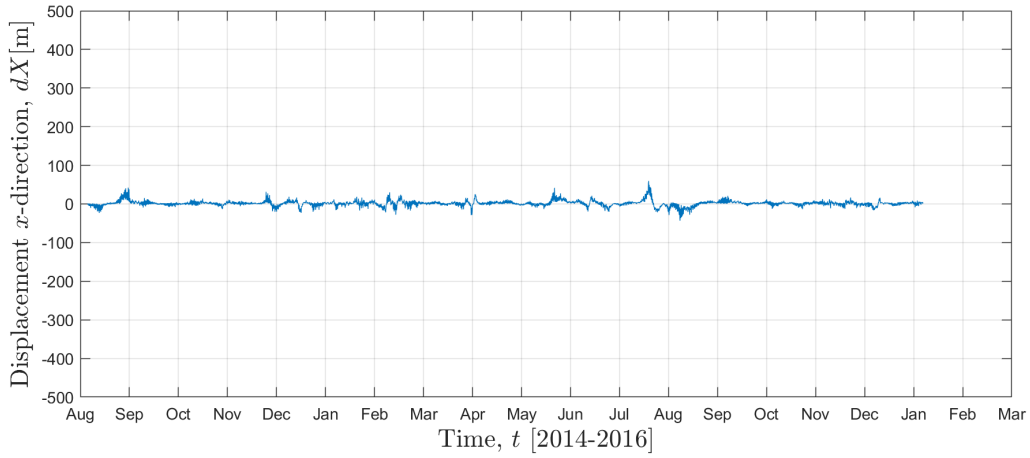

(a)

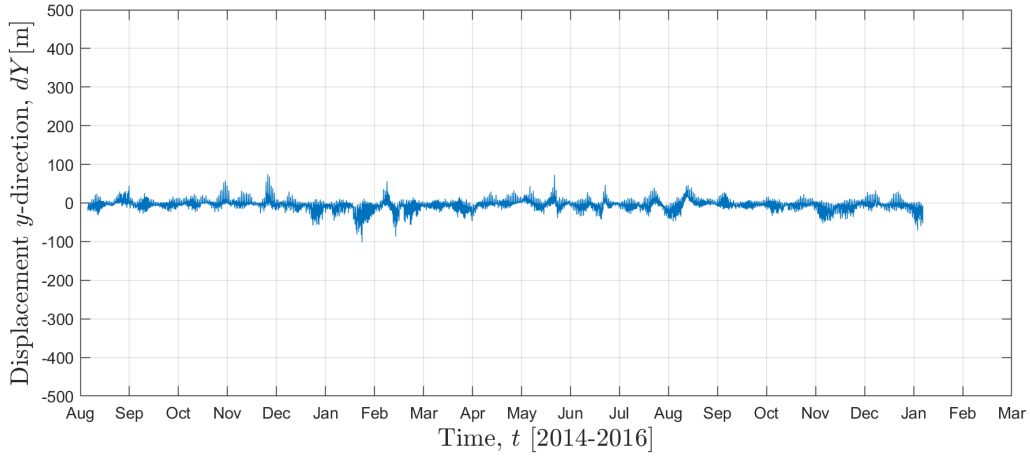

(b)

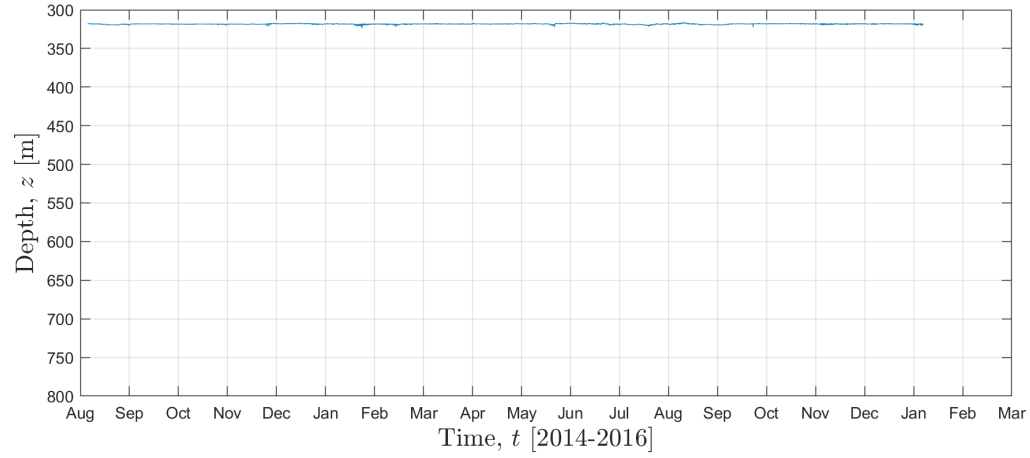

(c)

Figure 4.8: Observed mooring motion during the measurement period in the x-direction (a), y-direction (b), and z-direction (c) on UI4, as recorded by the DSTAR.

and movement in the z-direction. It is remarkable how stable it has been during the period, with a maximum pulldown of 8 m.

UI5

Figure 4.9 shows the mooring motion for UI5 both vertically and horizontally. It is much more movement in this mooring than observed in UI4. There are several reasons behind this, and one is probably because the water flow is generally stronger in this area. Another important aspect is the configuration of the mooring. As mentioned before, this mooring is equipped with a large acoustic source. This instrument adds a lot of payload and drag to the mooring, which definitely will affect the motion. Even though the ADCPs in the sphere contribute with buoyancy, it still seems insufficient to keep it from large knockdowns. In Figure 4.9 (c) the displacement in the z-direction is shown. It makes sense that the largest motion comes when there are strong currents.

Figure 4.9 (a) and (b) show the motion horizontally, movement up to 500 m from the origin is pretty much, and it could affect the measurements. This experiment makes it possible to correct the results according to these depth and location changes. In many oceanographic experiments, the only motion information is from pressure data from the instruments. Pulldowns like in Figure 4.9 (c) could be critical for certain instruments and hardware components. Many have depth/pressure ratings and can implode if they dive too deep. That could ruin the whole mooring, and all the data and instruments could get lost if, e.g., the top float fails.

4.2.3 Simulated Mooring Motion Using GECCO Ocean Model Data

This section covers the simulation of the mooring motion on UI4 and UI5. Firstly the simulation is conducted by importing data from the GECCO ocean model into the MD&D software. In MD&D the moorings have been modeled with all components included.

UI4

This section presents the simulated mooring motion on UI4 with environmental input from the GECCO ocean model.

Figure 4.10 shows the simulated mooring motion based on the simulation from MD&Dwith GECCO currents as input. The blue line under indicates the observed mooring motion. It shows barely any motion in either dX, dY, or dZ, which is not expected based on the observed motion. The stable mooring in the simulation could be explained by looking Fig-

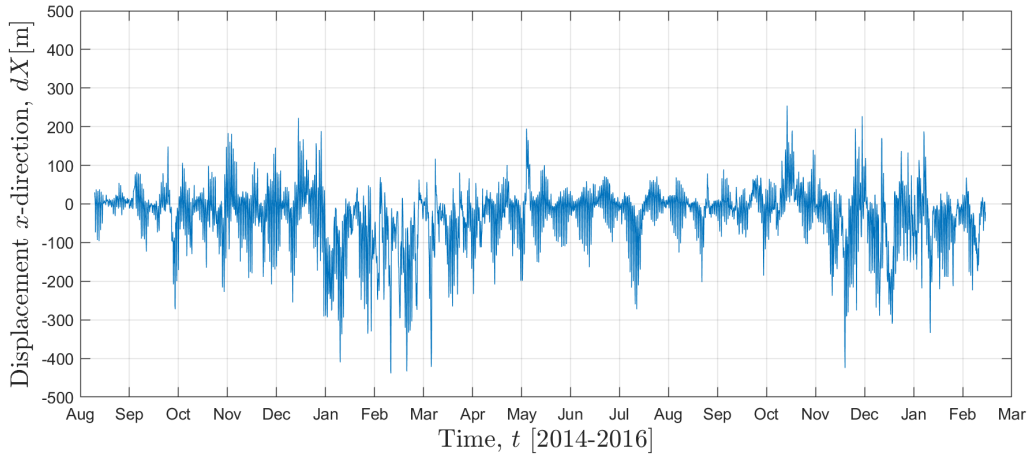

(a)

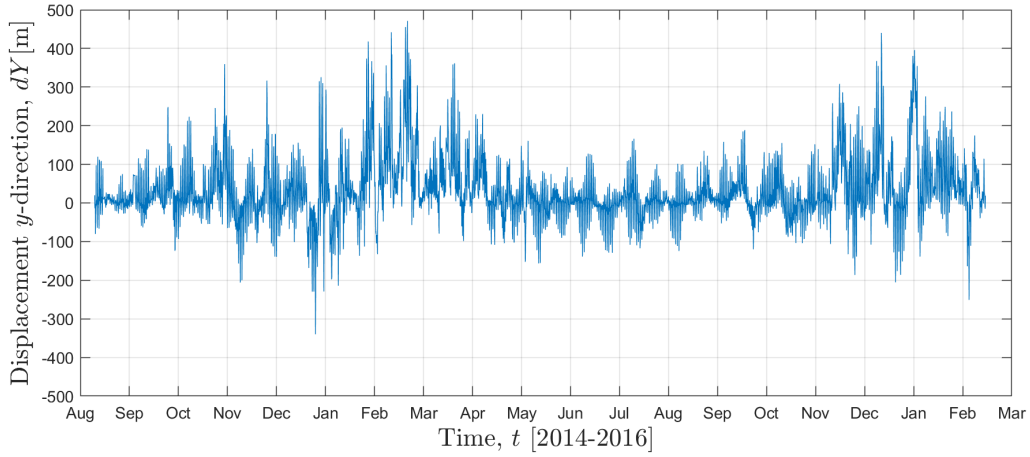

(b)

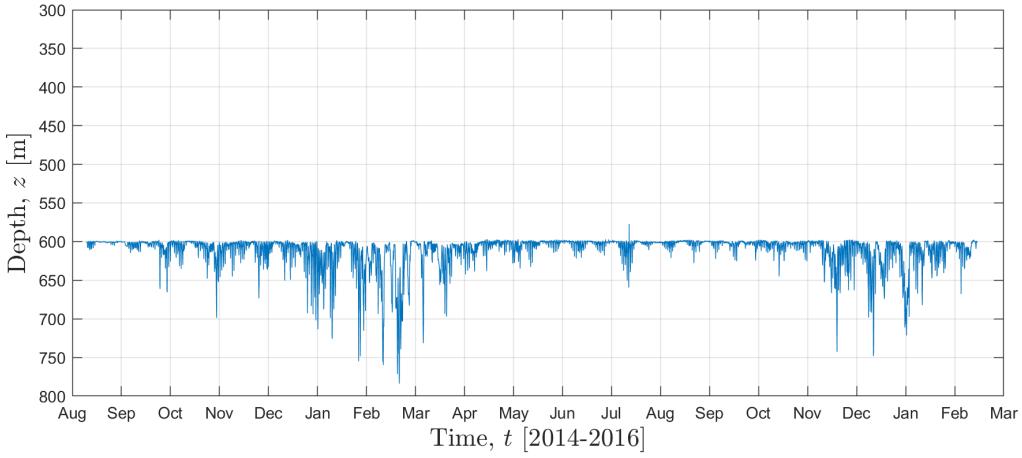

(c)

Figure 4.9: Observed mooring motion during the measurement period in the x-direction (a), y-direction (b), and z-direction (c) on UI5, as recorded by the DSTAR.

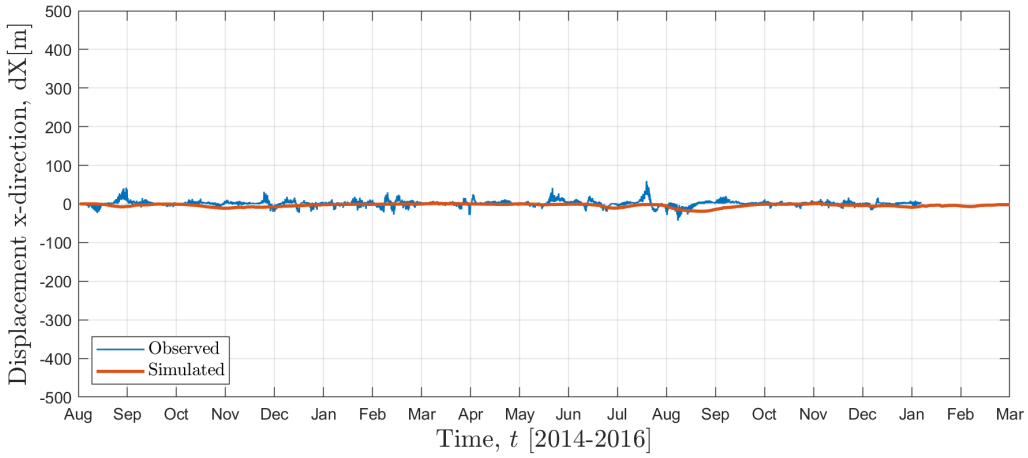

(a)

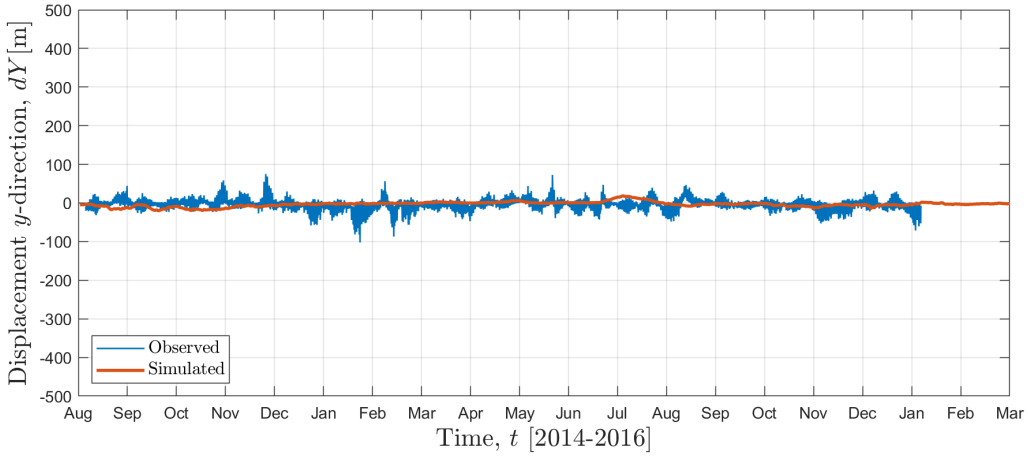

(b)

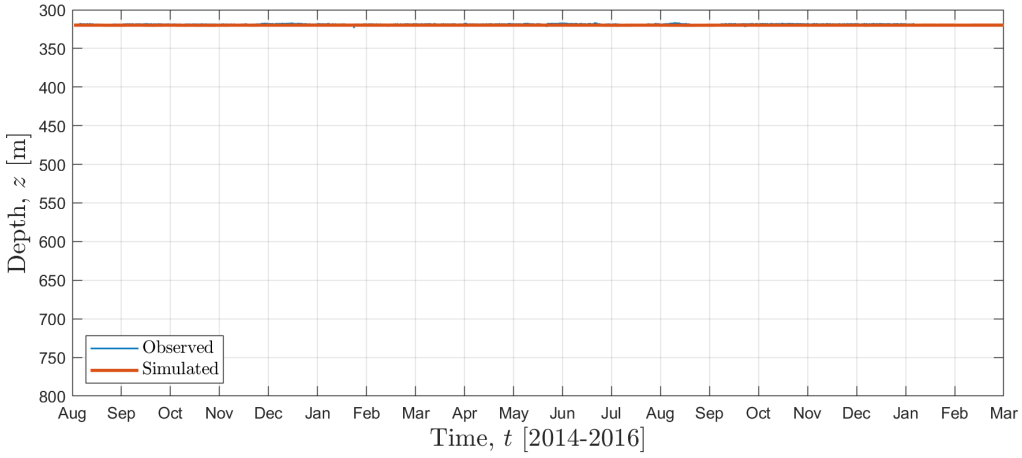

(c)

Figure 4.10: Simulated mooring motion of UI4 during the measurement period, with ocean currents from the GECCO ocean model as input.

ure 4.4 where the current given by the GECCO model was weaker than the measured ADCP current in Figure 4.5. However, it could also be due to uncertainties regarding how MD&D and how it runs. There are many components and also simplifications in the software. Consequently, getting it exactly right would be difficult, but to some degree, a similar motion pattern from the simulation is necessary to use this approach when predicting mooring motion.

UI5

This section presents the simulated mooring motion on UI4 with environmental input from the GECCO ocean model.

Figure 4.11 shows the simulated mooring motion on UI5 using input from the GECCO ocean model. This simulation has some motion in all directions. However, it is still insufficient relative to the observed motion in the experiment, as illustrated in the figure. Interestingly, the simulation seems to underpredict the motion in both cases. This could be critical if the observed pulldowns are about 150 m more than the simulated ones. Many instruments have depth-rating and can implode or get destroyed if they get pulled down too much. Also, in Figure 4.6 the currents from the GECCO ocean model are generally much lower than in the observed currents from the ADCPs from Figure 4.7.

4.2.4 Simulated Mooring Motion Using ADCP Data

This section presents the simulated mooring motion on UI4 and UI5 with new environmental input, which is more representative than the GECCO ocean model. Since the results from the simulations using GECCO currents as input was not satisfactory, it was decided to try and use measurements from the ADCP instead. However, the problem with using ADCP data is that many data points do not have values throughout the measurement period. As a result, it is challenging to use ADCP data directly in the software as was possible with the GECCO current. In effect, it was decided to multiply the GECCO currents by a factor of two to get the GECCO currents up to approximately the same level as measured by the ADCPs. The results from the new simulations are presented in Figure 4.12 for UI4 and Figure 4.13 for UI5.

UI4

This section covers the simulated mooring motion of UI4 with factorized currents representative of the *in situ* ADCP data.

Figure 4.12 shows the mooring motion in all directions from the simulation with modified

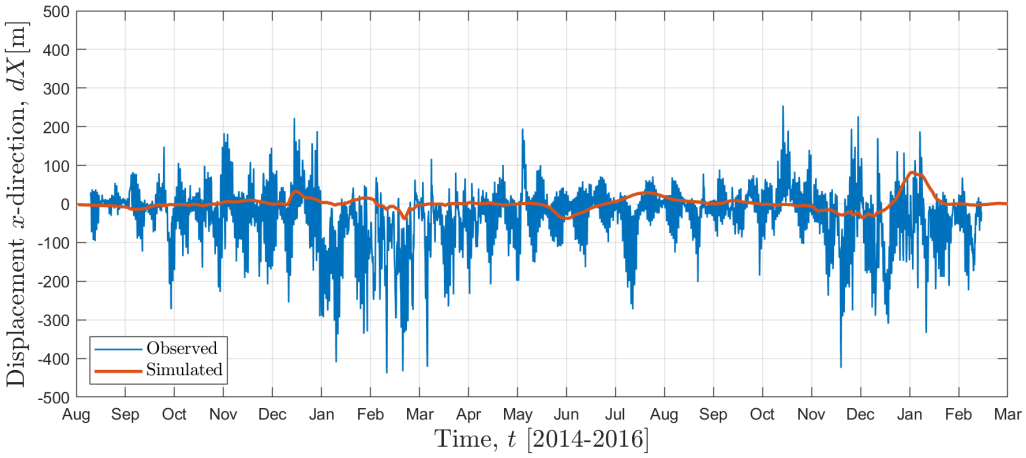

(a)

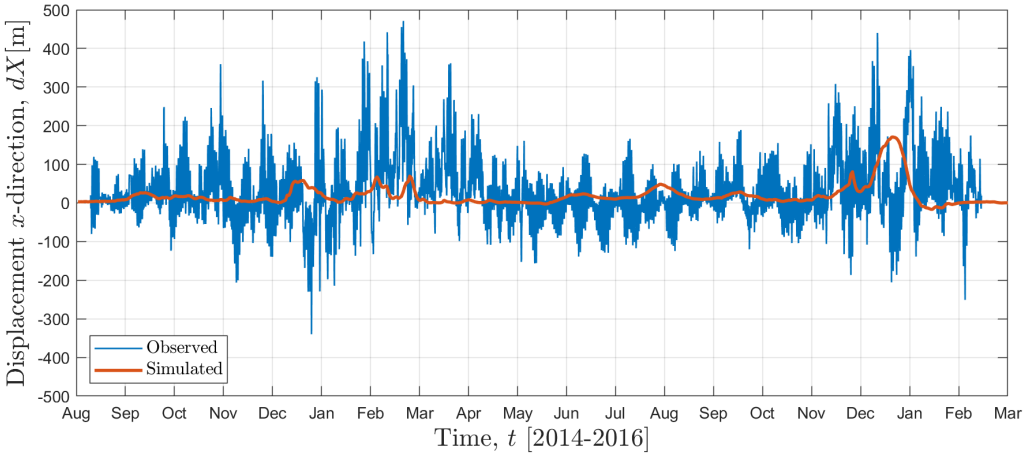

(b)

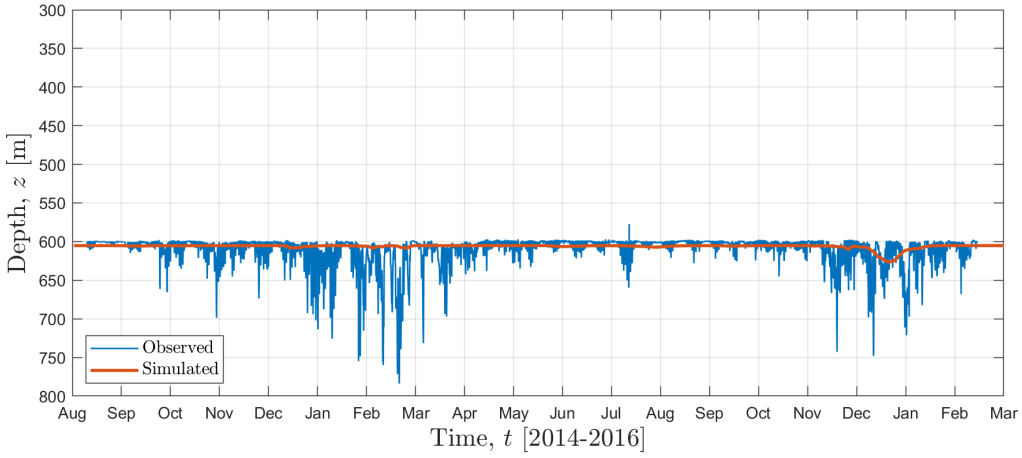

(c)

Figure 4.11: Simulated mooring motion of UI5 during the measurement period, with ocean currents from the GECCO ocean model as input.

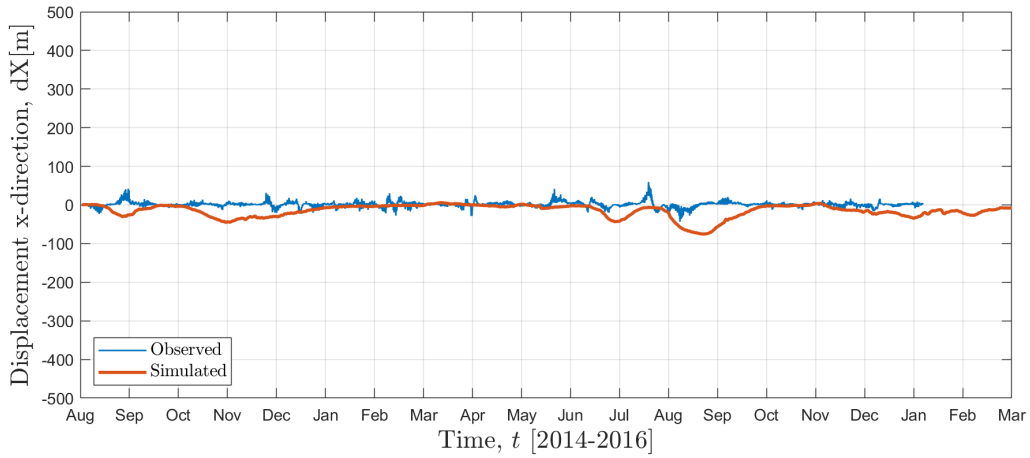

(a)

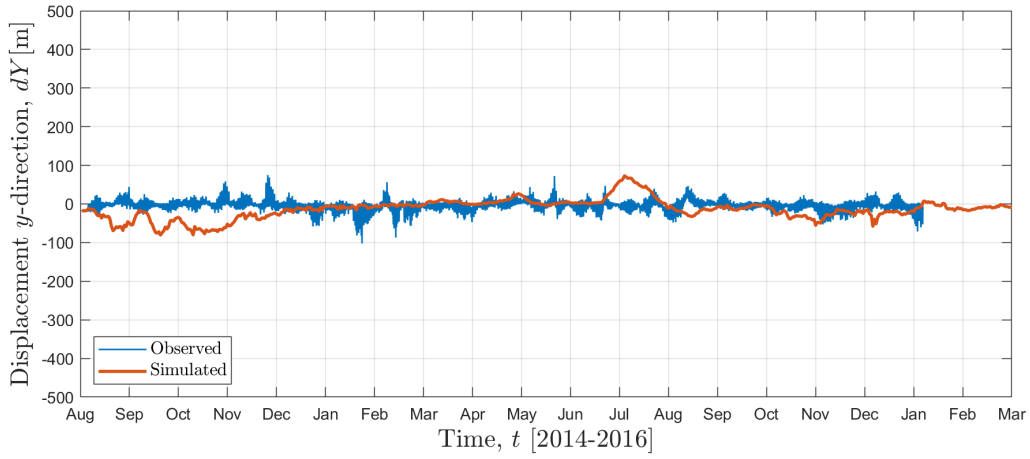

(b)

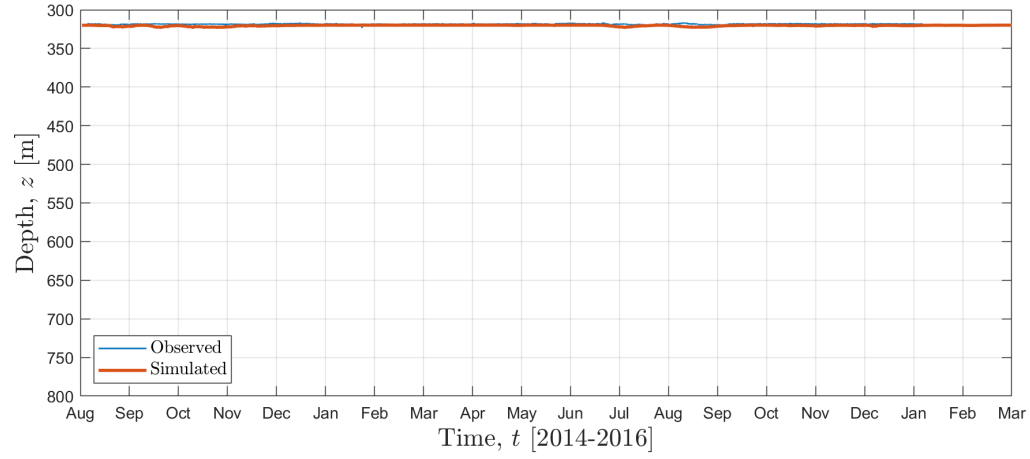

(c)

Figure 4.12: Simulated mooring motion of UI4 with modified currents from an upscaled GECCO model as input. It has been multiplied by a factor of two to represent a current more similar to the observed ADCP measurements.

GECCO currents. Interestingly, the movement in dX and dY is more like the observed motion at this point. The pulldowns in Figure 4.12 (c) is not easy to spot since the maximum dropdown was about 3 m. It is a difference of 5 m from the observed knockdown, which is considered narrow at this scale. That is why it is hard to spot the observed pulldown in this figure.

UI5

In this section, the simulation of the UI5 mooring is presented in Figure 4.13. This is also based on factor two of the GECCO currents, which is supposed to represent the ADCP current speed.

Figure 4.13 (a) and (b) shows that at certain points, it has a maximum displacement of around 400 m. Similarly, this is also spotted in the observed mooring motion in late December 2015, both in the x and y direction. The simulations are still pretty good if comparing the maximum displacement in the z direction in (c), where the pulldown is about 150 m. Hence, the simulations and observations are in a pretty good agreement during that period in December 2015. However, the observed motion hit a maximum pulldown of 184 m in February 2015, and at this point, the simulation is at only about 50 m. Although the simulations did not fully agree at all points, it is interesting that the same pattern is seen when comparing the motion. For instance in Figure 4.13 (b) the peaks of the simulations follows exactly in the shape. It is also spotted in (a) and (c), indicating that even though the GECCO model has a low current speed, the direction seems to be in good agreement.

4.2.5 Comparison Between the Observed and Simulated Mooring Motion

In the comparison between the simulated and observed mooring motion, some things need to be addressed. First, it was interesting to see the difference between the observed mooring motion on UI4 and UI5. It was expected that there would be differences between the moorings. This is because UI5 was deployed in an area with stronger currents and had large instruments like the acoustic source and the ADCPs in a sphere.

In theory, the same behavior would be expected in the simulation. However, when looking at the simulations conducted using currents from the GECCO model, the results had the same form, with little movement on UI4 and a bit more movement on UI5. Still, the displacement was significantly lower than observed in the experiment. As explained before, this could be critical when predicting mooring motion. As a result, it was necessary to try and do new simulations to investigate if this had something to do with the current differences spotted between GECCO and the ADCPs.

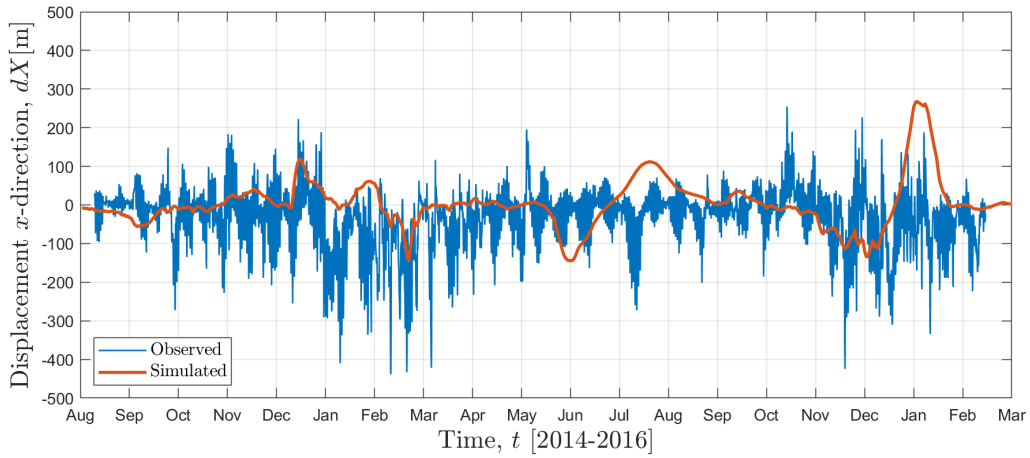

(a)

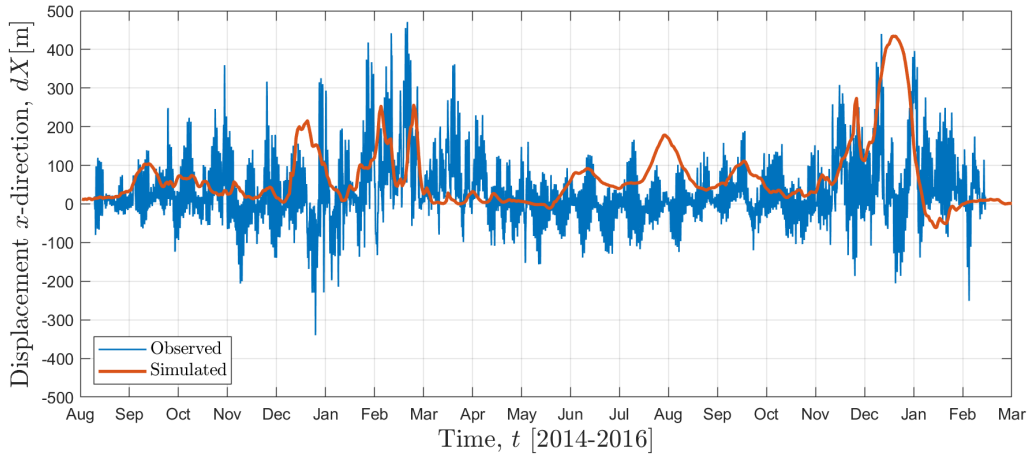

(b)

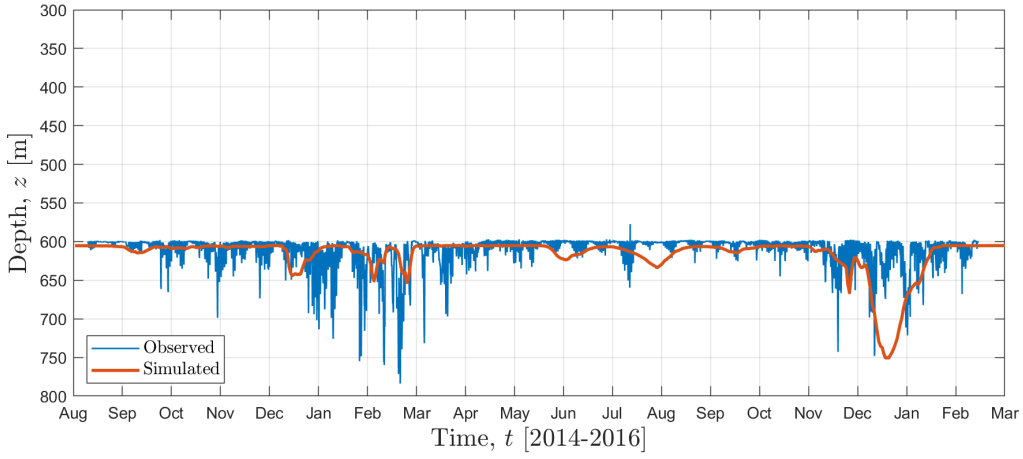

(c)

Figure 4.13: Simulated mooring motion of UI5 with modified currents from an upscaled GECCO model as input. It has been multiplied by a factor of two to represent a current more similar to the observed ADCP measurements.

Consequently, when simulating with more representative currents by factorizing the GECCO currents by two, the simulation results started to look more like what was observed. Moreover, especially on UI5, the motion was in good agreement in some periods. Hence, using GECCO with a factor gave better results, but it would have been interesting to try it with ADCPs covering the whole water column.

Chapter 5

Field Experiment in Stokksundet

This chapter describes the field experiment conducted in Stokksundet in the spring of 2022. The experiment involved the deployment of an observation mooring close to an aquaculture facility. It describes the process, from planning and preparations to mooring recovery.

5.1 Planning and Preparations

This section covers the preparation before deploying the mooring. The goal is to find a suitable location for the observation mooring and to help in mooring design and instrument configuration.

5.1.1 Layout of the Fish Farm

Figure 5.1 shows a map of the aquaculture facility in Stokksundet, located between Bømlo and Stord at the approximate position of N 59.78, E 5.33. The figure also gives an overview of the facility's components and the distances in the fjord. The fish farm consists of 9 circular fish cages with a diameter of 51 m organized in a 5x2 layout. However, the frame position of cage number six remains empty. The cages are surrounded by 18 buoys, which are moored to the seafloor with a series of anchors and chains. Only the anchors attached to the southern and eastern buoys are displayed on the map. In addition, the nets utilized in the cages are 38 m deep. Figure 5.1 also shows the EMBILINK sensors that measure oxygen, salinity, and temperatures at 5 m in fish cage number 9.

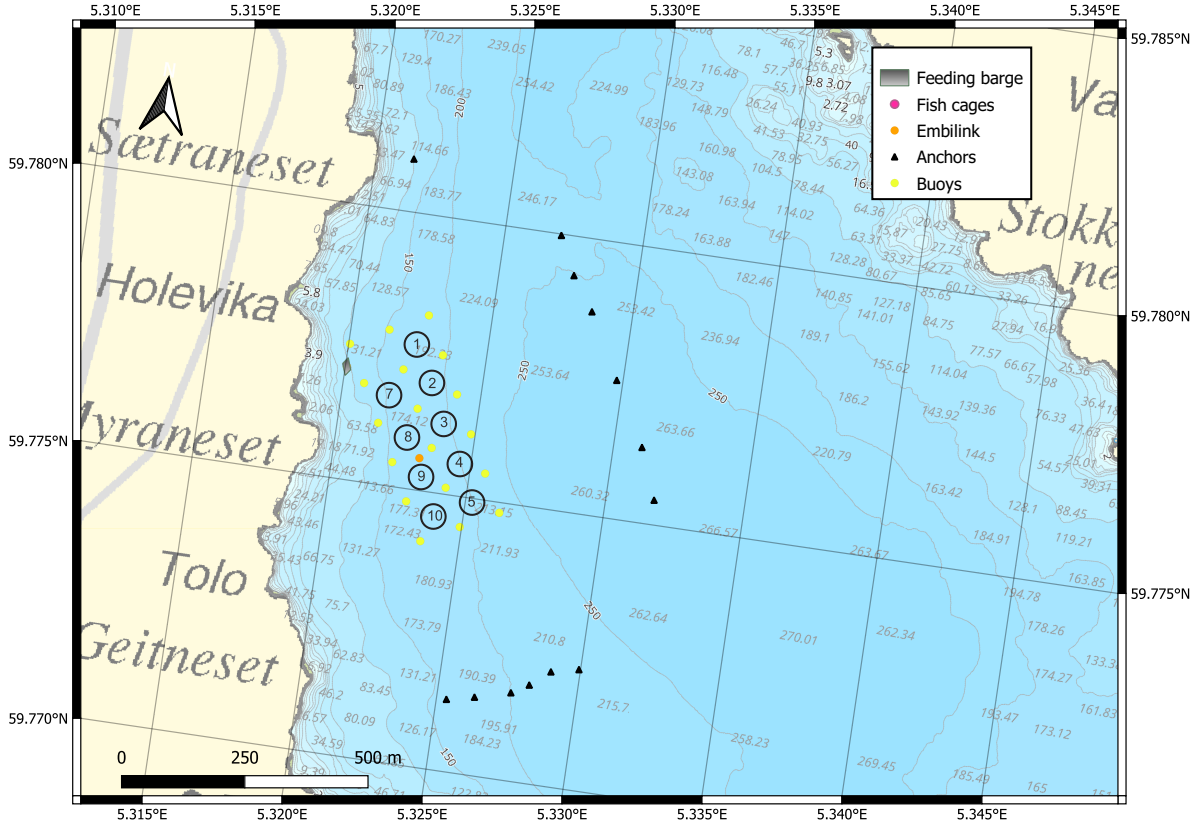

Figure 5.1: Map of the aquaculture facilities in Stokksundet. The orange dot represents the Embilink system that provides real-time data from inside fish cage number 9.

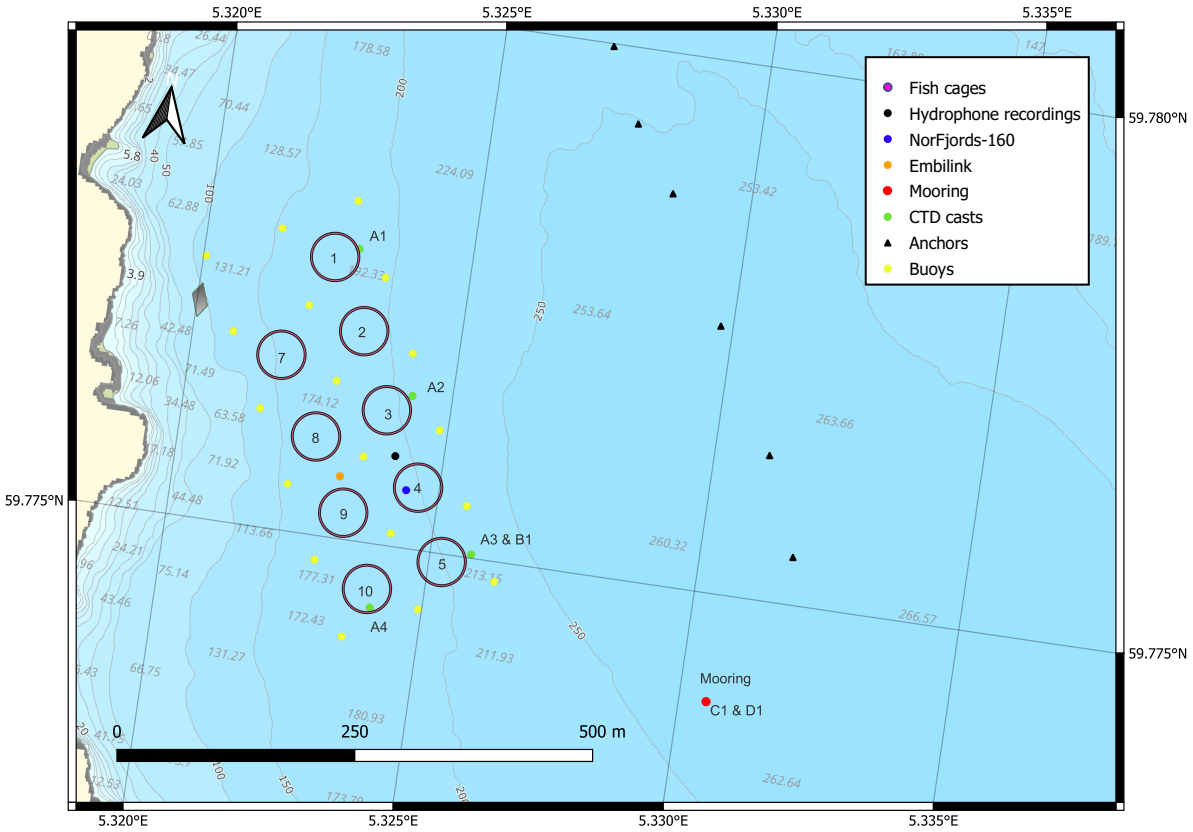

Figure 5.2: Map of the important locations that are involved in the field experiment.

5.1.2 Oceanographic Measurements

A Conductivity, Temperature, Depth sensor (CTD) was utilized to investigate the oceanographic conditions in the area to help determine a suitable location for the mooring and find optimal instrument depths. A SAIV SD204 CTD profiler [21] was used to measure temperature T and conductivity σ as a function of pressure p at a rate of 1 Hz. The CTD was lowered down manually in the water column from a ship while being moored to the fish cage on the starboard side. This method was carried out to obtain stable measurements in one location. In addition, the CTD was lowered on the port side to avoid conflict with the net and facility moorings. The descent rate was about 0.5 $\mathrm{m\,s^{-1}}$, resulting in a pressure resolution of 0.5 dbar (approximately 0.5 m resolution in depth). The processing software for the CTD, `MINISOFT SD200W` [21], was used to download the data and export it to text files. Accordingly, it is possible to compute the depth z, salinity S, and sound speed c according to the UNESCO formulas [22].

Eight CTD casts were conducted on different locations around the fish farm to examine the water layer variability around the fish farm. Table 5.1 shows the times and locations of the different CTD casts. Even though the depth was over 150 m, it was decided not to take the CTD deeper. This was to avoid the CTD hitting the seafloor due to uncertainties in the

ship's echo sounder. In addition, the upper water column was more interesting regarding the placement of the instruments.

Table 5.1: Times and positions of the CTD casts that were conducted in Stokksundet on four different days. The locations of these casts are shown on the map in Figure 5.2.

Cast ID	Start time (UTC)	Latitude	Longitude
A1	2021-11-28T09:55:00Z	59.7777 °N	5.3229 °E
A2	2021-11-28T10:34:00Z	59.7764 °N	5.3243 °E
A3	2021-11-28T11:09:00Z	59.7750 °N	5.3258 °E
A4	2021-11-28T11:32:00Z	59.7744 °N	5.3240 °E
B1	2022-02-12T12:33:00Z	59.7750 °N	5.3258 °E
C1	2022-03-17T16:14:00Z	59.7739 °N	5.3305 °E
D1	2022-03-18T12:27:00Z	59.7739 °N	5.3305 °E
E1	2022-04-28T17:40:00Z	59.7739 °N	5.3305 °E

Figure 5.3 shows the data obtained from the upcasts and downcasts from the CTD taken on 2021-11-28 around the aquaculture facilities. A 4° temperature span is seen in (a). The minimum temperature of 8 °C occurs at the surface and then again at around 150 m. Two distinct layers are seen in the uppermost 7 m, and from 12 m-20 m. Similar layering is seen in the salinity (b). Most freshwater is at the surface, and the salinity increases gradually with depth. The difference is that the temperature decreases again at 30 m, while the salinity continues to increase. The sound speed is shown in (c), which is a function of temperature, salinity, and depth has the same layering close to the surface and is slowly decreasing below 30 m like the temperature. The figure also shows that the spatial variation around the facility is small. The four casts have all similar curves. They indicate that the layers follow the same pattern, even though the fish farms might affect the results.

In order to investigate the seasonable variability, another CTD cast was conducted in February 2022. It is of interest to see if the layers are similar or have changed from the late fall season to the winter season. Furthermore, two casts were conducted in connection with deployment and redeployment on 2022-03-17, C1, and 2022-03-18, D1. That means another season to compare the layers with, the early spring season. These casts can also be compared to the measurements conducted on the instruments on the observation mooring. That could help investigate whether all the sensors are in agreement or if there are suspicions that some sensors are incorrect.

Additionally, casts were conducted in connection with the recovery operation on 2022-04-28, E1. Consequently, it is possible to compare with the sensors on the observation mooring again and investigate if the measurements still agree. Due to this, it could be possible to spot

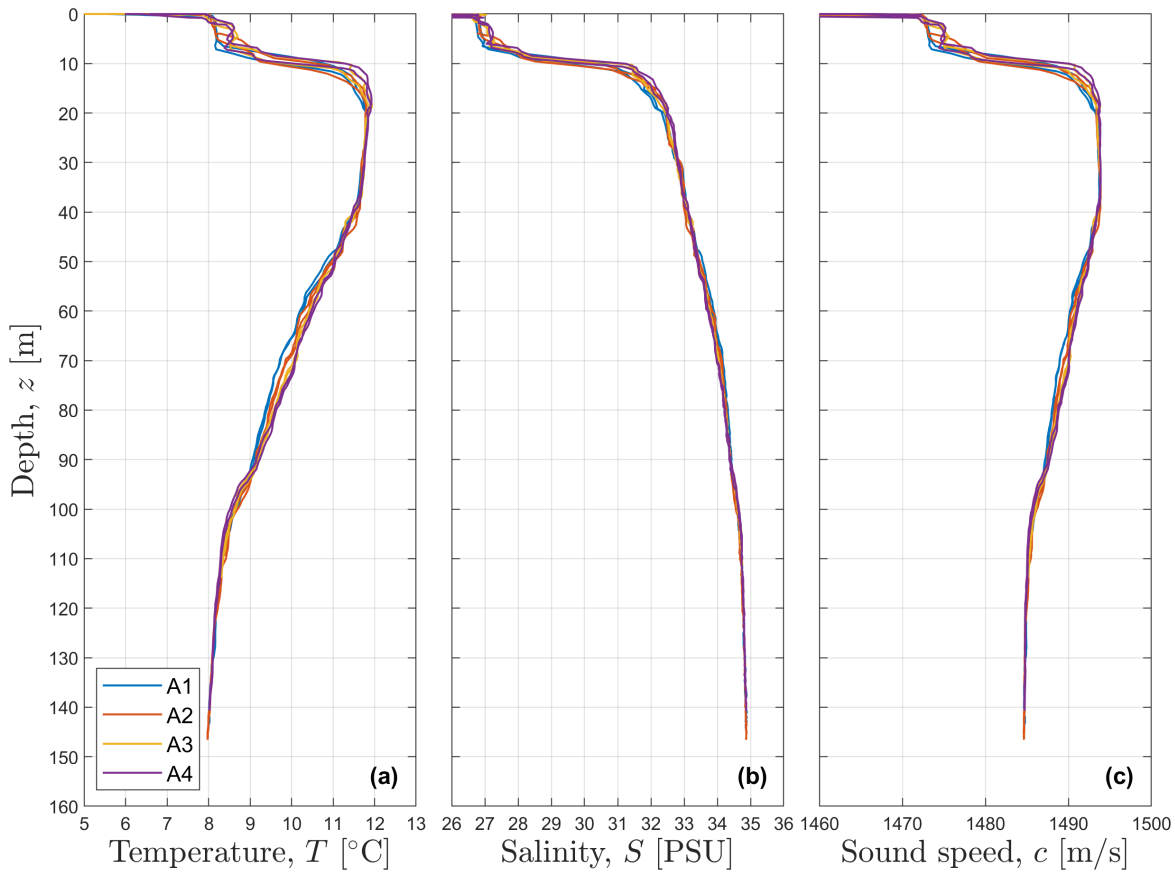

Figure 5.3: The CTD up- and downcasts from the measurements conducted in Stokksundet on 2021-11-28 around the aquaculture facilities. Temperature (a), salinity (b), and sound speed (c) are shown as a function of depth.

if, e.g., the conductivity sensors have been affected by biofouling.

Figure 5.4 shows the data obtained from the up- and downcasts from the different days. A3 and B1 were conducted on the eastern side of cage number five, and C1 and D1 at the mooring location, as shown in Figure 5.1. These two locations are about 250 m apart from each other. In (a), the B1 cast has a similar shape as the A3 cast also present in Figure 5.3. The difference is that the temperature variation is less, but there are still two distinct layers in the uppermost 7 m, and from 7 m-13 m. A3 and B1 also have a layer between 16 m-20 m that follows the same shape. Similar layering is seen in the salinity in (b). Most freshwater is at the surface, and then salinity gradually increases with depth until it seems to stabilize at depths below 140 m.

The C1 and D1 casts did not share the same shape as the earlier measurements. It seems that they do not have as distinct layers. In the C1 and D1 casts, the temperature (a), salinity (b), and sound speed (c) increase slowly with depth. Similarly, in the E1 cast conducted right after recovery, the salinity profile in (b) has the same shape as in B1, C1, and D1. However, something has changed when studying the temperature in (a) and sound speed in (c). It seems that the air temperature has started to warm up the upper layer. Hence the temperature decreases about 1.5 degrees from the surface and down to 25 m. Further, it steadily shrinks down in the water column. The sound speed follows the same pattern as the temperature.

5.1.3 Soundscape Measurements

This section is about conducting measurements of the soundscape near the aquaculture facility. The soundscape consists of ships, sounds of operations at the facility, marine mammals, etc. To optimize the quality of the recordings, e.g., choose the appropriate gain to reduce the risk of saturation.

A μAURAL (micro - Autonomous Underwater Recorder for Acoustic Listening) was deployed to measure sound in Stokksundet from 2022-02-12T07:01:00Z to 2022-02-12T16:42:00Z. The recorder was configured to measure at the maximum sampling frequency of the hydrophone, 96 kHz. The μAural is equipped with an HTI-96-MIN hydrophone with a sensitivity of -163.7 dB re 1 μPa. It has a vertical resolution of 24 bit and a peak voltage of 2.5 V in the Analog to Digital Converter (ADC). The voltage gain in the pre-amplifier is 18 dB (but can be manually adjusted to either 9 dB, 12 dB or 15 dB), and the frequency response of the hydrophone is flat from 2 Hz to 30 kHz. The data is stored as wav audio files on a 64 GB SD-card.

Furthermore, during the hydrophone recordings, there was an ongoing flushing operation at the facility. This happened in four different cages, from number two to five. The μAURAL was

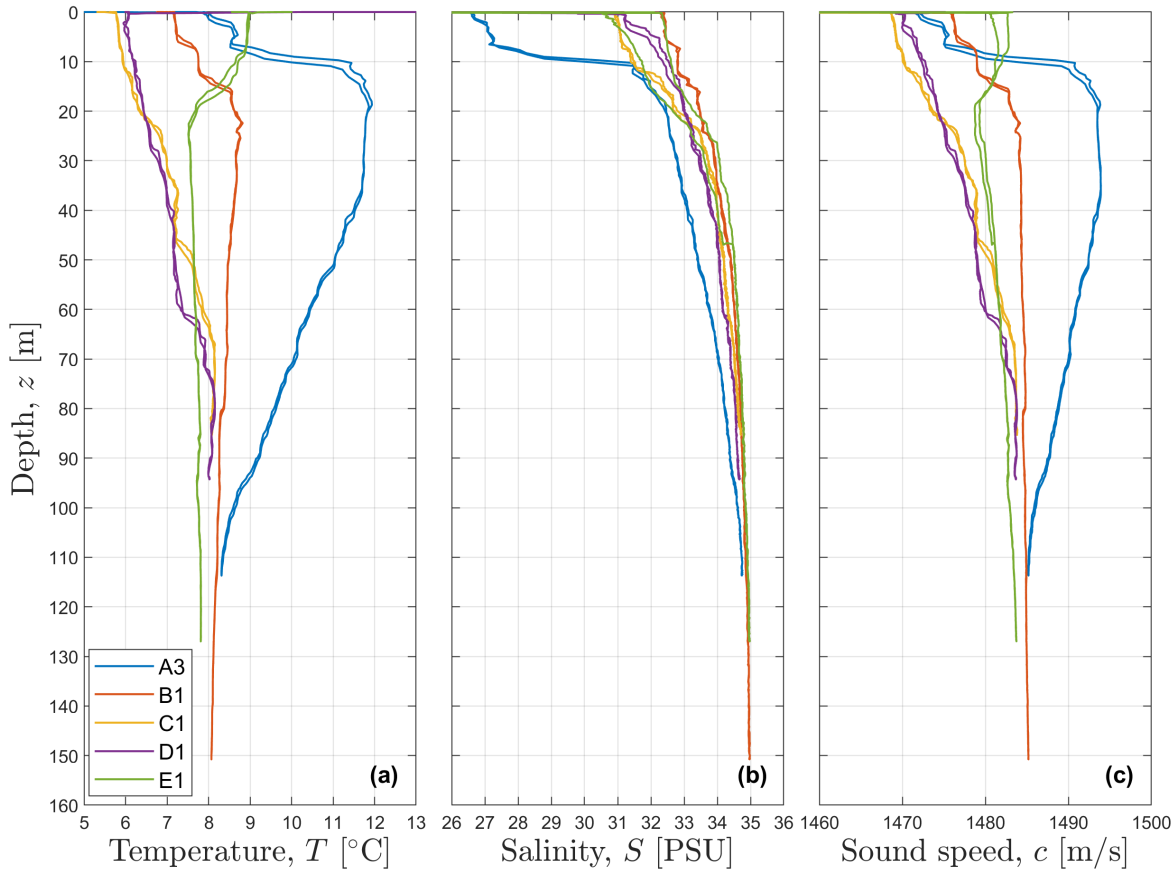

Figure 5.4: The CTD up- and downcasts conducted in Stokksundet on five different days as described in 5.1. The measurements were conducted on the southeast side of the aquaculture facilities. Temperature (a), salinity (b), and sound speed (c) are shown as a function of depth.

placed midway between cages three and four, at a depth of 25 m with a maximum distance of 160 m to the north end of cage number two. The operation time in each cage is approximately two hours and 20 minutes, followed by about 20 minutes of transit and preparation before starting again on another cage. In addition, to help identify the different sounds on the recording, a detailed event log from the day was conducted.

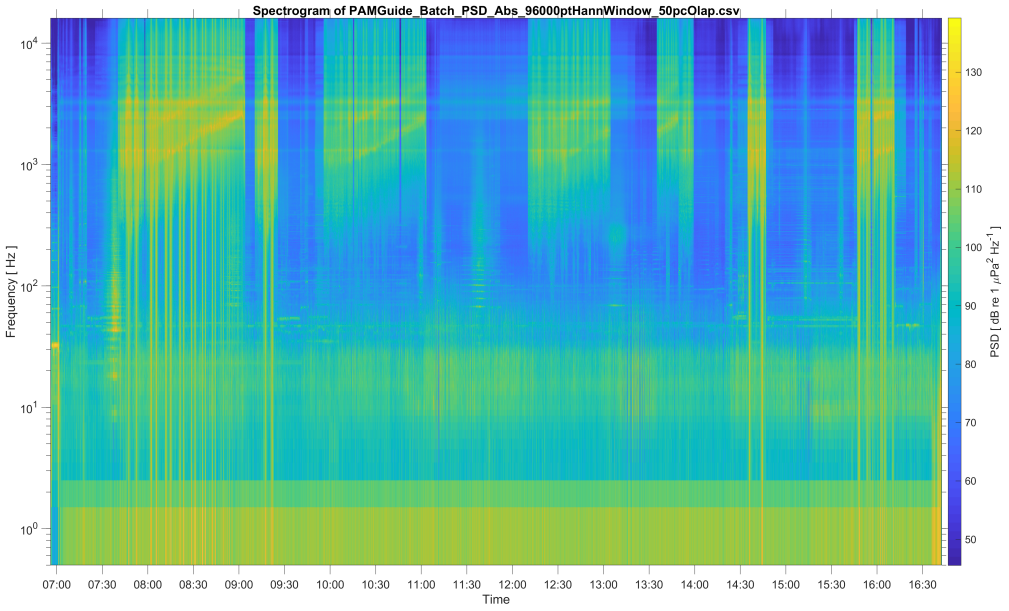

Figure 5.5: Spectrogram of the recording made by the μAURAL on the 12th of February 2022.

Figure 5.5 shows the spectrogram of the soundscape from the 12th of February. From this, it was possible to detect when the different flushing operations occurred. Furthermore, when comparing it to AIS data and the event log, it was possible to identify ships passing by in the fjord. Unfortunately, from the recordings, it was discovered that the μAURAL went into saturation at certain times. However, this only occurred when the flushing was as close as between 15 m and 75 m. Since the mooring is further away from the facilities, the voltage gain of 18 dB in the pre-amplifier should be fine.

5.1.4 Bathymetry

To be able to determine the water depth in and around the mooring location, depth information provided by the Norweigan Mapping Authority (NMA) was investigated. The data was collected through the Geonorge map catalog [23]. Unfortunately, the resolution of the depth data is limited to a grid of 50 m x 50 m since bottom data with a higher resolution is graded following the Safety Act [24]. It was controlled with various sea maps to investigate whether the depth data was consistent with the maps. Also, some control measurements were con-

ducted using the boat's echo sounder to validate that the depth was in agreement with the maps.

After review, the depth was relatively stable at around 262 m in the area of the planned deployment. This information was essential to get the instruments to the desired depth. In addition, it is easier to deploy the mooring at the preferred depth when the bathymetry is flat in the area, even though there are some more uncertainties to consider, like not knowing how deep the muddy bottom is. The tide must also be taken into account. The tidal variation is 62 cm between the average high and low tide in this region [25].

5.1.5 AIS Data

Stokksundet is an important shipping lane, with regular traffic day and night. Therefore, Automatic Identification System (AIS)-data from the area must be considered to lower the risk that the mooring conflicts with shipping. The AIS data is provided by the NMA and has a limit as it only shows ships larger than 45 m [26]. This means that many ships in the aquaculture industry and recreational vessels are not present in the dataset since they are often less than 45 m. Even though that is a limitation in the dataset, the data still indicates the traffic in the area. So firstly, the ship traffic through Stokksundet was investigated by looking at AIS data from May to September 2021 to get an impression of general traffic throughout the year. This is presented in Figure 5.6 (a) and shows that the regular traffic seems to follow the shipping lane.

Figure 5.6 (a) is from when the aquaculture facilities were fallowing [27]. Fallowing is about pausing the production of salmon for at least three months to neutralize the risk of spreading salmon diseases to new generations of salmon in the same production area.

Furthermore, shipping from September 2021 to March 2022 was evaluated to get a more specific overview of ships that regularly travel to and from the fish farms. These vessels were more relevant in this timespan since the salmon was delivered to the fish cages in September 2021. Figure 5.6 (b) shows the ship traffic in this period.

It was also essential to ensure that deployment happened outside the official safe water channel defined by the NMA. Based on the data shown in Figure 5.6 (a), most traffic is happening on the eastern side of the strait. The only boats operating in the mooring location are boats involved in the operation at the aquaculture facilities. Information about the mooring position should be provided to the NMA and boats involved in operating the facilities to ensure safety. As a result of the bathymetry survey, the AIS data evaluation, and considering the anchors mounted to the aquaculture facility, a suitable mooring location was detected. The mooring location is presented in Figure 5.2.

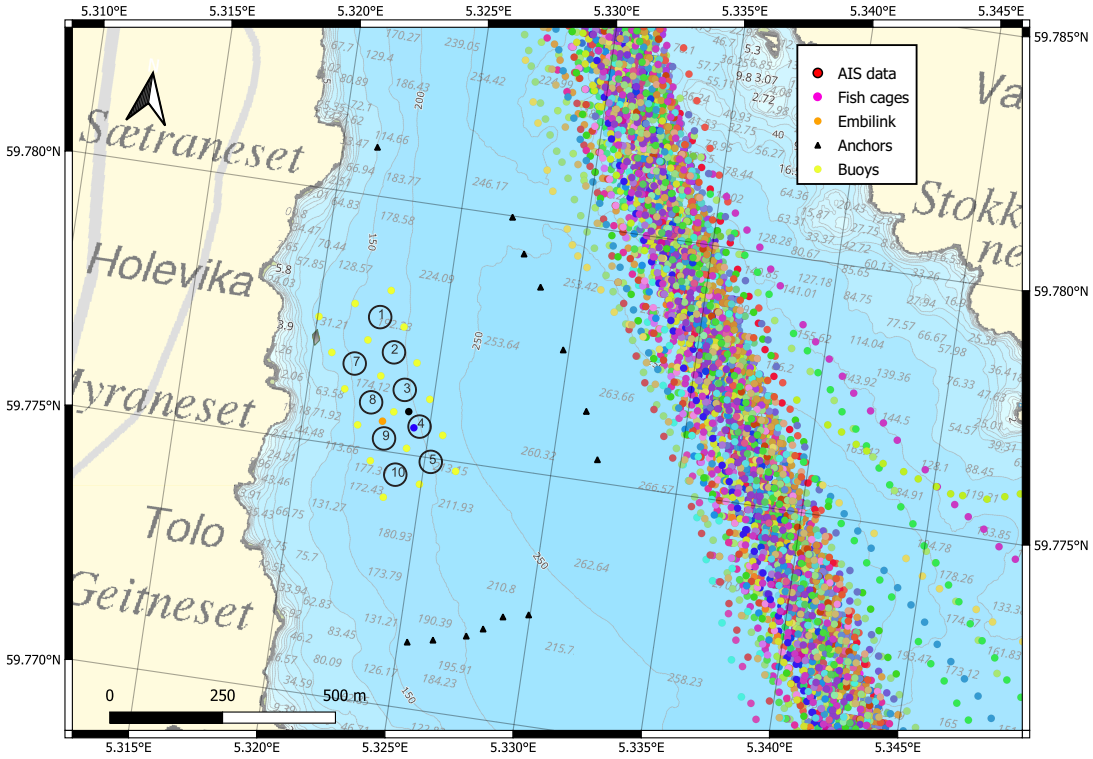

(a)

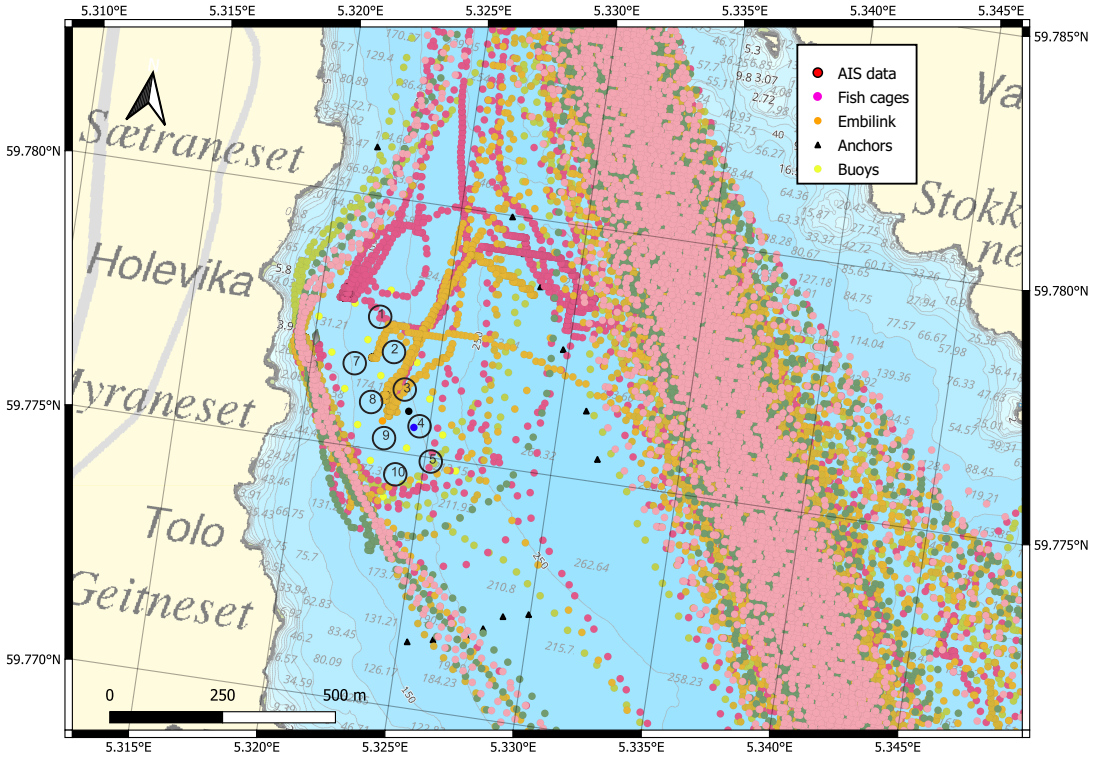

(b)

Figure 5.6: AIS data from May, June, July, and August 2021, the period when the aquaculture facility in Stokksundet was fallowing (a). In (b), AIS data from the facilities' operation period is included.

5.2 Mooring Design and Configuration

This section describes the main mooring components and instruments used in the field experiment. Moreover, it looks at the design and configuration of the observation mooring.

5.2.1 Hardware

This section describes the hardware used in the mooring design. A fishing floatation at the surface informs ships that it is something in the sea at this location. This float does not carry any payload on the mooring. Beneath this, the top float is located. This component is a SF-30 Spherical Float [28] and has a diameter of 76 cm a picture of it is shown in 5.7 (a). It ensures that the instruments do not sink to the bottom but stay in the correct position. Attached directly to the top buoy is a swivel to keep the mooring line from becoming twisted or entangled. In addition, there is a shackle-link-shackle connection between all the different segments of the mooring presented in 5.7 (b). There are some connections to consider since it has two in-line elements and various kevlar shots on the mooring line. The shackle used is a bolt-type anchor shackle with dimensions of 5/8 inches (1.6 cm). Segments of 5/16 inch (0.8 cm) kevlar were used as mooring lines between the anchor and the top float.

Four glass balls are attached above the acoustic release with 17 kg of buoyancy each. A picture of the glass balls is shown in 5.7 (c). These are added to ensure that the acoustic release does not get damaged by the bottom. In addition, five meters of anchor chain is used to connect the release with the anchor. This reduces the chances of the release failing to activate because objects like stones, marine growth, etc., could block the acoustic signals. A picture of the anchor is shown in 5.7 (d).

The anchor is made of concrete and is relatively big compared to the rest of the mooring. The exact weight of the anchor is unknown, however, an estimate has been calculated by using the anchor's volume and the concrete's average density. The dry weight on land is predicted to be around 1368 kg. The anchor is shaped like a cone frustum, with a height of 0.67 m, a bottom diameter of 1.1 m, and a top diameter of 1 m.

Based on the information provided by the technical report from Rådgivende Biologer AS [29], it was possible to simulate a scenario in MD&D with 50 years' values of currents in the deployment area. The safe anchor mass was calculated by MD&D using both drag and lift safety factors, considering the vertical and horizontal tensions. It was essential to ensure that the anchor was heavy enough to hold the mooring in position. Based on this simulation, a safe dry concrete anchor mass was calculated to be 871 kg. Therefore, even though the anchor's weight is estimated, it is still well within the safe anchor weight for this mooring.

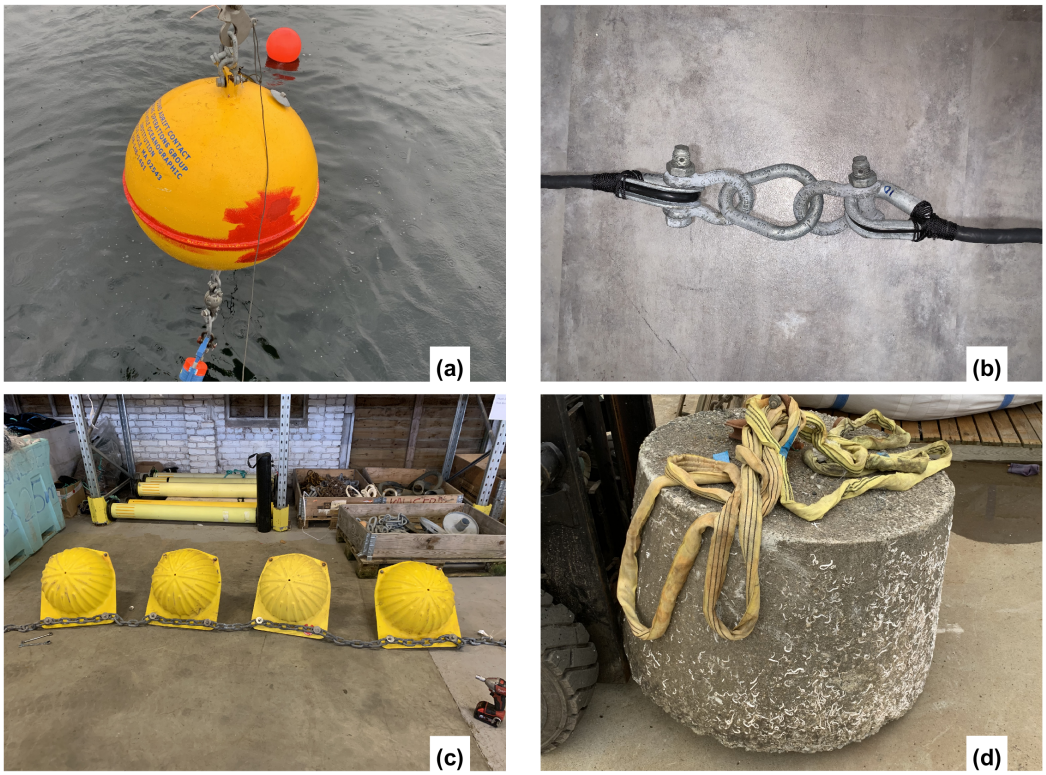

Figure 5.7: Shows the main hardware components used on the mooring. In (a), the top float is presented from the deployment, (b) shows the shackle-link-shackle connection between kevlar shots, (c) shows the glass balls used as floatation above the acoustic release, and (d) shows the anchor.

Table 5.2: Length and wet weight of the chains, shackles, links, and swivels used in the deployment. Nominal values as specified by the manufacturers, but some uncertainties and variances exist.

Name	Length (m)	Wet weight (kg)
Shackle 5/8"	0.049 m	0.56 kg
Shackle 3/8"	0.029 m	0.26 kg
Link 5/8"	0.092 m	0.45 kg
3 Ton Swivel	0.169 m	2.67 kg
1/2" Mooring Chain	5 m	15.47 kg

Table 5.2 describes the specifications of the smaller hardware components attached to the mooring.

Table 5.3: Length and buoyancy of the main hardware components used on the observation mooring. Nominal values as specified by the manufacturers.

Name	Length (m)	Buoyancy (kg)
SF-30 Spherical Float	0.762 m	149 kg
17" Glassballs	0.029 m	5.44 kg
Concrete Anchor	0.67 m	-820 kg
5/16" Kevlar	1 m	-0.02 kg

Table 5.3 describes the specifications of the main hardware components used on the observation mooring.

5.2.2 Instruments

The primary equipment on the mooring is the instruments. The first instrument from the top of the mooring is located in the upper section at about 5 m below mean sea level. This is a single-point current meter of the type Seaguard RCM [30] delivered by Aanderaa Data Instruments AS as shown in Figure 5.8 (a). This instrument measures the horizontal ocean current components locally at the depth. In addition, the Seaguard RCM platform also has sensors that measure temperature, dissolved oxygen, pressure, and conductivity connected.

At about 40 m, the Seaguard II RDCP [31] is located, as shown in Figure 5.8 (a). This is an acoustic Doppler current profiler (ADCP), which can measure the current on several different vertical layers in the ocean based on the doppler shift. Hence, the sensor can calculate the current based on the time the sound reflection uses to arrive back at the transducers. This instrument also has the same sensors as the Seaguard RCM to measure the other parameters locally at 40 m.

In between the two Seaguards, a 34.4 m kevlar shot has three clamp-on instruments. Starting with two moored CTDs of the type SBE 37-SMP MicroCAT as shown in Figure 5.8 (b), with high-accuracy conductivity, temperature, and pressure recorders [32]. They have been placed at depths of 10 m and 20 m. That is to monitor differences in temperature and salinity vertically in the water column.

The CTD casts conducted before deployment, as illustrated in Figure 5.4, were utilized to decide the instrument depths. The two casts before deployment A3 and B1 showed some distinct water layers from 7 m to 13 m and from 16 m to 20 m that were similar and made the

measurement depths logical.

At a depth of 30 m, a μAural hydrophone [33] as shown in Figure 5.8 (d), is configured to monitor the soundscape in the fjord. It focuses on operations like flushing and when well-boats are performing delousing of the fish. These operations tend to stress the fish. Therefore, it could be interesting to investigate if the noise could directly influence the appetite of the salmon.

The last instrument on the mooring is the acoustic release mentioned earlier. In this mooring, the Teledyne Benthos 866-A Transponding Release [34], as shown in Figure 5.8 (c) is utilized. This device allows subsurface moorings to be recovered since it can detach the anchor from the rest of the mooring. As a result, the floatation element will rise to the surface when the release is activated with an acoustic code. It also makes it easier to recover the other components when the anchor's weight is gone. Information about the configuration and measure parameters is presented in Table 5.4, and the appearance of the instruments is illustrated in Figure 5.8. Note that the measurement uncertainty is as defined in the instrument's manuals [30, 32, 33, 31].

Table 5.4: Sampling interval, instrument depth, and measuring parameters of the various instruments and sensors on the mooring.

Instrument	Depth (m)	Measured parameters	Sampling interval
Seaguard RCM	5 m	C,T,p, DO, U, V	5 min
SBE 37	10 and 20 m	C, T, p	1 min
μAural	30 m	Sound	30 min every 2 hours
Seaguard II RDCP	40 m	C,T,p, DO, U, V	5 min

5.2.3 Design

The design of the mooring is illustrated in Figure 5.9. The design is for a position where the water depth is about 263 m. The goal is to get the instruments on approximately the desired depth to compare with results from, e.g., the EMBILINK sensors. Another element necessary in the design process was having enough floatation to prevent the mooring from getting knocked down during extreme currents. Furthermore, the anchor should be sufficiently heavy to withstand the system's drag force and remain stationary at the same fixed position.

Another essential aspect is the tensile strength of the mooring line and other equipment. The tensile strength of the kevlar is about 4200 kg, and it is at loads over this that the kevlar

Figure 5.8: Instrumentation that is present on the observation mooring. In (a), the two different Seaguard platforms from Aanderaa Data Instruments AS are presented. The instrument on the right side is the Seaguard II with an ADCP profiler. In (b), the μAURAL is shown, (c) illustrates the acoustic release, and (d) shows the SBE 37-SMP MicroCAT.

rope can start to break. Since the anchor and the other equipment are not that heavy, it will probably not be because of high loads if the mooring line fails. The mooring must withstand the cyclic load and be strong enough to carry the anchor's weight if the release fails or the mooring has to be moved. Regarding the instruments, the configuration is essential to obtain as much data as possible without risking running out of power too early. It is also vital to try and utilize the available instruments for the deployment in the best possible way.

The Seaguard RCM was placed at approximately 5 m to compare it with the measurements conducted inside fish cage nine. In this cage, the EMBILINK sensors are located, continuously measuring salinity, oxygen, and temperature inside the fish's environment. The measurements are conducted as a part of the Aquaculture Stewardship Council (ASC) standard called ASC Salmon Standard Version 1.3 [35]. The measurement depth is standardized to be at 5 m.

Another important aspect is that the ocean current measurements must follow some guidelines to be approved as a fully worthy site survey [36]. Consequently, measurements must be done for at least four full weeks to get statistically accurate enough data, with a maximum interval between measurements of 10 minutes. The rules also say that the critical depths to measure currents are 5 m and 15 m. This was essential to consider in the configuration of the Seaguard instruments. Hence, ensure that the devices have the battery capacity to measure frequently enough, to meet these requirements. The SeaGuardII RDCP Power Calculator was utilized to evaluate the battery consumption of the Seaguard instruments. The short timeframe of the measurement period made it possible to make measurements every five minutes, according to the estimates. The SeaguardII RDCP was configured to measure currents at depths of 38-30 m, 20-10 m, and 10-3 m with 300 pings for every measurement. This gives good data at the bottom of the net at 38 m and data from the other instrument positions.

Table 5.5: Instruments mounted with clamp-on brackets on the observation mooring, the arrows in 5.9 shows the positions of the instruments.

Instrument	Depth (m)	Serial number	Label (A-C)
SBE37	10 m	9004	A
SBE37	20 m	9005	B
μAURAL	30 m	7016	C

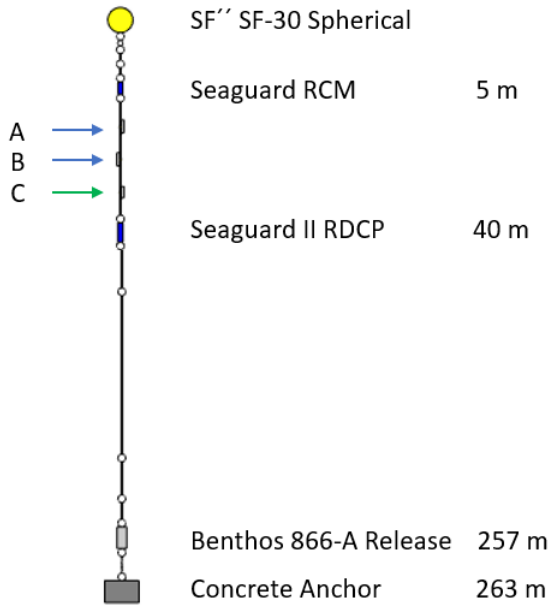

Figure 5.9: Schematic drawing of the observation mooring as deployed in Stokksundet. Instruments mounted with clamp-on brackets are described in Table 5.5.

5.3 Mooring Deployment

The mooring was deployed on the 17th of March, with one day of preparation and one day of deployment. This time was chosen because of the availability of the ship and the crew. It was also a factor to have sufficient good enough weather conditions to safely operate and deploy at the planned position. This was also a key element since the boat does not have a Dynamic Positioning (DP) system.

5.3.1 Preparation

On the 16th of March, the equipment arrived at Bremnes Seashore's storage building on Serklau about four nautical miles from the mooring position. It was essential to inspect and test all the equipment and instruments before the operation to ensure that all components were ready and in good condition. The top float had some damage on the paint that was repaired. This was done to prevent the exposed areas from corrosion. The glass balls were then mounted to a new chain. To ensure that the glass balls and release would withstand the anchor's weight, they were load tested at the dock by lifting it with a forklift. This also stretched the chain and ensured that the glass balls were correctly mounted.

The 34.4 m kevlar rope was also marked where the clamp-on instruments were supposed to be mounted. This was done using tape of different colors to differentiate the SBEs from the

μAURAL. The top float and the fishing floatation were also marked with name, address, and phone number as instructed by the Norwegian Directorate of Fisheries [37].

Furthermore, an overview of all the necessary tools and components was established for the operation. Then, when everything was ready to go, all the equipment was loaded onboard the deck of the workboat Randi. A picture of Randi is shown in Figure 5.10. During transit, the kevlar rope was spooled onto the winch to have control of the different lengths and pay out the rope safely during deployment. The first length spooled was the working line. It is not part of the mooring itself, but it was used to have control of the kevlar rope. Another security measure was to have a snatch block in the crane to maintain a safe method of managing the mooring line while deploying. Having a release hook was also helpful in keeping the deployment safe. It means that one can detach both the top float and anchor at a safe distance.

Figure 5.10: The workboat Randi used to deploy and recover the mooring is 14.99 m long with a crane and winch installed on deck.

5.3.2 Operation

The mooring is deployed with the anchor last, which means that the anchor may arrive at the seafloor 30 m to 35 m from the drop position, towards the top float [38]. This was taken into consideration before releasing the anchor.

The first step was to lay the boat up against the wind with a weak advance using engine power. This ensures that the equipment deployed first will extend away from the ship's stern, and the ship will remain approximately in the correct drop position. After getting into position, the top float and the Seaguard RCM were craned into the water and released using the release hook. The kevlar was then guided through a snatch block mounted in the crane. There were fixed tasks for each person throughout the operation: one captain, one crane operator, one winch operator, and one with a free role on deck.

Next, the three instruments with mounting brackets were mounted at specific depths on the first kevlar shot rope between 5 m and 40 m. The rope was marked with tape at the correct depth in advance, making it easy to see. When reaching the Seaguard II at 40 m, the mooring line was stopped, and the frame was attached directly between kevlar shots. During this operation, the rest of the mooring was secured to the boat, ensuring safety while working. Before going into the sea, it was essential to look over every kevlar shot and in-line element that all shackles were secured with split pins or wire.

After starting with many instruments, it was paid out about 200 m of rope before coming down to the bottom of the mooring. At the bottom, the glass balls were attached between the mooring line and the acoustic release. Then, the anchor was connected to the release with 5 m of chain. From this point, the release hook was connected directly to the anchor. It was then craned over the row and down to the sea surface. This gives a good overview of the situation since the top float was stretched long behind the ship. Finally, the anchor was released and dropped down to the bottom after adjusting the boat's position slightly.

5.3.3 Redeployment

After deployment, the top float was supposed to be 5 m under the sea surface, but it suddenly came to the surface. It was evident that the mooring was too long for the depth at this location. The crane was then attached to the top float, and the entire mooring was lifted from the seafloor to check how long the mooring was relative to the depth. The sphere was about 3 m above the surface when the anchor's load was felt. At this point, there were two alternatives to make this a subsurface mooring: 1) recover, adjust and redeploy the mooring, and 2) move the mooring to deeper water. However, redeploying is time-consuming, and there is a risk of damaging the equipment. Therefore it was decided to try and move the mooring further

out in the fjords towards deeper water. Unfortunately, sufficient depth was not as close as expected and too far into the shipping lane.

Consequently, to avoid conflict with shipping in the fjord, it was opted to tow the mooring towards the aquaculture facility and accept it as a surface mooring. This operation was conducted the day after deployment on the 18th of March. In addition, since the instrument layout was about 4 m closer to the surface than planned when becoming a surface mooring, 4 m of kevlar was added between the top float and the Seaguard RCM instrument. With this adjustment, the instruments were placed at the correct depth. It also helped make the buoy easier to spot at the surface. Another improvement was that a blinking light was mounted to the top float to make it more visible at night. This was added on the 25th of March, one week after the redeployment.

5.4 Mooring Recovery

The recovery was planned for the end of April to ensure more than a month's worth of data. Hence, the recovery operation was conducted on the 28th of April, six weeks after deployment. Before starting the primary operation, a small boat was used to prepare the mooring. Firstly, the blinking light was removed from the top float and replaced with a lifting sling. In addition, a Teledyne Benthos UDB 9400 deck unit [39], and transducer was used to enable the acoustic release to ensure it was still powered up. That confirmed that the release mechanism was more likely to work correctly.

Furthermore, the necessary equipment was loaded on board Randi after the initial preparation. Next, the working line of kevlar was spooled onto the winch again to connect it directly to the mooring line during recovery. The main difference from the deployment operation was that, in this case, the idea was that the anchor should stay on the seafloor. Therefore, when arriving approximately 200 m from the mooring position, the pinger was again lowered 10 m into the water column. A unique acoustic code was then transmitted from the pinger to the acoustic release at the seafloor. The code was configured through the Benthos deck unit that handles the command of the pinger. The code worked when finding the correct angle and distance, and the release unattached the chain from the anchor. Since the mooring was equipped with four floatation glass balls at the bottom, these floated up after a few minutes.

First, a lifting sling was attached to the bottom of the mooring. This made it a reversed operation from deployment except without the anchor. Next, the release and glass balls were craned on the deck of Randi. Then the kevlar shot was connected to the working line, and the winch was used to spool in the mooring line. After around 150 m of the mooring line, the

Seaguard II RDCP was located and lifted on deck. Since this was an in-line element, it had to be removed to spool on the remaining kevlar. At this point, the three clamp-on instruments came with a spacing of 10 m, and since the tension was low, they were all lifted on board with hand power. After the kevlar shot with the clamp-on instruments, the Seaguard RCM came at about 5 m below the surface. Lastly, the lifting sling on the top float was connected to the crane and lifted on deck. Immediately after arriving on deck, every component and instrument was inspected and photographed to look for damages and marine growth.

5.5 Post Recovery

After recovery, all the equipment and mooring components were transported to the storage at Serklau with Randi. The mooring line was detached and coiled at the deck. The other elements were lifted by hand or craned up at the pier. Finally, the hardware was lined up at the dock and flushed with fresh water and soap to remove the marine growth and avoid corrosion. The instruments were also gently rinsed and cleaned with fresh water to remove dirt and salt. After this, the instruments were opened up and shut down before removing the SD cards to download and backup the raw data. It was also essential to clean all the o-rings and mating surfaces and apply silicone grease to maintain them and prevent leaks in the future. The results from the experiment are presented in Chapter 6.

Chapter 6

Results - Field Experiment

This chapter describes the results of the field experiment conducted in Stokksundet.

6.1 Temperature

This section aims to evaluate the temperature differences over the measurement period. Consequently, analyze the vertical variability based on the sensors on the mooring and horizontally by comparing the Seaguard RCM data with the EMBILINK data.

6.1.1 Comparison Vertical Temperature

In this section, the temperature vertically on the mooring location is evaluated. It also describes some events that occurred during the measurement period, which could help identify outliers in the dataset.

Figure 6.1 (a) illustrates the different depths of the various instruments and the spacing between them. Some events need to be addressed to explain the pulldowns and other variances. At first, the Seguard RCM was designed to be directly beneath the top float at about 5 m depth. This was later adjusted since the mooring was rearranged as a surface mooring. Moreover, since this instrument also started measuring on power-up, the first small segment on 1 m is from the 17th of March. The SBE-37s also did some sampling about 5 m over the design depth at 10 m and 20 m. That was before the mooring was adjusted on the 18th of March.

Ideally, the Seaguard instruments should be on 5 m and 40 m, but since the kevlar shots were not designed for this specific mooring, it was difficult to hit that precisely with the kevlar shots available. Nevertheless, the clamp-on Seabird instruments hit the design depth quite

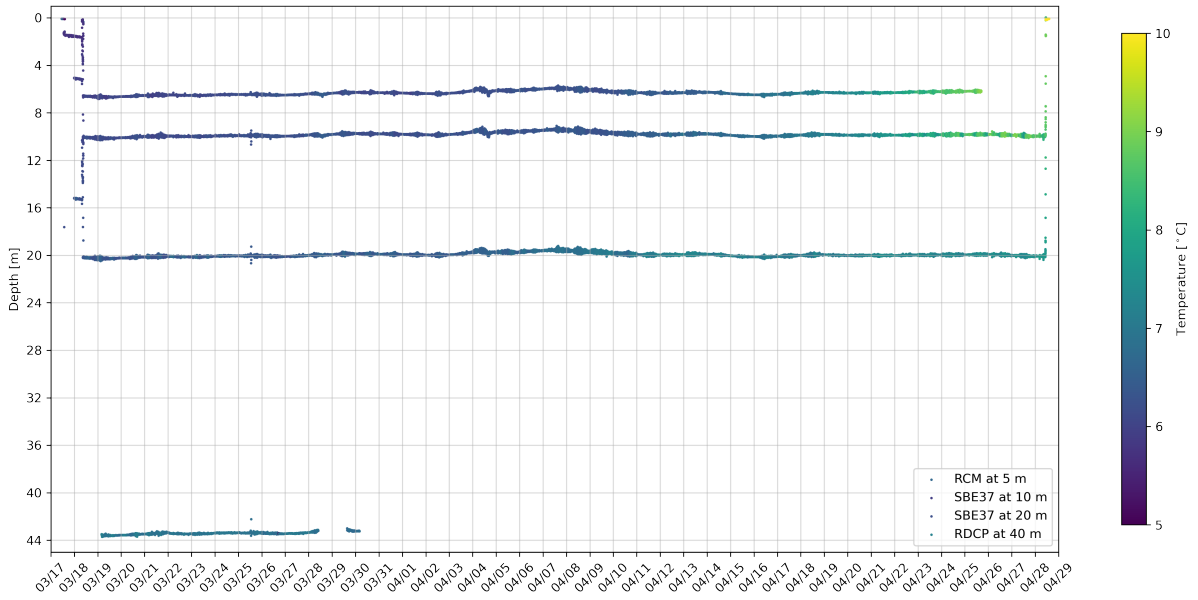

(a)

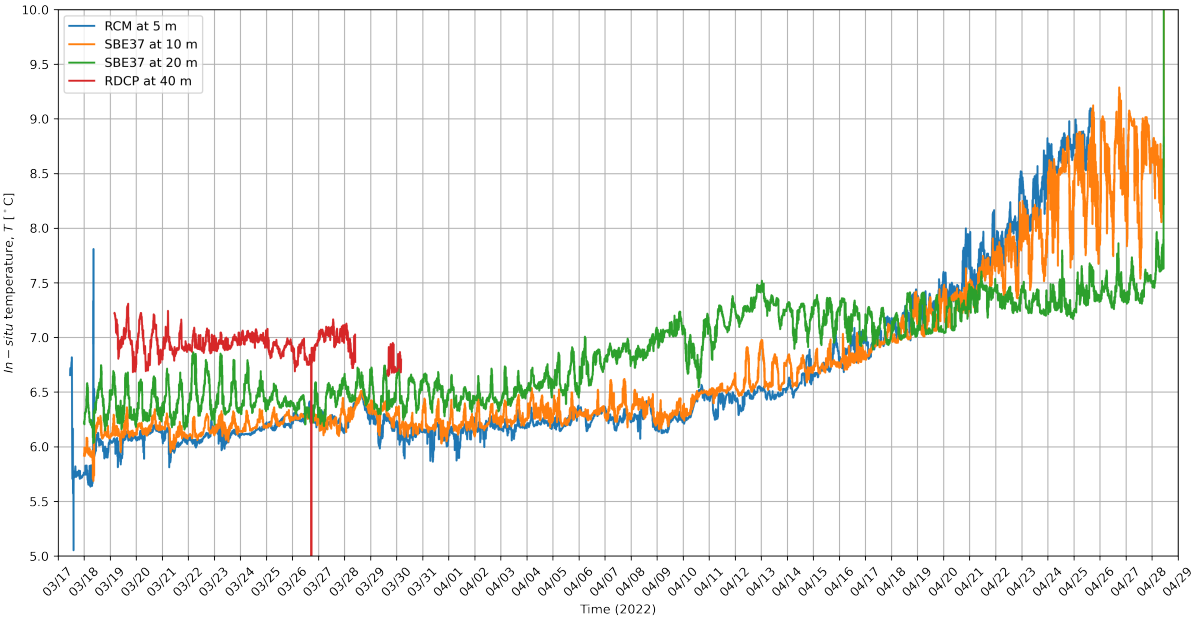

(b)

Figure 6.1: Time-series of the temperature measurements conducted on the observation mooring with instrument depth in (a) and temperature variability in (b).

well. So on the 18th of March, the instrument depths stabilize. The new depth is about 6 m for the RCM, 10 m and 20 m for the SBE37s, and approximately 44 m for the RDCP.

Another important note is at the 25th of March, a blinking light was added to the top float for visibility. It is possible to see this operation accordingly to the measurement points that deviate from the line. This is illustrated more evident on the SBE37s in Figure 6.1 (a), since they have a sampling interval of 1 min, to the Seaguards five minutes. The two Seaguards do not have the same outlier on the line since the five-minute sampling interval was not synchronized.

Furthermore, some other points with significant mooring motion were during events with strong wind and ocean currents. For instance, on the 21st of March, there were strong winds and currents towards the Northwest. In addition, on the 29th of March, the 4th of April, and from the 7th to the 11th of April, strong currents and wind occurred towards the Southeast.

Furthermore, based on the temperature difference between the RCM and SBE37, it looks like a pretty mixed layer, which corresponds to the mixing of layers seen in the CTD cast conducted on the deployment day in Figure 5.4 with label C1. Even though the instrument depths were based on the CTDs completed during the winter, there were excepted more differences between the two sensors at 6 m and 10 m. These two sensors follow the same temperature pattern during the whole period, which indicates that the sensors are within the same water masses. It is also interesting to see that the temperature towards the surface was colder than the seabird at 20 m until mid-April. That may be because of a period with warm air temperature. At the start, the temperature was warmer the deeper the instruments were. However, as the spring emerged more and more, the two sensors in the uppermost column of the water started to surpass the deeper one. The deeper one on 20 m was more stable, and the RDCP would probably be even steadier. Deeper waters need more time to get warm.

Figure 6.1 (b) shows the temperature variation measured by the different oceanographic instruments. It also shows some inconsistencies and outliers in the period. For instance, the RCM was out of the water for a period when moving the mooring. Another interesting moment was on the 26th of March when something happened with the batteries on the RDCP. Furthermore, looking at the variability at different depths was interesting when investigating the results. For example, the temperature seemed more stable towards the surface and bottom at the start while varying more at 20 m. However, towards the end of the measurement period, the instruments closest to the surface had more variability. It was also possible to recognize that the difference between depths was reduced during strong currents.

From the 6th of April, the difference between the two uppermost sensors and the seabird at 20 m increased to about 1 degree. Later they converged on about the 17th of April when

the water masses towards the surface started to warm up faster and eventually surpassed the SBE37 at 20 m. From the comparison, it seems like all the curves follow somewhat the same pattern. It is an indication that both tidal water and the time of the day play a part in the temperature swings. At the end of the deployment period, the uppermost seabird is the one that varies the most.

6.1.2 Comparison Horizontal Temperature

This section compares the temperature data collected on the RCM and the EMBILINK. The horizontal distance between the sensors is about 450 m.

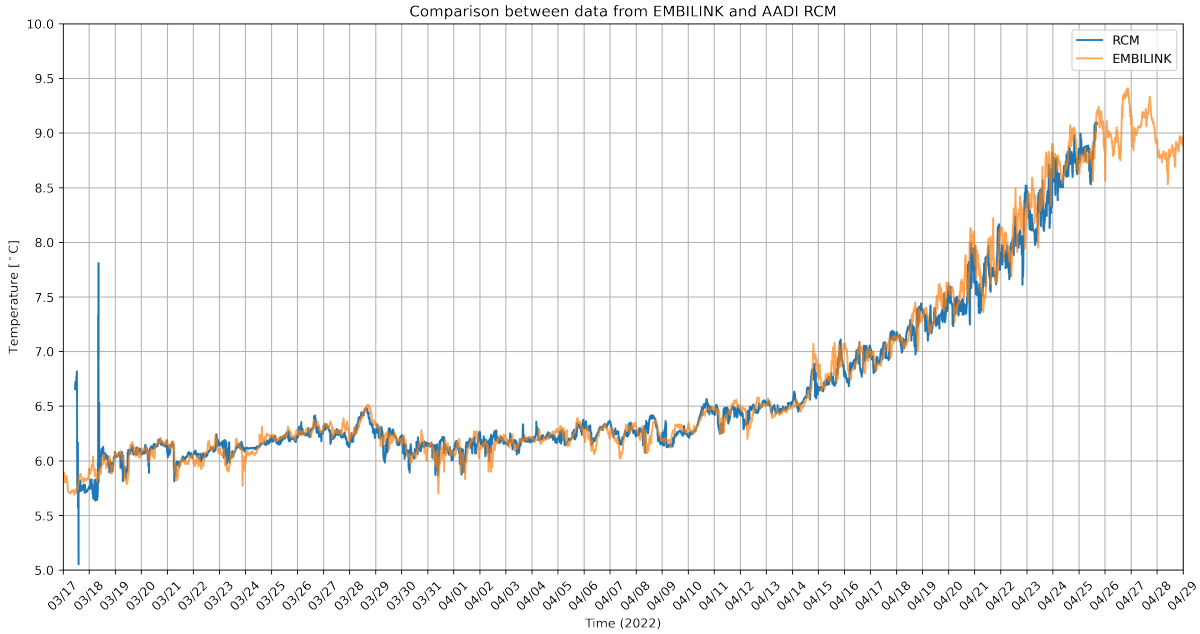

Figure 6.2: Comparison between measurments of temperature on the EMBILINK and RCM at about 5 m depth.

In Figure 6.2 the differences between the measurements inside fish cage number nine and the RCM are compared. It was interesting to investigate how, e.g., the marine growth on the net in the cage influences the different ocean parameters. Of course, another factor is whether the fish will make a difference, but it is hard to say what might affect it in this case. Figure 6.2 shows the same outliers as before, during deployment and redeployment. Nevertheless, the temperature curves seem to follow each other closely after that. Except for some places were on or the other has some more significant spikes. An important outlier is from the end of the 23rd of April. At this point, Ronja Vest is located along the same fish cage as the EMBILINK during a delousing treatment. The EMBILINK is removed from the fish cage to prevent damage during the operation. This is more clearly illustrated when looking at the salinity comparison in Figure 6.5.

The figure also shows how the temperature has increased since the deployment date, except for a little setback in early April. The temperature change is essential in the aquaculture industry. It is a good sign since the salmon digest the food faster and increase growth. The problem is that also the salmon lice grow more quickly with temperature. That can undoubtedly stop the salmon's development and increase the noise levels in the fjord and the cost of the production.

6.2 Salinity

This section aims to evaluate the salinity changes during the measurement period. However, since the same outliers as in the temperature plots are also present in these figures, it is not described here.

6.2.1 Comparison Vertical Salinity

This section aims to describe the vertical salinity variation throughout the period. It includes pressure data to understand at what depth the sensors are located. In addition, some Temperature-Salinity (T-S) diagrams are presented to help describe the variability at different depths.

As illustrated in Figure 6.3 the salinity has a similar tendency as the temperature that it looks like it varies with tidal water. On the temperature plot in Figure 6.1 the same pattern was spotted at the start of the measurement period, which is that the salinity is increasing with depth. They also connect with the curves, with salinity increasing when the temperature rises. At the RDCP depth, it was the most stable, and at the three uppermost instruments, the variability was more during the day. It also looks like the layers are diverging from the 5th of April, and also, here, the two uppermost instruments have a similar curve. Unlike in Figure 6.1 the salinity does not increase on the two uppermost, but it seems like they stabilize at a certain level. The variations have the same pattern but swing more on the deepest SBE37. It appears that the uppermost layer is influenced when there are wind-induced currents.

Figure 6.4 shows the TS diagrams for the different instruments. It is interesting to observe that the variation is more severe in the upper layer. On the RDCP at 40 m, the situation is much more stable at a certain point. It is important to note that the variability is also less since there were recordings from a shorter period. Moreover, measurements from the whole period would probably show more variation.

The temperature variation is also more minor at a depth of 20 m, explains, even though the salinity distribution of measurements has the same shape at both 10 m and 20 m. The

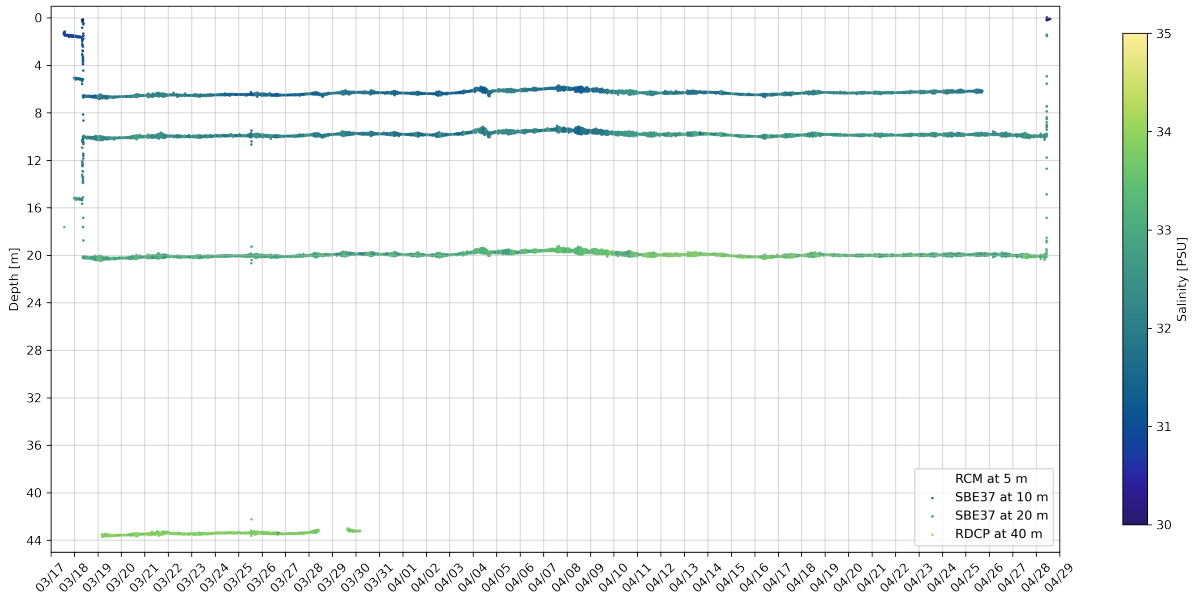

(a)

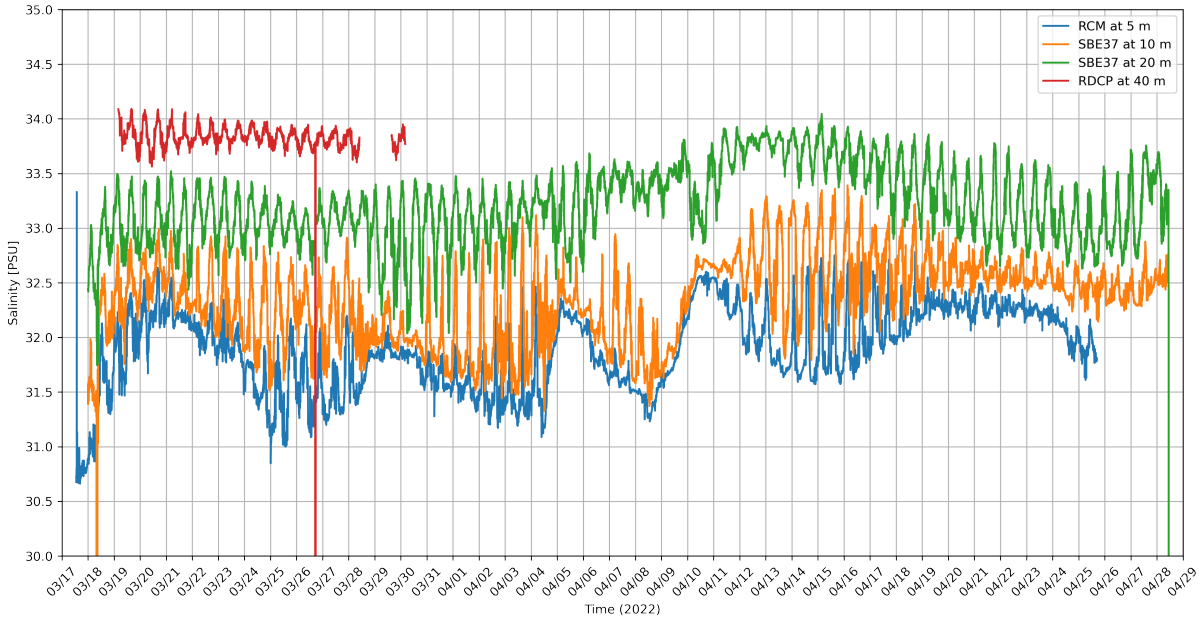

(b)

Figure 6.3: Time-series of the salinity measurements conducted on the observation mooring with instrument depth in (a) and salinity variability in (b)

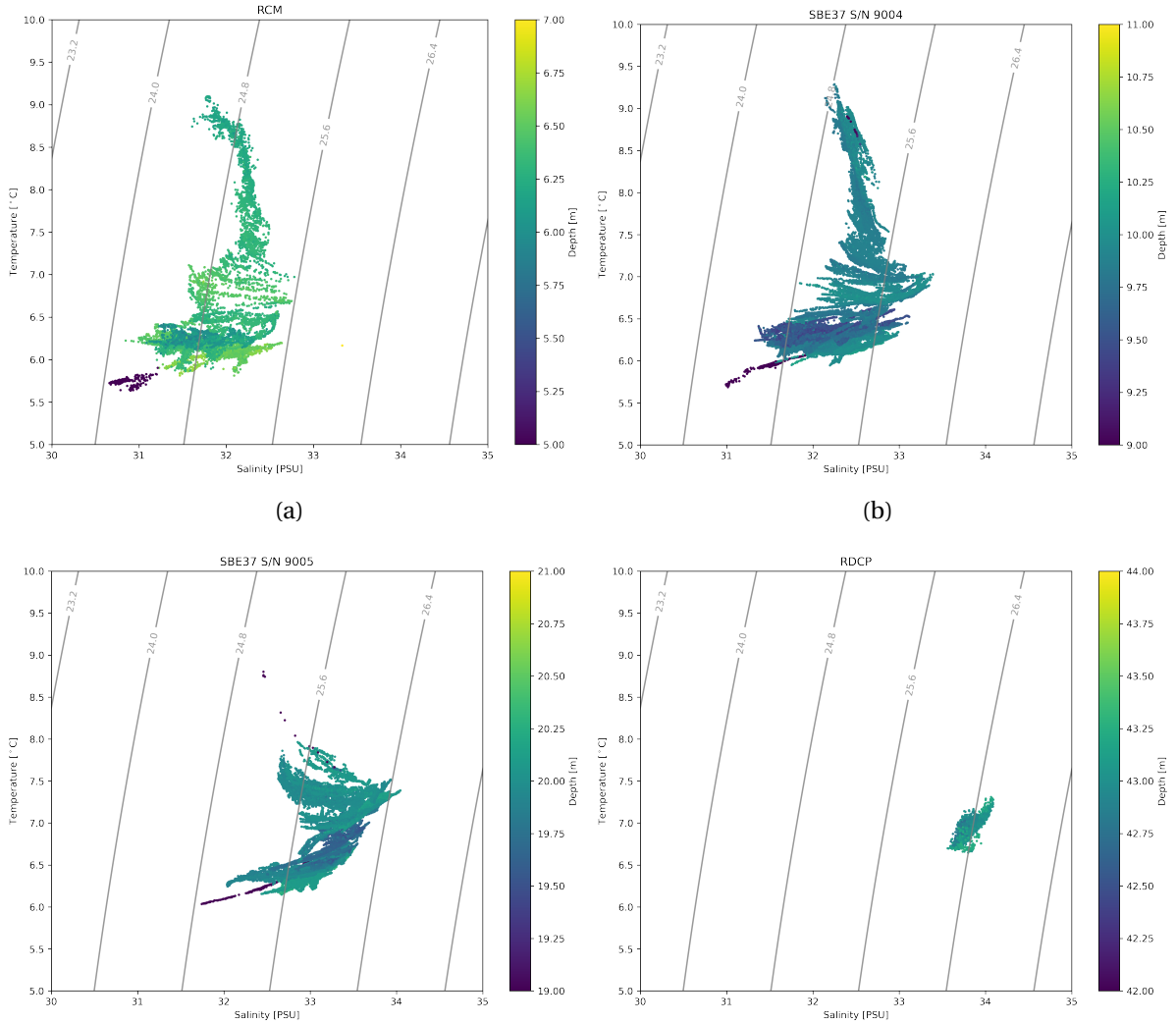

(a) (b)

(c) (d)

Figure 6.4: T-S diagrams (a)-(d) of measurements conducted by the four different instruments observing temperature, salinity, and pressure. Diagram (a) shows the RCM at about 6 m depth, (b) shows the SBE37 S/N 9004 at 10 m, (c) shows the SBE37 S/N 9005 at 20 m, and (d) shows the RDCP at 43 m.

difference is that the salinity is about one PSU less at 10 m. The temperature swings are almost four degrees on the two uppermost instruments, about two degrees on the SBE37 S/N 9005, and within one degree on the RDCP. Looking at (a) could help explain the differences in salinity observed on the EMBILINK in Figure 6.5, since it seems to be varying quite a bit with just a 1 m depth gap.

6.2.2 Comparison Horizontal Salinity

This section describes the salinity comparison between the RCM and EMBILINK.

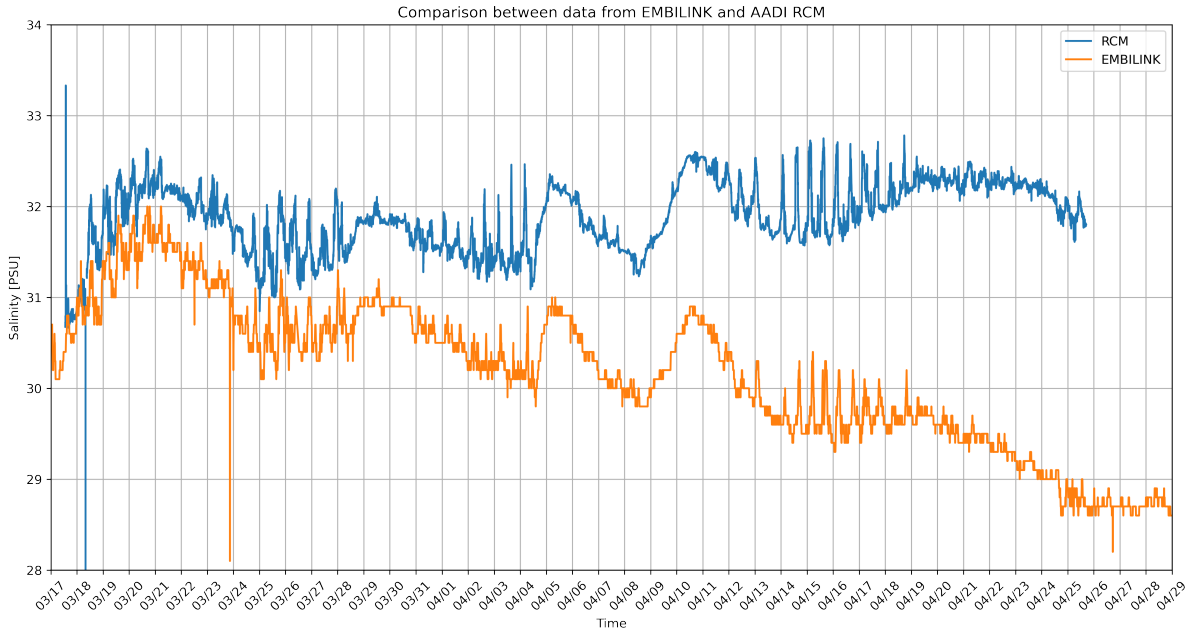

Figure 6.5: Comparison between measurments of salinity on the EMBILINK and RCM at about 5 m depth.

Figure 6.5 shows the salinity recorded by the EMBILINK compared to the data from the RCM on the observation mooring. Regarding the curves, the trend is clear, and the salinity follows the same pattern on the RCM and EMBILINK. However, the difference between salinity and temperature is an offset between the curves in this case. It starts at about half a PSU before gradually increasing to almost three PSU differences at the end of the period. One potential explanation could be that the EMBILINK and RCM were not at the same depth, even though they should ideally be at 5 m. Based on the pressure sensors on the RCM, this is known to be a bit deeper. Unfortunately, the EMBILINK does not have a pressure sensor, so that the depth could have been adjusted during this period. Another factor could also be the amount of marine growth on the sensors. That last confirmed rinsing of the EMBILINK sensors was on the 19th of February. It could affect the measurements if it has not been cleaned after this.

There are also some interesting variations from the CTD casts shown in Figure 5.4. The C1

and especially D1 cast from deployment and redeployment show that the salinity can vary significantly towards the surface. So it makes sense that there is some variation at the start of the measurement period. The increasing variation in salinity could also come from the warm weather that led to faster snow melting. Since Stokksundet is a part of the Hardangerfjord, it could influence the amount of fresh water, especially towards the surface. However, marine growth is probably the essential factor that could explain the salinity decrease towards the measurement period's end. Since the temperature increases, it means that the marine growth also increases. Since the Embilink has been in the sea for several weeks more, it could help explain the curve falling earlier than on the RCM.

Nevertheless, from the 23rd of April, the RCM also starts to have a downgoing salinity. It is reasonable that the conductivity sensors measure less conductivity when a film is on the sensor. Furthermore, thereby, the calculated salinity is also decreasing. Based on the CTD cast conducted post-recovery on the 28th of April presented in Figure 5.4 with label E1 in Chapter 5, the salinity on 5 m was about 31 PSU. The RCM curve seems like it is creeping toward 31 PSU, but unfortunately, the battery died on the 25th of April. However, by comparing it with the SBE37s, the salinity measurements agreed.

6.3 Oxygen

This section describes the variations in oxygen levels throughout the period. However, since the RDCP had a limited sample size of Oxygen measurements, it was decided only to present the comparison between the RCM and EMBILINK data.

6.3.1 Comparison Horizontal Oxygen

This section describes the oxygen comparison between the RCM and EMBILINK. The oxygen measurement is conducted using oxygen optodes which measure dissolved oxygen, DO.

Figure 6.6 shows a comparison of the air saturation as a function of time, based on the measurements from the RCM and the EMBILINK. On the 23rd of April, the EMBILINK sensors were brought onshore, which may have damaged the oxygen optode. At the start of the period, the RCM and Embilink follow the same curve at about 100 % air saturation. However, especially after the 23rd, the measurements from the Embilink start to vary much more than on the RCM.

There could potentially be several reasons behind this. First, it is a pattern that the oxygen levels are higher in the middle of the day and at the lowest points during the night. It also makes sense that the differences increase along with the algae bloom during the spring. The

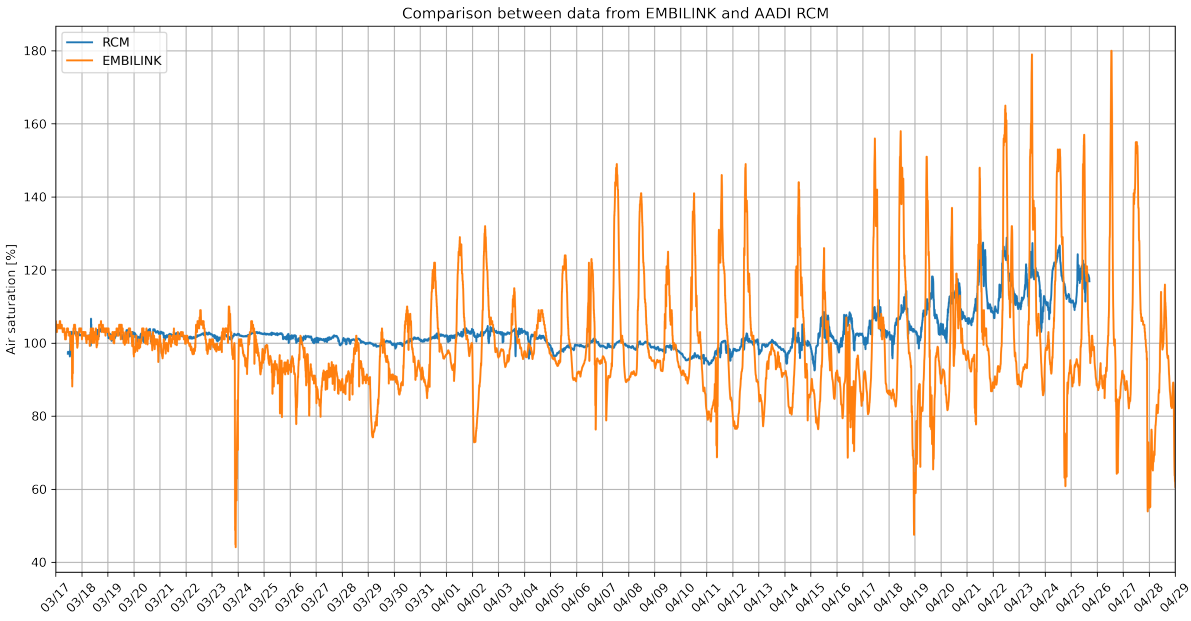

Figure 6.6: Comparison between measurments of oxygen on the EMBILINK and RCM at about 5 m depth.

algae produce oxygen when the sun is up and use oxygen during the night. This trend is seen in both cases, but the variability is higher inside the fish cage. It could be because of fertilization from the fish itself, but it is at this point only speculation.

6.4 Ocean Currents

This section will describe information about ocean currents in Stokksundet related to the observation mooring.

Figure 6.7 shows the distribution of current directions during the period. Again, the currents are dominated heading towards the North, but the most extreme events happen towards the Southeast.

Figure 6.8 shows the current speed in cm/s over time given in the format day-month (dd/mm). The orange curve represents the current in the East-West direction. In this figure, the East is upwards in the positive direction, and currents toward the West are downwards in the negative direction. The blue curve represents the current in the North-South direction. In this case, the North direction is the positive and the South negative. The green curve shows the absolute value of the current, and based on the shape of the orange and blue curves, the current direction can be roughly estimated.

The spikes on the 17th of March are from adjusting the observation mooring. As discussed earlier, the smaller spikes on the 18th and 25th could be affected by work done on the moor-

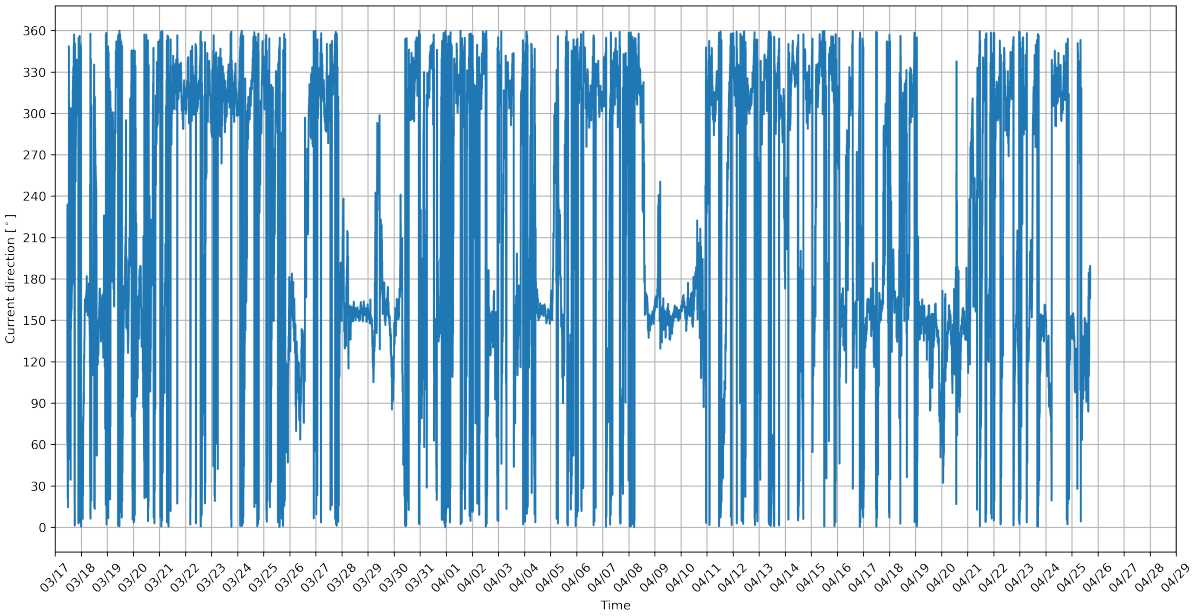

Figure 6.7: Time-series of the current directions during the measurement period.

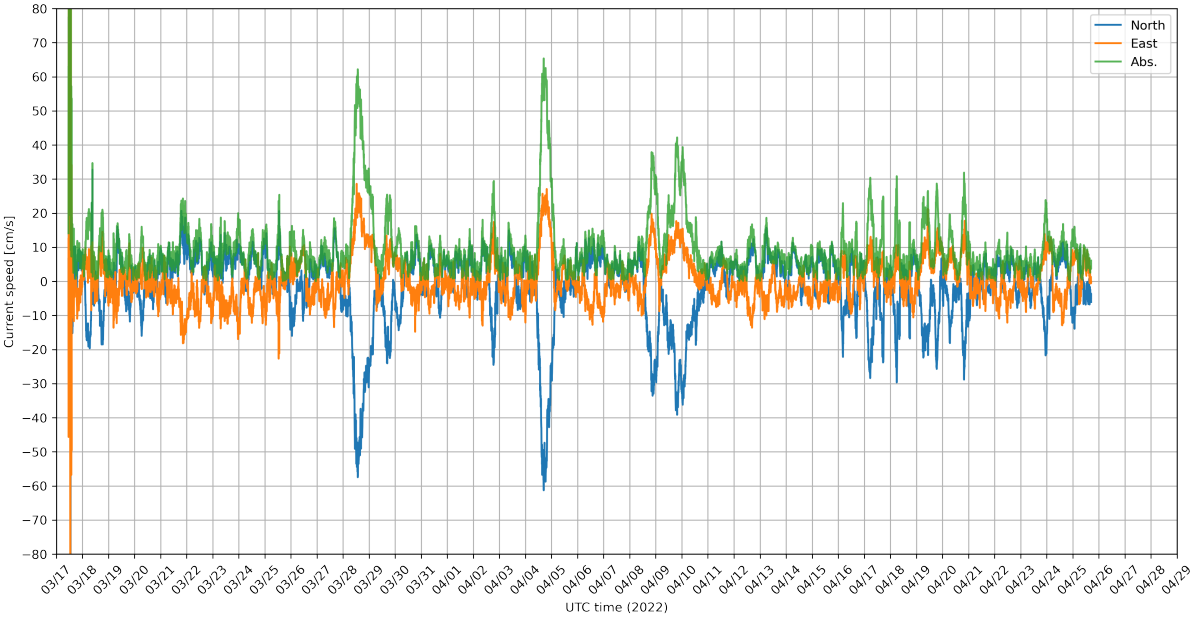

Figure 6.8: Time-series of the current speed in cm/s during the measurement period, positive currents are towards North and East.

ing. A trend seen throughout the period is that currents towards the Northwest dominate the water transportation in the fjord. Interestingly, the most extreme currents observed with the highest maximum current were currents in the opposite direction towards the Southeast. This could be explained because the fjord is more narrow on the northern side of the mooring. Ultimately this will press the water masses to go faster since it is limited space.

Another explanation of the currents up to almost 70 cm/s is explained in Figure 6.9. Especially at the most extreme spikes, it is clear that there are winds up to nearly 20 m/s at the strongest currents. Since the current meter on the RCM is only at a depth of about 6 m, it makes sense that the wind highly influences it. Therefore, the 28th of March, the 4th of April, and from the 8th to the 11th of April are the periods with the highest current and wind values measured.

In general, the oceanic current seems to be relatively affected by tidal currents on the surface, and the current direction changes regularly between the Northwest and Southeast. This makes sense since it is the longitudinal direction of Stokksundet, and the currents typically follow the fjords.

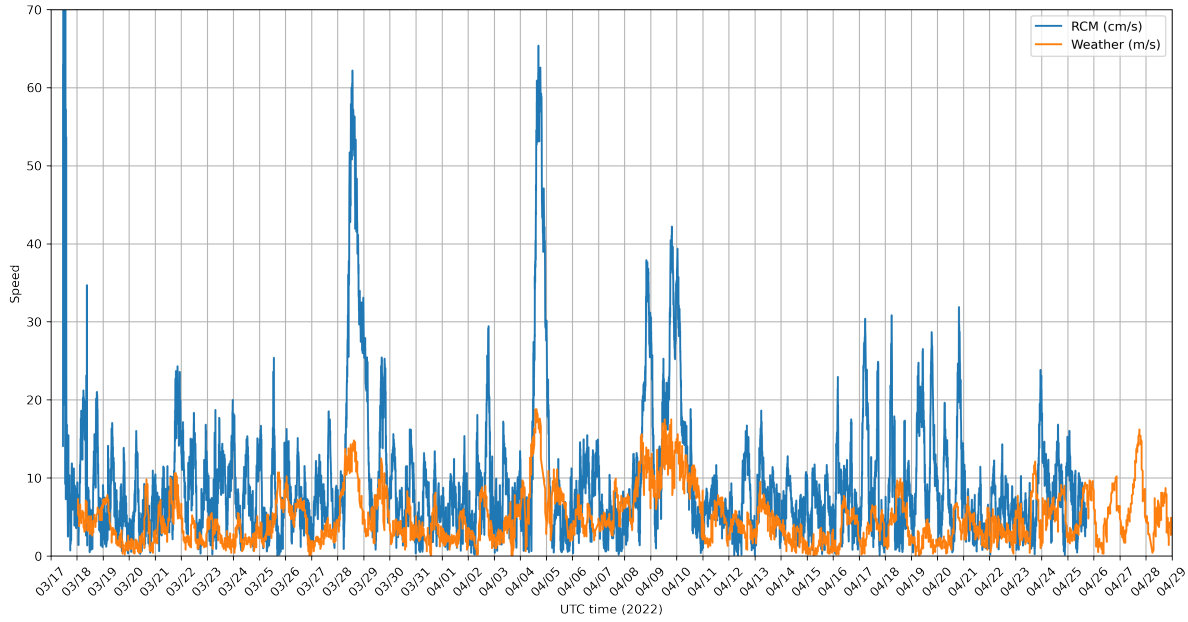

Figure 6.9: Time-series of the current speed in cm/s and the corresponding wind speed in m/s during the measurement period.

Figure 6.7 shows the distribution of current directions during the period. Again, the currents are dominated heading towards the North, but the most extreme events happen towards the Southeast. It is also interesting that it has measurements in all directions, likely connected to when the tide changes. The periods with considerable winds and currents are the only periods when the tidal waters do not seem to affect them. The current direction is pretty stable towards the Southeast at about 150 °.

In Figure 6.13 (b), the histogram of the RCM direction distribution confirms the trends seen in Figure 6.7. The counts towards the northern directions have more data points but are less focused. Toward the Southeast, the current seems more focused, which could help explain the strong currents. This is also expected based on the geometry of Stokksundet shown in Figure 5.1, where the fjord narrows down North of the aquaculture facilities.

Figure 6.13 (a) shows a histogram of the RCM current speed distribution. Interestingly, the current is at around five m/s with some strong currents. There were few observations of no currents and weak flow below two m/s. That is preferable in a location where there are aquaculture activities. The fish cages will have fresh water masses with oxygen transported through the net.

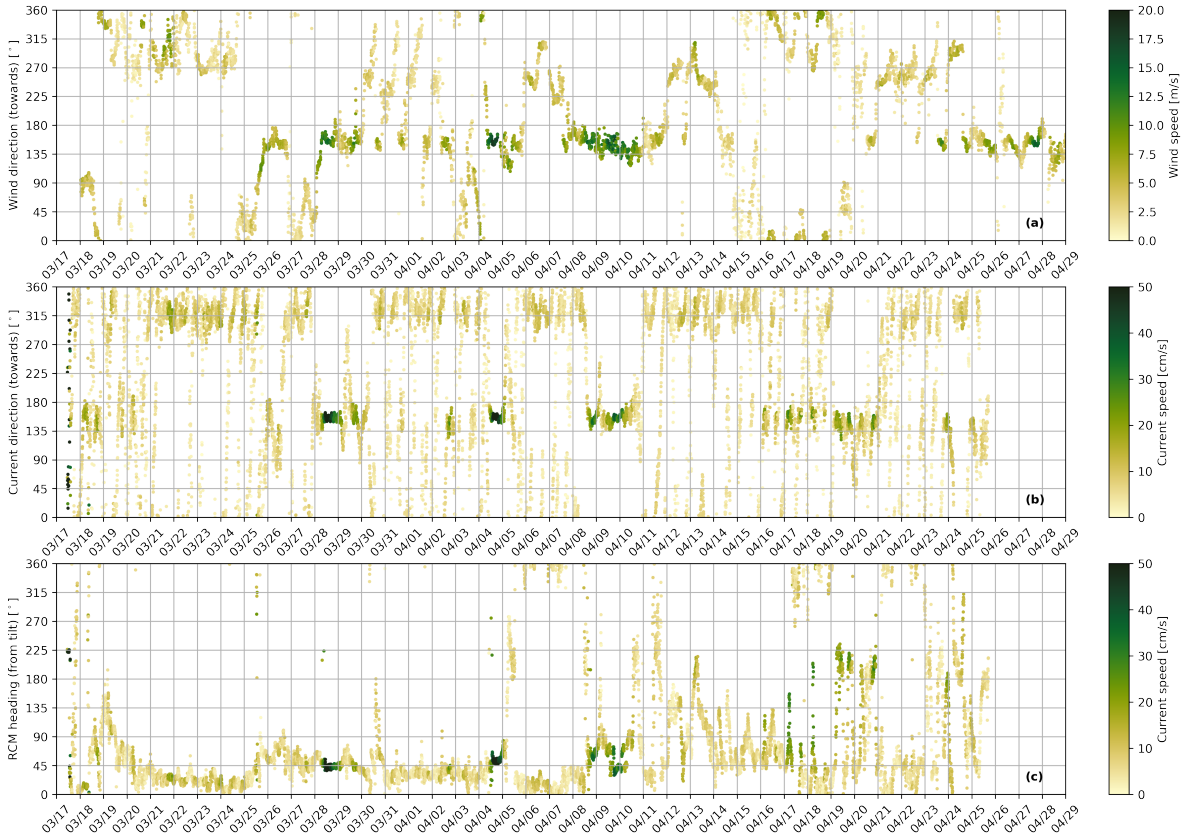

Figure 6.10: Time-series of the connection between wind direction (a), current direction (b), and the RCM heading (c).

Figure 6.10 shows the connection between the wind direction in (a), current direction in (b), and heading from the RCM in (c). The weather data is obtained from the weather station at Bømlabrua [40]. The surprising part is that when there are strong wind and currents from the Southeast, the tilt is towards the Northeast, not the Northwest as expected. This could potentially be a source of error within the compass of the tilt sensor.

Figure 6.10 shows the wind direction distribution in Stokksundet. The most common wind direction is towards the South/Southeast, which can explain why the highest current values

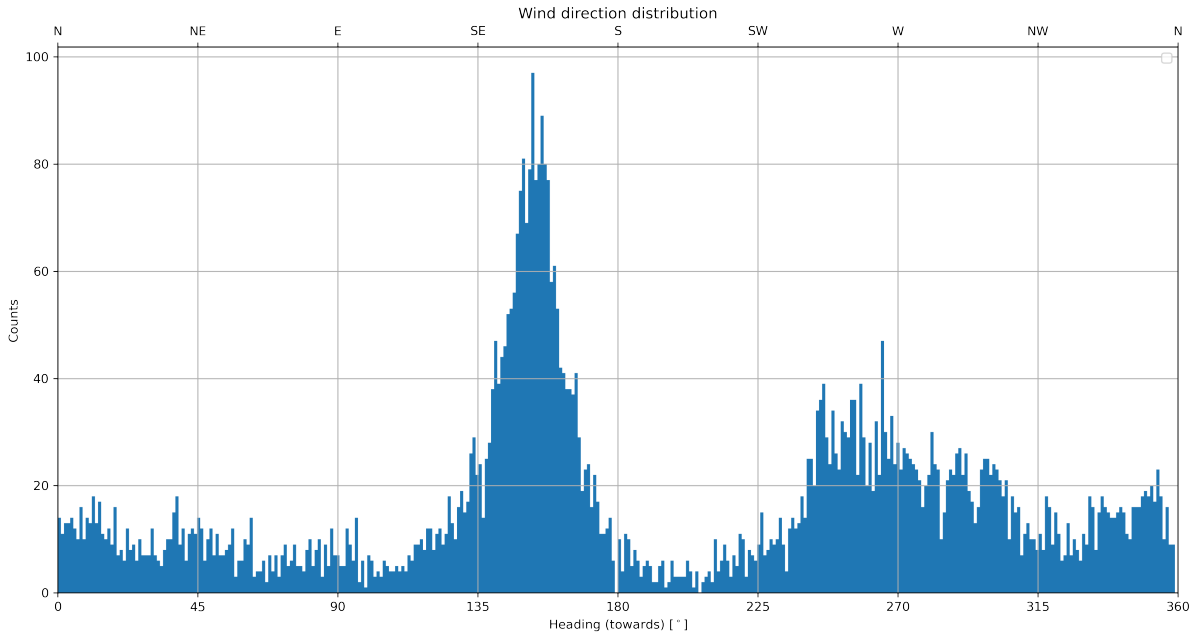

Figure 6.11: Histogram of the wind directions in Stokksundet.

measured also were towards the South/Southeast.

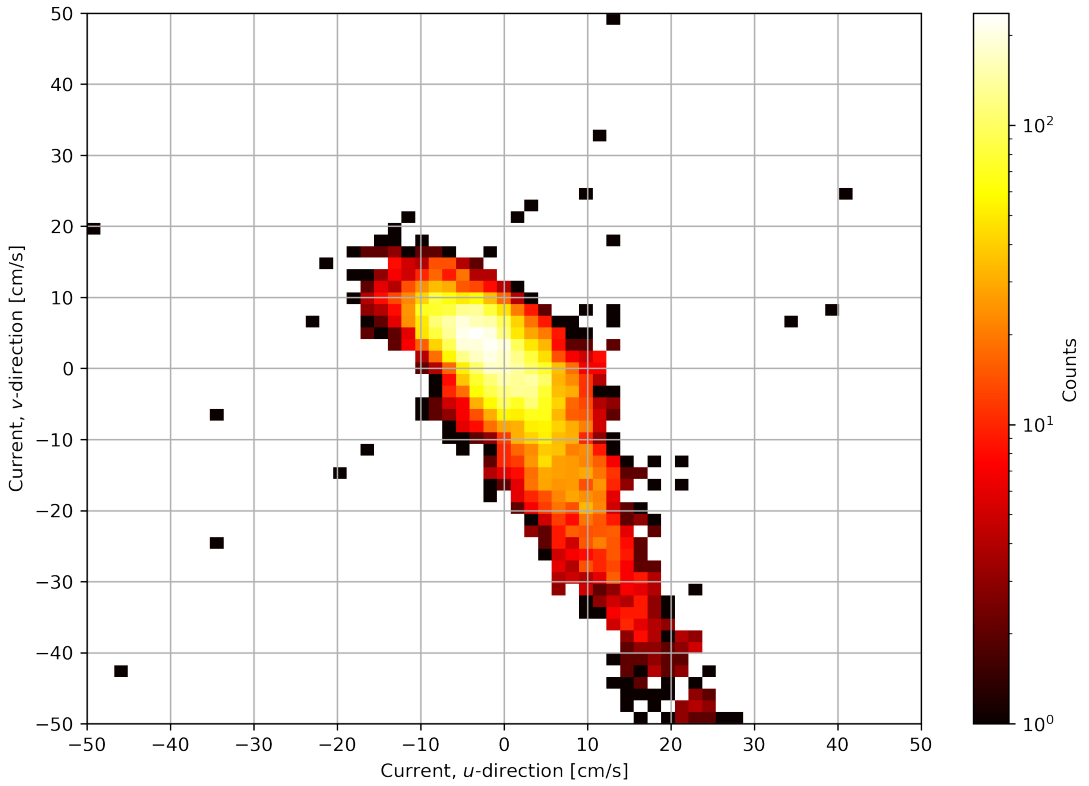

Figure 6.12: 2D histogram of the current distribution in Stokksundet.

Figure 6.12 shows the current distribution of the currents in Stokksundet. Interesting to note that the most counts are not in the center of the figure but a little towards the Northwest. There are also more measurements in that direction, but the most significant ones are to-

wards the Southeast. Some of the black dots towards the Southwest and Northeast are probably outliers from operations done on the mooring.

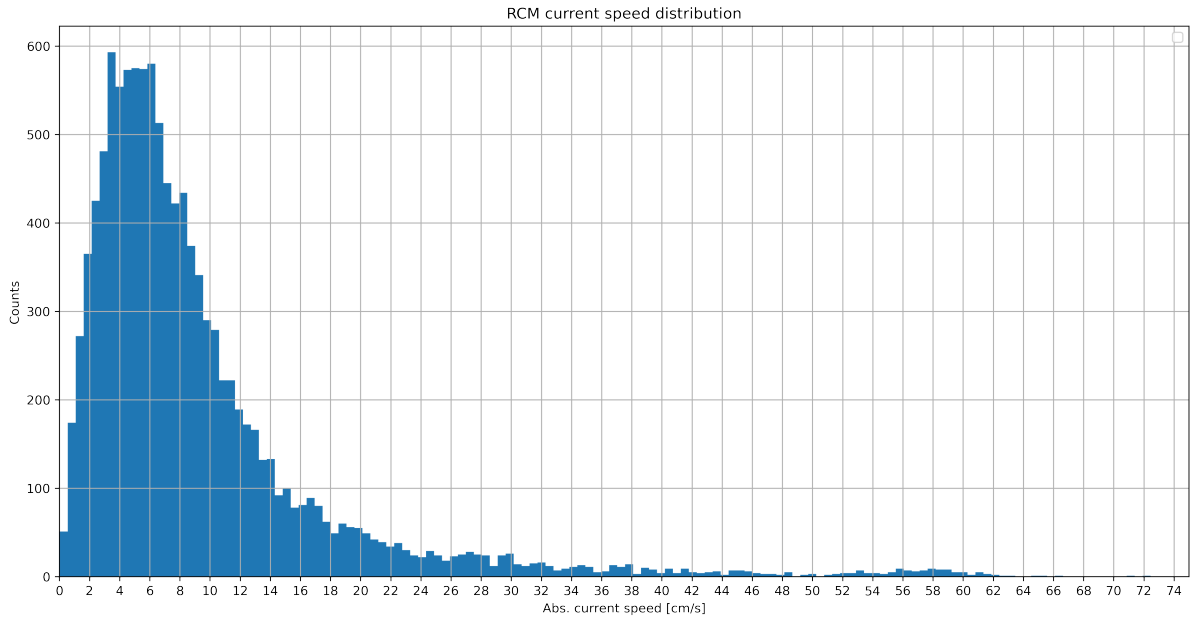

(a)

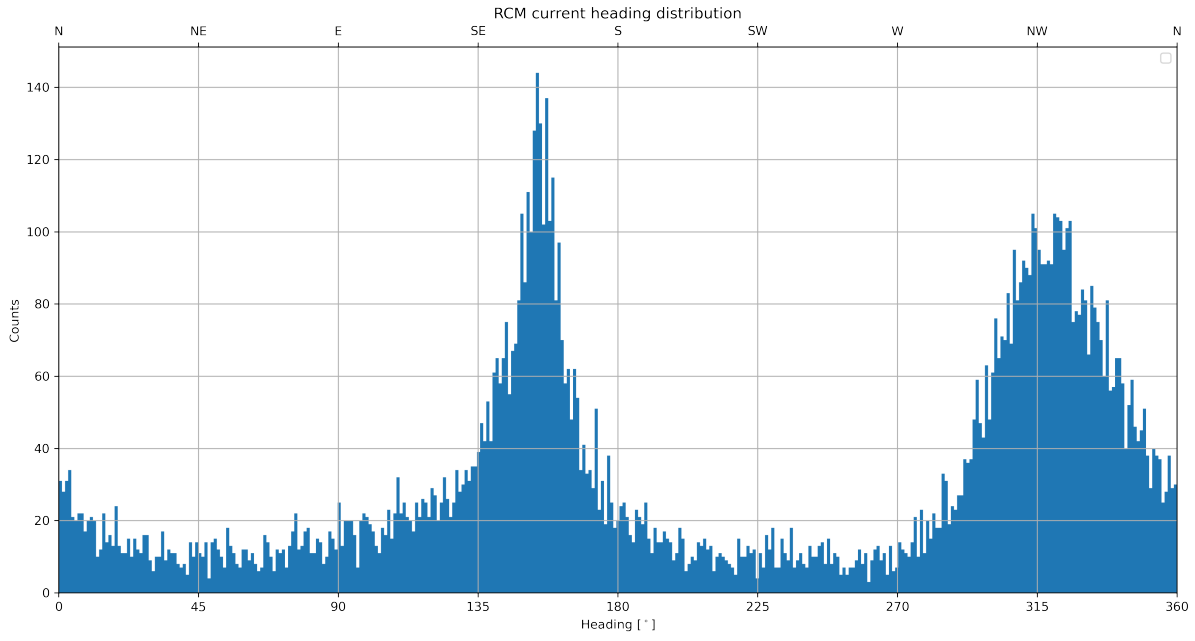

(b)

Figure 6.13: Histogram of the most common current speed (a), and current heading (b).

Figure 6.14 (a) shows the instruments' lifetime during the measurement period. The RCM was configured to start recording on power-up to minimize the risk of any problems while conducting the operation. Before loading the instrument onboard the vessel, it was turned on to avoid opening the instrument on deck. It then did measurements every five minutes until approximately the 25th of April. It needed to record at least every 10 minutes for four

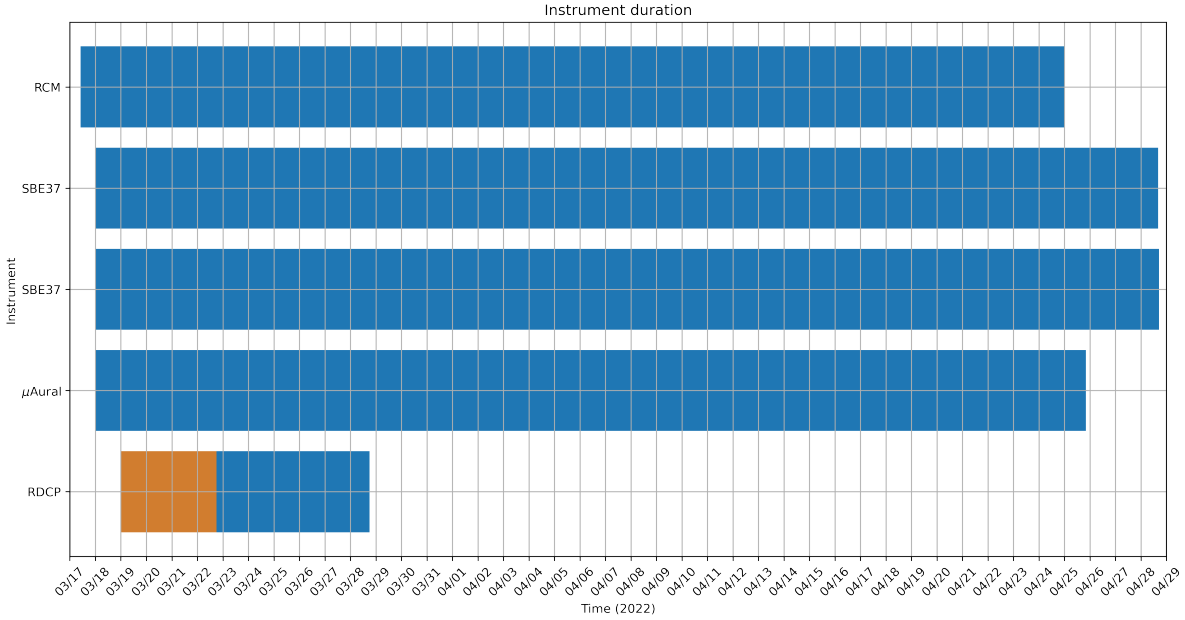

(a)

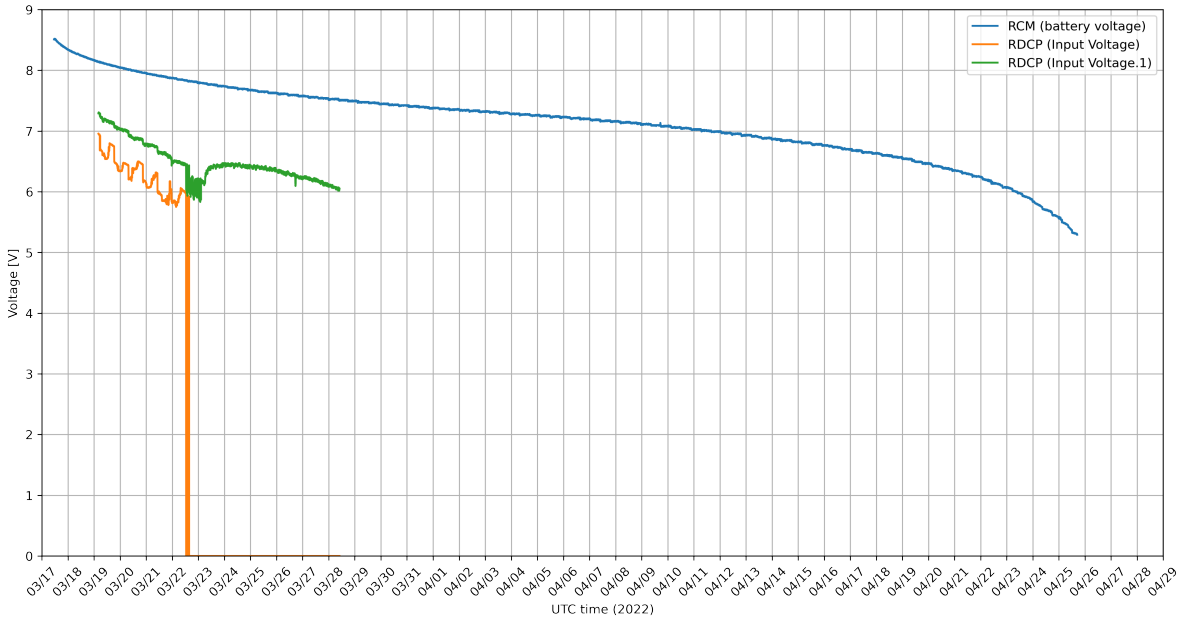

(b)

Figure 6.14: Instruments recording periods showed in (a), in (b) the battery voltage from the AADI instruments during the measurement period is illustrated.

weeks to get enough samples based on the ASC Standard. That was achieved with measurements for more than five weeks.

The other instruments were configured to start measuring at 2022-03-18T00:00:00Z. The SBE37s did measurements every minute for the whole period and had to be turned off after recovery. The μAural did survive until the 25th of April, just like the RCM. Unfortunately, the SeaGuard II instrument did not deliver the desired results. It only did current measurements for about five days before conducting an internal error. Based on Figure 6.14 (b), it looks like a problem with the battery. However, even though the RDCP stopped working on the 23rd of March, the other sensors on the instrument continued to measure for six more days. The input voltage suddenly went up for the additional sensors when the RDCP stopped.

6.5 Comparison of Observed Horizontal Mooring Motion and Simulations

This section was supposed to compare the vertical mooring motion from the simulation with the actual movement from the field experiment. However, this comparison did not make much sense since the observation mooring ended up as a surface mooring instead of a subsurface mooring. Ideally, there should have been a GPS tracker on the top float when this happened. That could have helped track at least the horizontal movement of the mooring and how it moved.

Another way to try and estimate the mooring motion is by looking at the absolute tilt of the RCM. Figure 6.15 shows that the tilt is as expected, connected to the strength of the wind and currents at the time. The green dots show the times with rough environmental conditions, and the tilt follows that pattern. Based on Eq. (2.1) one can estimate the horizontal distance between the top float and the mooring position. Since the depth at the mooring location was about 260 m, and the maximum tilt (α) was about 9.5 ° on the 4th of April, the horizontal distance could be estimated using Pythagoras. Thus, the distance Z_H is calculated by multiplying tan (α) with the mooring depth. That approximates a distance of 44 m from the anchor position at max. The mooring length can then be calculated by taking the square root of Z_H and Z_d squared to find the mooring length to be about 263 m. That is an estimation that makes sense based on observations reported from the field experiment while moving the mooring.

Figure 6.16 shows a 3-D plot of the motion of the observation mooring. This simulation compares movement on the day with the most observed tilt. Ocean current data from the NorFjord ocean model [19] and wind data obtained from [40] were used as input in MD&D. The

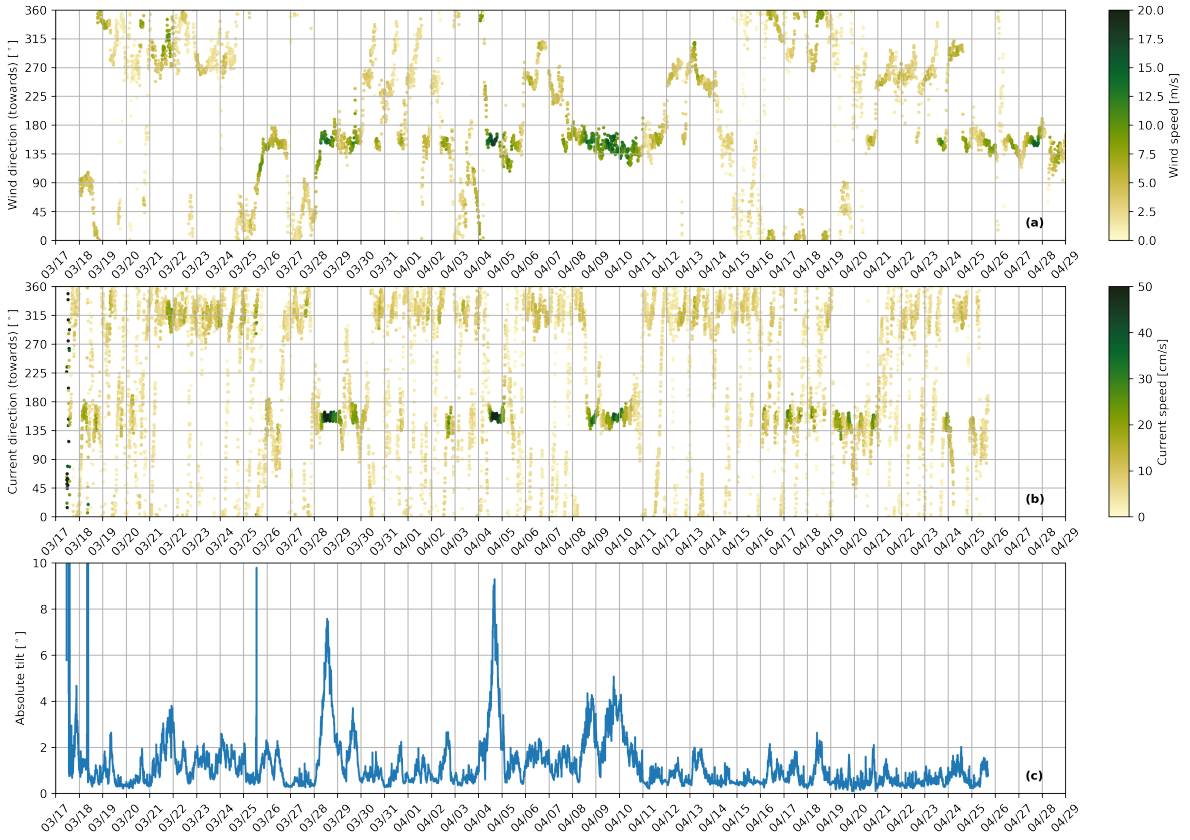

Figure 6.15: Time-series of the connection between wind direction (a), current direction (b), and absolute instrument tilt (c) on the RCM.

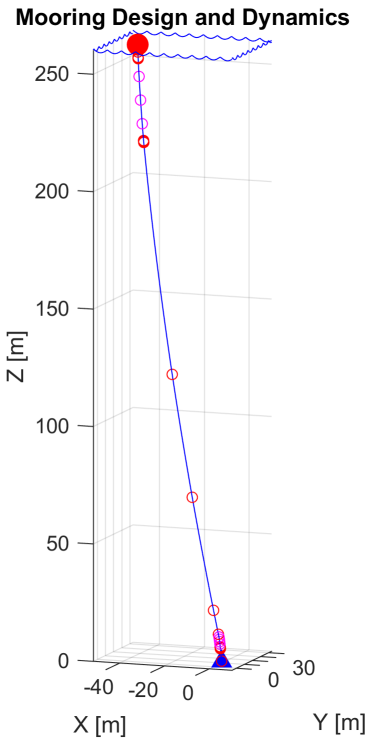

Figure 6.16: A simulated 3-D plot of the mooring motion on the observation mooring.

4th of April was one of the days with the strongest winds and currents during the measurement period. Furthermore, based on the calculations from Eq. (2.1), the observed horizontal motion was estimated to be 44 m. In the simulations, the result was a horizontal movement of 42.5 m with the surface mooring almost submerged. Consequently, it is a good agreement between the simulation and the observed motion. However, this comparison is based on many approximations, but it looks plausible.

Chapter 7

Discussion, Conclusions, and Further Work

This chapter aims to discuss the main results and investigate the potential limitations of the project. Furthermore, look at the main conclusions and experiences learned before lastly proposing suggestions for further work.

7.1 Discussion

Firstly, discussing simplifications, limitations in the approach, and work conducted regarding the UNDER-ICE experiment in the Arctic Ocean. Secondly, evaluate the same problems in the field experiment and investigate if similarities occur.

7.1.1 Mooring Motion - UNDER-ICE Experiment

The MD&D software has some limitations and simplifications that must be addressed. For instance, it is only possible to define the shape of the mooring elements as spheres or cylinders. Even though many instruments are shaped like cylinders, it can be challenging to define advanced structures. Of course, calculating the surface area and choosing a good drag coefficient can create a good approximation. It has a library with standard mooring components that have been tested before and have the correct specifications. Unfortunately, the library is from 1999 and newer instruments are not in there. However, there are often similarities in appearance, and older versions can be used as inspiration.

MD&D also uses the seafloor at the anchor position as $z = 0$. In contrast, most other instruments and persons working with marine research reference the surface as the $z = 0$. That

means it is crucial to be careful when preprocessing the environmental input data.

Furthermore, another limitation is that the software only shows the solution when it is static, assuming it has had time to reach a stable position. Therefore, datasets with a short sampling interval are necessary to capture the motion change from, e.g., tidal currents. Exactly how short of an interval is needed depends on the application, but with something like hourly and shorter, it would be possible to spot the trends. Consequently, having a time-series of current data, which only has data points daily, is not ideal.

This thesis utilized the GECCO model to try and simulate the mooring motion. Unfortunately, this model only has daily data points and some other limitations. For instance, it has a low spatial resolution, making it hard to get data from the correct positions. However, it is easily accessible and has a dataset covering the measurement period. It was also discovered that the GECCO model generally seemed to underpredict the currents. Accordingly, it was decided to use current data from the ADCPs when simulating the mooring motion. Since the simulations based on the GECCO currents also underpredicted the mooring motion.

Unfortunately, it required much preprocessing to use ADCP data directly in MD&D. Hence, it was decided to scale the GECCO current profiles to approximately the same level as the ADCPs showed. However, comparing the simulated with observed motion with ADCP data as direct input would have been very interesting.

Additionally, the impact of the mooring components' drag coefficients on the simulated mooring motion was investigated. The acoustic source was the instrument that had the most uncertainties regarding drag. Consequently, it was a process where the drag coefficient was gradually increased to look at the changes in the simulation. Even though it made a difference, it was not sufficient, and it appeared that the accuracy of the simulations was more dependent on having time series of precise ocean current data.

7.1.2 Field Experiment - Stokksundet

In the field experiment, the initial idea was to analyze the motion of a subsurface mooring in the same manner as in the first part of the project. Hence, it was mainly the pulldowns on the instruments based on pressure data that were going to be investigated. To look at the horizontal displacement would be challenging without a transponder network.

However, since the deployment did not go as planned, and the mooring ended up as a surface mooring, this was not an option. Therefore, a GPS on the surface mooring would have been very interesting in investigating the horizontal movement. Unfortunately, since the plan was to have a subsurface mooring, this was not something that could be improved at the time of deployment.

Even though it did not go exactly according to the plan, the new configuration as a surface mooring had some benefits. For instance, the top float was more visible, which was probably wise in an area with much shipping. It also made it easier to get the instruments at approximately the planned depth by adjusting kevlar shots from the float. On the other hand, it had some downsides, e.g., waves and wind affecting the top float. Consequently, this led to more movement in the horizontal directions and low-frequency noise on the μAural due to waves and wind hitting the top float.

Furthermore, regarding the EMBILINK sensors, there are some uncertainties. For example, when were they cleaned, how are they cleaned, when were they last calibrated, and at what depth. Unfortunately, they do not have pressure sensors. These things could be a part of some of the deviations seen in the measurements. In addition, in connection with an operation conducted on the 23rd of March, the sensors were suspected to be in the air for a while. Consequently, it seemed that at least the oxygen sensors were more in agreement before this event. It could potentially have been damaged in some way.

The measurements could also be affected by biofouling. For instance, the differences in salinity could have to do with the fact that the EMBILINK had more marine growth on the conductivity sensor than the RCM. Although not proven, it could be a part of the explanation. Biofouling is not as important to consider during the winter season, but when the spring and summer emerge, it is potentially challenging for observation moorings like this. Biofouling could compromise the measurements on, e.g., the conductivity sensors. In addition, it could also increase the drag force working on the mooring line and other mooring elements. Some biofouling was present on the observation mooring, especially on the instruments near the surface, like the RCM at 6 m and SBE-37 at 10 m. Consequently, it is important to consider this when deploying moorings in coastal areas since it happened after only six weeks in the ocean.

Furthermore, an essential difference between the mooring and the EMBILINK is that the EMBILINK is observing the conditions in real-time. This is critical inside the fish cage since sudden drops in oxygen levels could be fatal for the fish. Therefore, a solution with real-time or near real-time data transmission to shore would have been preferable on the observation mooring. That could potentially be used to spot trends with currents or other parameters that increase the chances of salmon lice infecting the fish. However, implementing a system like that would require more resources.

7.2 Conclusions

This thesis focuses on modeling and simulating mooring motion using simulation software. In addition, investigate if ocean models can be used to predict the movement and help optimize mooring design when deploying moorings in new areas. This is conducted by comparing observed and simulated motion on moorings that have *in situ* data. It also focuses on designing, deploying, and recovering an observation mooring in coastal areas. The intention is to evaluate the quality of the data collected and look at how the system has performed. Finally, compare the results with data collected from the EMBILINK and investigate the vertical structure.

It was discovered that when simulating mooring motion in MD&D having a good time series with ocean current data is essential. Hence, using environmental input from the GECCO model was insufficient. However, when using data from the ADCPs as input arguments, the simulations and observed mooring motions are within a reasonable agreement. Consequently, it is critical to have input currents representing the area to predict mooring motion before a new deployment. Using *in situ* data or a well-validated ocean model is possible. However, it is also wise to investigate the movement using 50 or 100 years values as a safety measure.

The deployment and recovery operations were conducted successfully and safely using the workboat Randi. Having a good plan and procedure was vital in the process. Consequently, no personnel or instruments were injured/damaged during the operations. Even though the mooring ended up as a surface mooring, the design and planning phase was critical to everything going as well as it did.

The observation mooring proved a capable system when conducting measurements under the given circumstances. Moreover, the transition from subsurface to surface mooring did not seem to influence the measurements in a suboptimal way.

The current measurements showed that the area was dominated by short-term current peaks, with some periods of more continuous current. Moreover, the current direction changes between Northwest and Southeast along the longitudinal direction of the fjord. Hence, it is significantly affected by tidal waters. However, the wind heavily influenced the current in some periods with the highest current speeds. With winds from 15 m/s to 20 m/s, the tidal change was less prominent, and the water layers from 10 m to the surface started to mix.

Evaluating horizontal motion on a surface mooring would have been very interesting with a GPS tracker on the top float. Unfortunately, since the initial plan was to deploy a subsurface mooring, a GPS tracker was not in the toolbox when deploying. Therefore, it is hard to say something concrete about the motion when it is only current and tilt data from the RCM

available.

The examination of the soundscape before deployment provided valuable information regarding selecting appropriate gain on the hydrophone. Although the μAURAL went into saturation during the measurement period, it was during two of the four flushing operations. Hence, it only happened when the distance to the hydrophone was less than 75 m. As a result, since the mooring is approximately 250 m away from the closest fish cage, a gain of 18 dB should be fine.

7.3 Further Work

This section looks at possible improvements in the present work in this thesis and recommendations for future work to find solutions in optimizing mooring design. It also looks at how observation moorings can be utilized better in aquaculture. Firstly, it would be interesting to try and simulate mooring motion on UI4 and UI5 using other ocean models covering the measurement period in the UNDER-ICE experiment. It would also be exciting to use ADCP data from the moorings directly in MD&D.

Deploy a new observation mooring that is either subsurface or surface. Either deploy a subsurface mooring with a transponder network or a surface mooring with a GPS tracker. Probably more cost-effective to use a GPS tracker. It would also be interesting to transmit data from the mooring near real-time. That would especially be beneficial when cooperating with aquaculture companies. For instance, moorings could be utilized to observe oxygen levels and algae concentration in a fjord system.

Consequently, the moorings could notify aquaculture companies if the water conditions are deadly for the fish. Then it would be possible to take measures before it is too late. For example, over the years, there have been cases of deadly algae suddenly killing salmon. However, to detect these changes in time, it would probably be necessary to have several moorings in the fjord or position the mooring in the fjord inlet.

Another point is to investigate how currents, salinity, and temperature affect when the lice spread to the salmon. As a result, it could be possible to spot patterns that, e.g., with currents going towards the Southeast, the chances of lice increased a lot. Consequently, measures like lowering the fish farms below 15 m in periods could be used to try and limit the spread.

Finally, using other simulation software with the same current input. Then, compare the different software based on how well the motion predictions are. It could also be helpful to evaluate the various software based on other factors like functionality, performance, and usability. For instance, ProteusDS and NOYFB would be interesting to look into further.

References

[1] D. S. Nath, P. Pujari, A. Jain, and R. Vikas, "Drag reduction by application of aerodynamic devices in a race car," Advances in Aerodynamics **3**, 20 (2021) doi: https://doi.org/10.1186/s42774-020-00054-7.

[2] D. Nelson, "Laminar vs. turbulent flow," Science Trends (2018) doi: https://doi.org/10.31988/SciTrends.5067.

[3] R. Dewey, "Mooring design & dynamics—a matlab® package for designing and analyzing oceanographic moorings," Marine Models **1**, 103–157 (1999) doi: https://doi.org/10.1016/S1369-9350(00)00002-X.

[4] E. Storheim, H. Sagen, and F. Geyer, "Analysis of signal propagation in the UNDER-ICE experiment," in *Proc. UACE2021*, Proceedings of Meetings on Acoustics (2021), Vol. 44, p. 070031, doi: https://doi.org/10.1121/2.0001500.

[5] T. Soltwedel, E. Bauerfeind, M. Bergmann, A. Bracher, N. Budaeva, K. Busch, A. Cherkasheva, K. Fahl, K. Grzelak, C. Hasemann, H. E, M. Jacob, A. Kraft, C. Lalande, K. YM, K. Metfies, E.-M. Nöthig, K. Meyer-Kaiser, N.-V. Quéric, and M. Klages, "Natural variability or anthropogenically-induced variation? insights from 15 years of multidisciplinary observations at the arctic marine lter site hausgarten," Ecological Indicators **65**, 89–102 (2016) doi: https://doi.org/10.1016/j.ecolind.2015.10.001.

[6] Beaufort Gyre Exploration Project, "About the Beaufort Gyre Exploration Project" , https://www2.whoi.edu/site/beaufortgyre/ (2022) [Accessed: 2022-06-09].

[7] D. Moller, "A Computer program for the design and static analysis of single-point subsurface mooring systems : NOYFB," Technical Report 083-004, Woods Hole Oceanographic Institution, 86 Water St, Falmouth, MA 02543, USA (1976), doi: https://doi.org/10.1575/1912/665.

[8] Dynamic Systems Analysis Ltd. 2022, "Flexible Marine Dynamic Analysis Software" , https://dsaocean.com/proteusds/overview/ (2022) [Accessed: 2022-06-09].

[9] N. Panicker, L. Schultz, and D. Schmidt, "Analysis of surface mooring dynamics," Offshore Technology Conference **2**, 12 (1974) doi: https://doi.org/10.4043/2071-MS.

[10] J. Davidson and J. Ringwood, "Mathematical modelling of mooring systems for wave energy converters—a review," Energies **10**, 46 (2017) doi: https://doi.org/10.3390/en10050666.

[11] S. Edward, K. Ira, and S. James, *Introduction to Fluid Mechanics* (Oxford University Press, New York, 2005).

[12] J. C. Yunus Çengel, *Fluid Mechanics – Fundamentals and Applications* (McGraw-Hill, New York, 2006).

[13] National Oceanic and Atmospheric Administration, "What is a current?" , https://oceanservice.noaa.gov/facts/current.html (2019) [Accessed: 2022-05-07].

[14] MATLAB, *version 9.10.0 (R2021a)* (The MathWorks Inc., Natick, Massachusetts, 2021).

[15] P. Worcester, S. Carey, M. Dzieciuch, L. Green, D. Horwitt, J. Lemire, and M. Norenberg, "Distributed Vertical Line Array (DVLA) acoustic receiver," Proc. UACE 113–118 (2009).

[16] G. Lyu, A. Köhl, N. Serra, D. Stammer, and J. Xie, "Arctic Ocean-Sea ice reanalysis for the period 2007-2016 using the adjoint method," Quarterly Journal of the Royal Meteorological Society **147**, 22 (2021) doi: https://doi.org/10.1002/qj.4002.

[17] G. Lyu, N. Serra, A. Köhl, and D. Stammer, "Arctic Ocean synthesis 2007-2016" Available online: "http://thredds.nersc.no/thredds/catalog/gecco/GECCO/catalog.html" (2022).

[18] "These data were generated by the INTAROS H2020 project (ref. Goukun Luy, Nuna Serra, Armin Koehl and Detlef Stammer, University of Hamburg) and made freely available by the Nansen Center, Norway.".

[19] S. Dalsøren, J. Albretsen, and L. Asplin, "New validation method for hydrodynamic fjord models applied in the Hardangerfjord, Norway," Estuarine, Coastal and Shelf Science **246**, 13 (2020) doi: https://doi.org/10.1016/j.ecss.2020.107028.

[20] A. Beszczynska-Moeller, E. Fahrbach, U. Schauer, and E. Hansen, "Variability in atlantic water temperature and transport at the entrance to the arctic ocean, 1997-2010," ICES Journal of Marine Science **69**, 852–863 (2012) doi: https://doi.org/10.1093/icesjms/fss0567.

[21] Saiv AS Environmental Sensors & Systems, "CTD profiler model SD204" , https://saiv.no/sd204-ctd-profiler (2022) [Accessed: 2022-03-14].

[22] UNESCO, "Tenth report of the joint panel on oceanographic tables and standards," Technical Papers in Marine Science **37**, 1–144 (1970).

[23] Geonorge, "dybdedata.no" , https://kartkatalog.geonorge.no/metadata/dybdedatano/5d07be67-9737-419e-afae-f5631a6070b0 (2022) [Accessed: 2022-03-25].

[24] Lovdata, "Lov om informasjon om bestemt angitte områder, skjermingsverdige objekter og bunnforhold" , https://lovdata.no/dokument/NL/lov/2017-06-21-88 (2022) [Accessed: 2022-03-25].

[25] Kartverket, "Se havnivå" , https://www.kartverket.no/til-sjos/se-havniva (2022) [Accessed: 2022-03-28].

[26] Kartverket, "AIS tetthetsplott" , https://kartkatalog.geonorge.no/metadata/ais-tetthetsplott/fe1c9df5-d350-45e6-95d3-2723d04de4b1 (2022) [Accessed: 2022-03-28].

[27] M. Beveridge and J. A. Grøttum, *A review of cage culture: northern Europe.*, 129–158 (FAO, Rome, Italy).

[28] Mooring System Inc., "Spherical ADCP Buoys and Floatation (SYNTACTIC)" , https://www.mooringsystems.com/buoyancy.htm?fbclid=IwAR36v_HXsAn8zyKZ7oksDCnj1nACSdd0Rf_SGkQLKJVwKlINZ-pv0bcXb-o (2022) [Accessed: 2022-03-29].

[29] S. Klem, "Straummåling ved lokalitet Holevik i Bømlo kommune. November-desember 2020.," Technical Report 3295, Rådgivende Biologer AS, Edvard Griegs vei 3, 5059 Bergen (2021), available online: "https://www.radgivende-biologer.no/rapporter/ar-2021/straummaling-ved-lokalitet-holevik-i-bomlo-kommune-november-desember-2020/" [Accessed: 2022-02-05].

[30] Xylem Inc. | Aanderaa Data Instruments AS, "Single-point current meter" , https://www.aanderaa.com/single-point-current-meter (2022) [Accessed: 2022-03-29].

[31] Xylem Inc. | Aanderaa Data Instruments AS, "SEAGUARD® II DCP - Doppler Current Profiler" , https://www.xylem.com/en-il/products--services/analytical-instruments-and-equipment/data-collection-mapping-profiling-survey-systems/data-collection-systems-sensors/seaguardii-dcp/ (2022) [Accessed: 2022-03-29].

[32] SEA-BIRD Scientific, “SBE 37 MicroCAT” , https://www.seabird.com/moored/sbe-37-sm-smp-smp-odo-microcat/family?productCategoryId=54627473786 (2022) [Accessed: 2022-03-29].

[33] Multi-Electronique (MTE) Inc., “µAURAL” , http://www.multi-electronique.com/uaural.html (2017) [Accessed: 2022-03-29].

[34] Okeanus An Advanced Ocean Systems Company, “Teledyne Benthos Acoustic Release” , https://okeanus.tscstrategic.com/rentals/metocean/teledyne-benthos-acoustic-release (2022) [Accessed: 2022-03-29].

[35] The Aquaculture Stewardship Council (ASC), “ASC Salmon Standard Version 1.3,” Technical Report 34389683, Aquaculture Stewardship Council, Arthur van Schendelstraat 650 3511 MJ Utrecht, the Netherlands (2019), available online: "https://www.asc-aqua.org/wp-content/uploads/2019/12/ASC-Salmon-Standard_v1.3_Final.pdf" [Accessed: 2022-04-04].

[36] Lovdata, “Forskrift om krav til teknisk standard for flytende akvakulturanlegg (NYTEK-forskriften)” , https://lovdata.no/dokument/SF/forskrift/2011-08-16-849 (2015) [Accessed: 2022-04-06].

[37] Norwegian Directorate of Fisheries, “Merking av reiskap” , https://www.fiskeridir.no/Fritidsfiske/Reiskap/Merking-av-reiskap (2022) [Accessed: 2022-04-06].

[38] J. Kemp, K. Newhall, W. Ostrom, R. Krishfield, and A. Proshutinsky, “The Beaufort Gyre Observing System 2004 : Mooring recovery and deployment operations in pack ice,” Technical Report WHOI-2005-05, Woods Hole Oceanographic Institution, 86 Water St, Falmouth, MA 02543, USA (2005), available online: "https://www.whoi.edu/beaufortgyre/pdfs/BGOS_Technical_Report_2004.pdf" [Accessed: 2022-03-30].

[39] Okeanus An Advanced Ocean Systems Company, “Teledyne Universal Deck Box UDB-9400” , https://okeanus.com/rentals/metocean/teledyne-benthos-universal-deckbox-udb-9400 (2022) [Accessed: 2022-06-12].

[40] Norsk Klimaservicesenter, “Observations and weather statistics” , https://seklima.met.no/observations/ (2022) [Accessed: 2022-06-13].